Gastrointestinal Motility Variation and Oral Drug Absorption

by

John Inn Chung

A dissertation submitted in partial fulfillment
of the requirements for the degree of
Doctor of Philosophy
(Pharmaceutics)
in The University of Michigan
2008

Doctoral Committee:

Professor Gordon L. Amidon, Co-Chair
Associate Professor Naír Rodríguez-Hornedo, Co-Chair
Professor H. Scott Fogler
Associate Professor Steven P. Schwendeman

2008

To my parents,
who have sacrificed so much on my behalf and
who are my role models

To my brother, James,
whom I am very proud of

and

To my wife, Christine,
who I love dearly

Acknowledgements

First I would like to praise God, who makes all things possible.

I would like to express my sincere gratitude to my co-advisors, Dr. Gordon L. Amidon and Dr. Naír Rodríguez-Hornedo for giving me the opportunity to do rewarding and challenging research under their guidance. I have learned many things from them and I have a tremendous respect for their knowledge, dedication and contributions to the pharmaceutical field.

I would also like to sincerely thank Dr. Mary Lee Ciolkowski, Dr. Brian Rohrs, and Dr. Jeffrey Koup who have mentored me over the years and who have positively impacted my decision to pursue a career in pharmaceutical research and my development as a scientist.

I am especially grateful for the many friends, brothers and sisters I have met at the College of Pharmacy, Lighthouse, and Cornerstone. They have made my eight years in Michigan even more enjoyable.

Most of all, I would like to thank my wife, parents, and my brother for their unconditional love, support, and patience. I thank God for their presence in my life.

Finally, I am indebted to the College of Pharmacy, Ara G. and Shirley W. Paul Scholarship, Chinju Wang Sheu Graduate Student Fellowship, Fred W. Lyons Fellowship, Harold and Vivian Shapiro Award, and Warner-Lambert/Parke-Davis Fellowship for their generous support of my graduate studies.

Table of Contents

Dedication....ii
Acknowledgements....iii
List of Figures....vi
List of Tables....vii
List of Appendices....viii
Abstract....ix
Chapter
I. Introduction and Background....1
Anatomy and Physiology of the Gastrointestinal Tract
The Migrating Motor Complex
Migrating Motor Complex Effects on Gastric Emptying
Carbamazepine
Nictotinamide
Carbamazepine:Nicotinamide Cocrystal
Research Objectives
References

II. Development of the Pulsatile Emptying Transit (PET) Oral Absorption Model....23
Introduction
Theoretical
Methods
Results and Discussion
Summary
References

III. A Pharmacokinetic Model Incorporating Gastrointestinal Motility Variation Coupled with Discontinuous Gastrointestinal Absorption to Examine the Appearance and Absence of Double Peaks in Oral Ranitidine Plasma Concentration-Time Profiles....50
Introduction
Theoretical
Methods
Results
Discussion
Summary
References

IV. Applying Solubility Product and Solution Complexation Relationships to Preliminary Cocrystal Dissolution Studies.....73
Introduction
Theoretical
Methods
Results
Discussion
Summary
References

V. Conclusions.....94

Appendices.....97

List of Figures

Figure

1-1. Diagram of small intestine....13
1-2. Diagram of (a) villus and (b) microvilli....14
1-3. Aboral migration of phase III....15
1-4. Timing of bolus injection and intestinal transit....16
1-5. Contractile coordination between antrum and duodenum....17
1-6. Gastric emptying pattern for non-nutrient liquids and solids....18
1-7. Chemical structures of (a) carbamazepine and (b) nicotinamide....19
1-8. Molecular assembly of carbamazepine:nicotinamide cocrystal....20
2-1. Weibull dissolution varying shape factor (b)....39
2-2. Weibull dissolution varying time scale factor (A)....40
2-3. Weibull dissolution varying time lag (t_{lag})....41
2-4. 3-D plot of fraction of dose absorbed vs. Do vs. Dn....42
2-5. Simulated plasma concentration-time profiles of cetirizine....43
2-6. Schematic of PET model with 2-compartment pharmacokinetic model....44
2-7. Amount of drug in solution vs. time (a) TTP = 80 min (b) TTP = 18 min....45
2-8. 3-D plot of C_{max} vs. TTPIII vs. t85....46
2-9. 3-D plot of C_{max} vs. TTPIII vs. P_{eff}....47
3-1. Oral ranitidine plasma concentration-time profiles for 12 patients....62
3-2. Plasma concentration-time profile varying time to next phase III (TTPIII)...63
3-3. Plasma concentration-time profile varying dissolution rate (t85)....64
3-4. Plasma concentration-time profile varying P_{eff} in the duodenum....65
3-5. Plasma concentration-time profile varying P_{eff} in the ileum....66
3-6. Plasma concentration-time profile varying k_{12}....67
3-7. Plasma concentration-time profile varying k_{21}....68
3-8. Plasma concentration-time profile varying k_{out}....69
3-9. Plasma concentration-time profile varying V_c....70
4-1. Theoretical CBZ:NCT phase solubility diagram in ethanol....85
4-2. Theoretical CBZ-NCT phase solubility diagram in 2-propanol....86
4-3. Theoretical CBZ:NCT phase solubility diagram in ethyl acetate....87

List of Tables

Table

4-1 Compression conditions for compact formation.....88
4-2 Solubility of CBZ:NCT, CBZ & NCT in three organic solvents.....89
4-3 K_{sp} and $K_{1:1}$ for CBZ:NCT in three organic solvents.....90
4-4 Comparison of estimated and experimental relative dissolution rates.....91

List of Appendices

Appendix

A. Parameter values used for simulations in Chapter II.....98
B. Parameters values used for simulations in Chapter III.....105
C. Mathematical phase solubility diagrams.....114

Abstract

Gastrointestinal Motility Variation and Oral Drug Absorption

by

John Inn Chung

Co-Chairs: Gordon L. Amidon and Naír Rodríguez-Hornedo

Gastrointestinal (GI) motility is a physiological factor that affects oral drug absorption by controlling a drug's residence time in the GI tract. The development of an oral drug absorption model, the pulsatile emptying transit (PET) model, which takes into account variations in GI motility due to the migrating motor complex (MMC) is described. The absorption rate outputted by the PET model can be used as an input for pharmacokinetic models to estimate drug plasma concentration-time profiles. The effect of variations in GI motility on the drug plasma concentration-time profiles of high permeability and high solubility (BCS Class I) drugs was simulated. Simulations showed that increases in the maximum plasma concentration (Cmax) greater than 10% can occur when drugs that have an effective permeability greater than 0.04 cm/min and a high dissolution rate (85% of the dose dissolves within 15 minutes) are dosed during phase III of the MMC.

Many explanations have been given for the appearance of double peaks in oral ranitidine plasma concentration-time curves. Using a discontinuous PET model with a 2-

compartment pharmacokinetic model, parameter sensitivity analysis was done on the following parameters: dosing time relative to the MMC, dissolution rate, effective permeability in the duodenum and ileum, and intravenous pharmacokinetic parameters (k_{12}, k_{21}, k_{out}, V_d). Simulations suggest that the variety of shapes for ranitidine plasma concentration-time profiles with double peaks is a result of differences in these parameter values between individuals. In addition, simulations showed that the dosing time relative to the MMC coupled with discontinuous absorption sites along the small intestine can explain the absence and presence of double peaks in oral ranitidine plasma concentration-time profiles.

Cocrystals are non-covalently bonded crystal complexes with two or more components. The formation of cocrystals offers a means to alter the dissolution rate of a solid without changing covalent bonds. Dissolution experiments with CBZ:NCT cocrystal and CBZ(III) crystal in ethanol, 2-propanol and ethyl acetate were conducted and the relative dissolution rates were compared with estimated relative dissolution rates based on stoichiometric cocrystal solubility. Statistically significant differences in relative dissolution rates were not observed in all three solvents.

Chapter I

Introduction and Background

The simplicity of swallowing a tablet with a glass of water to treat a disease stands in stark contrast with the difficulty of developing an orally delivered pharmaceutical product. To achieve a desired pharmacologic effect, therapeutic amounts of drug need to be absorbed by the gastrointestinal tract, enter the systemic circulation and reach the sites of action. Many factors can affect how well orally delivered compounds are absorbed. These factors fall into three categories: physicochemical properties of the compound, formulation of the compound, and human gastrointestinal physiology (Yu, Lipka et al. 1996). A crucial step during early drug development is determining whether a new compound that shows promising *in vitro* pharmacologic activity can be absorbed adequately by the human body without actually dosing the compound in humans. If it is determined that sufficient absorption can be achieved, another key step in the development of the compound is determining a safe and effective dosing regimen in humans. Predictive oral absorption models can significantly aid compound selection and optimization decisions at important drug development stages by providing reasonable estimates of human oral drug absorption for newly synthesized compounds and by allowing pharmaceutical scientists to run simulations to quantitatively understand how changing specific parameters may affect the rate, extent and variability of human oral drug absorption

The migrating motor complex (MMC) is a rhythmically recurring cycle of contractile activity in the stomach and small intestine that occurs during the fasted state. One of the primary roles of the MMC is to clear remaining ingested material from the stomach and small intestine into the colon. As a consequence, the MMC influences the rate of gastric emptying and the intestinal residence time of drugs taken orally, which can be important determinants of the rate and extent of drug absorption in the fasted state. Additionally, the MMC may be a major source of inter-subject and intra-subject variability in oral drug absorption due to variable gastric emptying times and transit times caused by MMC cycle length differences between and within people and random dosing of drug during different phases of the MMC. For these reasons, the MMC is an important physiological process to include in fasted state oral absorption modeling. Including the effects of the MMC into predictive oral absorption models can help quantify variability in oral drug absorption, which would be especially useful for estimating a dose and dosing regimen selection of a drug candidate to be tested in clinical trials and for developing criteria to evaluate the bioequivalence between two formulations of a drug.

Most drugs are given orally as a solid dosage form such as a tablet. One of the fundamental processes for oral drug absorption is dissolution because a drug must be dissolved before it can be absorbed by the gastrointestinal tract. An extremely slow dissolution rate may limit the absorption capability of a promising new compound such that a decision to stop its development is made. The physicochemical properties of a drug and drug formulation are important factors for drug absorption. Synthesizing different solid forms of the same drug such as forming salts, hydrates, or polymorphs is a strategy used to change the physicochemical properties of drugs and improve their

absorption. The formation of cocrystals offers another way to improve the physicochemical properties of a drug by making a new solid form of the drug. Cocrystals are noncovalently bonded multiple component crystal complexes. Improved dissolution rates of cocrystals compared to the single component drug crystal have been reported (Remenar, Morissette et al. 2003; Childs, Chyall et al. 2004; McNamara, Childs et al. 2006). However, the mechanisms for improved dissolution rates of cocrystals compared to the single component drug crystal have not been well studied. A better understanding of cocrystal dissolution mechanisms may aid in the selection of cocrystal components to achieve a desired drug dissolution profile and thus improve oral drug absorption.

Anatomy and Physiology of the Gastrointestinal Tract

The GI tract consists of the mouth, esophagus, stomach, small intestine (duodenum, jejunum, ileum), and large intestine (caecum, colon, and rectum). The GI tract not only serves as a region in the body where digestion of ingested food and absorption of necessary nutrients to maintain life occur, but it also prevents potentially harmful xenobiotics from entering the systemic circulation by acting as a barrier. Furthermore, it excretes any unabsorbed GI contents from the body. The diversity in structure and environment of the GI tract is a reflection of the many essential functions that this part of the body performs. The stomach serves as a temporary reservoir for ingested food and is not considered to be a major site of absorption for most drugs due to its small surface area. The acidic environment of the stomach ($pH \approx 2$) may inhibit the growth of microrganisms and can denature ingested proteins to expose peptide bonds. At the terminal end of the stomach is the pyloric sphincter, a ring like opening that controls

the flow and size of gastric contents that enter into the small intestine from the stomach. When strong contractions take place in the stomach, contents small enough to pass through the pylorus can empty out of the stomach. The remaining contents in the stomach are mixed with stomach secretions and reduced in size so that they can pass through the pylorus upon subsequent contractions.

The small intestine is the predominant site for absorption in the GI tract due to its large surface area. The different regions that make up the small intestine are the duodenum, jejunum, and ileum (Figure 1-1). Finger-like projections, known as villi and microvilli which are located on the walls of the small intestine greatly increase the small intestine surface area (Figure 1-2).

The duodenum connects to the stomach through the pylorus and is approximately 25-35 cm long. Bile, digestive enzymes, and bicarbonate are secreted into the duodenum through the Sphincter of Oddi. Bicarbonate is released from the pancreas to help neutralize acidic contents that are emptied from the stomach and prevent ulceration from occurring in the duodenal wall. Bile secreted from the liver and gall bladder helps emulsify fats for absorption while digestive enzymes secreted from the pancreas help break down components of food such as peptides and triglycerides.

The jejunum is located between the duodenum and ileum. This part of the small intestine is where most of the nutrients are absorbed. It is approximately 100-200 cm long and has an approximate pH of 7.5.

The ileum makes up the distal part of the small intestine. It is approximately 200-400 cm long and has an approximate pH of 7.4. Notably, the ileum is the main absorption site for both vitamin B12 and bile salts.

The large intestine receives unabsorbed material from the small intestine and stores it before it is excreted. During the time that unabsorbed material stays in the large intestine most of the remaining water is absorbed to compact the material into feces. It has been commonly thought that drug absorption in the colon is low due to a low surface area and tighter tight junctions compared to the small intestine. However, studies that evaluated regional permeabilities in rats using an Ussing chamber technique, showed that some drugs may be absorbed well in the colon. It was found that hydrophilic compounds had decreased permeabilities in the colon compared to the jejunum. However, hydrophobic compounds had similar or increased permeabilities in the colon compared to the jejunum (Ungell, Nylander et al. 1998). This study suggests that significant absorption of hydrophobic drugs can occur in the colon.

The digestive system is unique in that veins converge from the stomach, small intestine and large intestine to form the portal vein, which brings venous blood to the liver instead of the right atrium of the heart. Thus substances that are absorbed from the GI tract and enter the portal vein must pass through the liver before entering the systemic circulation.

The Migrating Motor Complex

The stomach and small intestine have recurring cycles of intense contractile activity that occur during the fasted state known as the migrating motor complex (MMC). In the fed state, the MMC is disrupted and takes approximately 3.5 hours to return (Vantrappen, Janssens et al. 1977), although times of 10 hrs for the MMC to return have been observed (Kerlin and Phillips 1982). The MMC is commonly described as having three phases; however, a fourth phase is sometimes mentioned. Phase I is a quiescent

phase. Phase I is followed by Phase II, which is described as having infrequent and irregular contractions. During late Phase II, there is a period of increasing contractile activity. This period is followed by an abrupt onset of regular and intense contractile activity that is characteristic of Phase III, which has been referred to as the housekeeper of the small intestine (Szurszewski 1969). Phase IV, is described as a brief transition period between Phase III and Phase I (Code and Marlett 1975).

Phase III contractile activity typically originates from the antrum/duodenum in humans. However, Phase III may start in the proximal jejunum. In one study it was found that 52 of the 66 recorded MMCs started in either the duodenum or antrum and 14 of the 66 started near the proximal jejunum (Vantrappen, Janssens et al. 1977). Phase III migrates aborally along the small intestine and when it reaches the terminal ileum, another Phase III begins in the proximal intestine (Figure 1-3). At any given time during the fasted state, Phase III occupies a definite length of the small intestine. The length of small intestine occupied by Phase III decreases as it migrates aborally. In humans, Phase III was measured to occupy 35 cm in the duodenum and 25 cm in the jejunum (Fleckenstein 1978). The mean propagation velocity of Phase III decreases as well as it migrates aborally. Mean propagation velocities of Phase III in human duodenum, jejunum, proximal ileum and terminal ileum are approximately 12 cm/min, 6 cm/min, 4.7 cm/min, 1.3 cm/min, and 0.9 cm/min, respectively (Fleckenstein 1978; Kerlin and Phillips 1982).

Similar to animals, the MMC appears with great regularity in man (Fleckenstein and Oigaard 1978); however values of MMC duration between and humans can vary widely. In studies done in the proximal part of the intestine of five human subjects, it

was found that the duration of MMCs ranged from 122 to 172 minutes (Fleckenstein 1978). In subsequent studies done in the entire small intestine, measured MMC durations ranged from 40 to 180 minutes with 80% of the MMC durations between 60 to 140 minutes. The mean MMC duration was 110 ± 14 min (Fleckenstein and Oigaard 1978). Other researchers measured a MMC duration that ranged from 67 to 218 minutes with a mean of 144 ± 46 min (Takamatsu, Welage et al. 2002). In measurements taken from the duodenum, the duration of Phase III activity remains fairly constant in the range of 3 to 11 minutes. The durations of Phase I and Phase II are variable and inversely related (Fleckenstein 1978; Takamatsu, Welage et al. 2002). Intraluminal contents and nerve activity have been found to influence Phase II activity. Increases in intraluminal contents increase the duration of Phase II activity and cholinergic nerves enhance Phase II activity (Takamatsu, Welage et al. 2002).

It has been suggested that one of the major purposes of the MMC is to clear unabsorbed contents from the stomach and small intestine into the large intestine in preparation for the next meal (Szurszewski 1969; Vantrappen, Janssens et al. 1977). The movement of contents in the small intestine is mostly attributable to Phase III. In radiological observations in humans, when a small amount of barium was injected into a jejunal segment that was in Phase III, it was propelled a distance of 25 to 35 cm with an estimated speed of 2.5 cm/s. When contrast agent was injected during phase I, it remained stationary. When injected during Phase II, a back and forth segmentary phenomena was observed with no significant net progression of the barium. Occasionally two or three consecutive contractions that occurred during phase II would progress the barium longer distances (Vantrappen, Janssens et al. 1977). The time to

clear contents from a specific region of the intestine is dependent on the time it takes Phase III to migrate to that region. In studies in dogs and sheep, major differences in intestinal transit times were observed depending on what phase of the MMC a bolus of phenol red was injected. When the bolus was injected before Phase III was present, relatively short transit times were observed. The longest transit times occurred when phenol red was injected during Phase I, after Phase III had already passed (Bueno, Fioramonti et al. 1975) (Figure 1-4).

Migrating Motor Complex Effects on Gastric Emptying

The emptying of stomach contents predominantly occurs in a pulsatile manner and is a well coordinated event between the stomach, pylorus, and duodenum. The coordination is especially apparent during Phase III of the MMC. When the antrum contracts during Phase III, the pyloric sphincter relaxes and the duodenal bulb briefly stops contractile activity to accept a bolus from the stomach. Once a bolus is emptied from the stomach the pyloric sphincter contracts preventing further flow of contents into the duodenum and Phase III contractile activity resumes in the duodenum (Figure 1-5).

Physical properties of the gastric contents such as volume, caloric content, viscosity, density, and particle size can influence gastric emptying rates. Major differences exist in the gastric emptying patterns of digestible solids and nonnutrient liquids. The emptying pattern of digestible solids is typically characterized by a lag time followed by a zero order decline. Nonnutrient liquids empty from the stomach more rapidly than solids and their emptying follows a first order process (Figure 1-6).

In addition to the physical properties of the gastric contents, the gastric emptying rate is influenced by gastrointestinal motility in the fasted state. In a study that investigated the human gastric emptying rate of 50 mL and 200 mL of water during different phases of the MMC, it was found that the gastric emptying of liquids can be greatly influenced by the different phases of the MMC (Oberle, Chen et al. 1990). The mean gastric emptying rate for 50 mL of water increased with increasing contractile activity. The gastric emptying half lives for 50 mL of water were 61 min, 17 min and 9 min for Phase I, Phase II and Late Phase II/Phase III, respectively. The gastric emptying lag time for 50 mL of water also depended on the phases of the MMC and decreased with increasing contractile activity. The gastric emptying lag times for 50 mL of water were 19 min, 7.6 min, and 4 min for Phase I, Phase II and Late Phase II/Phase III, respectively. The gastric emptying of 200 mL of water was influenced differently by the phases of the MMC than 50 mL of water. During Phase I and Phase II the gastric emptying rates were found not to be statistically different from each other. The gastric emptying half lives for 200 mL of water were 14 min, 10 min, and 5 min for Phase I, Phase II and Late Phase II/Phase III, respectively. The gastric emptying lag times for 200 mL of water were 7 min, 4 min, and 2 min for Phase I, Phase II and Late Phase II/Phase III, respectively. The results of the study suggest that the gastric emptying of small volumes of liquid are more sensitive to stomach motility changes than larger volumes of liquid. However, both 50 mL and 200 mL of liquid had significantly increased rates of gastric emptying during Late Phase II/Phase III activity.

The MMC patterns in the stomach and duodenum are closely related. In a study that observed 109 MMC cycles in the stomach and duodenum of five dogs, it was

observed that in all cases that the same recurrent cyclic pattern of action potential activity was seen in both the antrum and duodenum (Code and Marlett 1975). Furthermore, the Phase III activity in the antrum and duodenum ended simultaneously for 14% of the cycles and within 3 minutes of each other for the remainder, which demonstrated a near simultaneous relationship in the MMC patterns between the antrum and duodenum.

Carbamazepine

Carbamazepine (Tegretol, dibenz [b,f] azepine-5-carboxamide) (Figure 1-7(a)) is a drug indicated for the treatment of epilepsy and trigeminal neuralgia. It has a molecular weight of 236.28. Four anhydrous polymorphs of carbamazepine have been identified. These include triclinic CBZ(I), trigonal CBZ(II), monoclinic CBZ(III) and a second anhydrous monoclinic form, CBZ(IV). In aqueous environments, carbamazepine transforms from the anhydrous polymorphs to a dihydrated form, CBZ(D) (Kaneniwa, Ichikawa et al. 1987; Kobayashi, Ito et al. 2000; Murphy, Rodriguez-Cintron et al. 2002). The marketed form of carbamazepine is CBZ(III).

Nicotinamide

Nicotinamide (3-pyridine carboxamide) (Figure 1-7(b)), is one of the water-soluble vitamin B-complex vitamins. More specifically, nicotinamide is the amide form of vitamin B3 also known as niacinamide. It has a molecular weight of 122.12. Nicotinamide (NCT) is used to prevent and treat niacin deficiency and has low toxicity.

Nicotinamide has been used to solubililize many poor aqueous soluble drugs. The mechanism of solubility enhancement has been reported to be due to stacking

complexation between drug and nicotinamide and not cosolvency or micellar mechanisms (Sanghvi, Evans et al. 2007).

Carbamazepine:Nicotinamide Cocrystal

A supramolecular design strategy was used to create 13 cocrystals with carbamazepine including carbamazepine:nicotinamide cocrystal (CBZ:NCT). The formation of CBZ:NCT uses a homosynthon approach where carbamazepine dimers with the carboxamide moiety take advantage of additional electron donors and acceptors to interact with nicotinamide molecules (Fleischman, Kuduva et al. 2003). As a result of the interactions, a hydrogen-bonded network forms (Figure 1-8).

Research Objectives

The use of mathematical modeling methods to aid the development of potential drugs has been increasing. Mathematical models are especially beneficial for providing human estimates of oral absorption, pharmacokinetics, and pharmacodynamics for new drug candidates, since the drug candidates can not be dosed in humans without extensive animal experiments showing reasonable assurances of safety. Realistic estimates of the rate and extent of human oral drug absorption by mathematical modeling methods require that the major factors affecting drug absorption by this route are accounted for. Therefore, the research objectives for this dissertation are:

1. To develop an oral absorption model that takes into account pulsatile gastric emptying and the effects of the migrating motor complex on drug transit time through the small intestine and gastric emptying.

2. To incorporate the absorption rate estimated by oral absorption model into a compartmental pharmacokinetic model to simulate plasma concentration-time profiles.

3. To simulate the effect of gastric emptying on the maximum concentration (C_{max}) of plasma concentration-time profiles for BCS Class I drugs.

4. To simulate oral drug absorption variability due to dosing at different phases of the migrating motor complex (MMC).

5. To simulate discontinuous absorption sites along the intestine and dosing at different phases of the MMC to explain the absence and presence of double peaks in oral ranitidine plasma-concentration-time profiles.

6. To use mathematically constructed phase solubility diagrams to guide an investigation of the validity of using the stoichiometric solubility to estimate the relative dissolution rates between CBZ:NCT and CBZ(III) in three organic solvents.

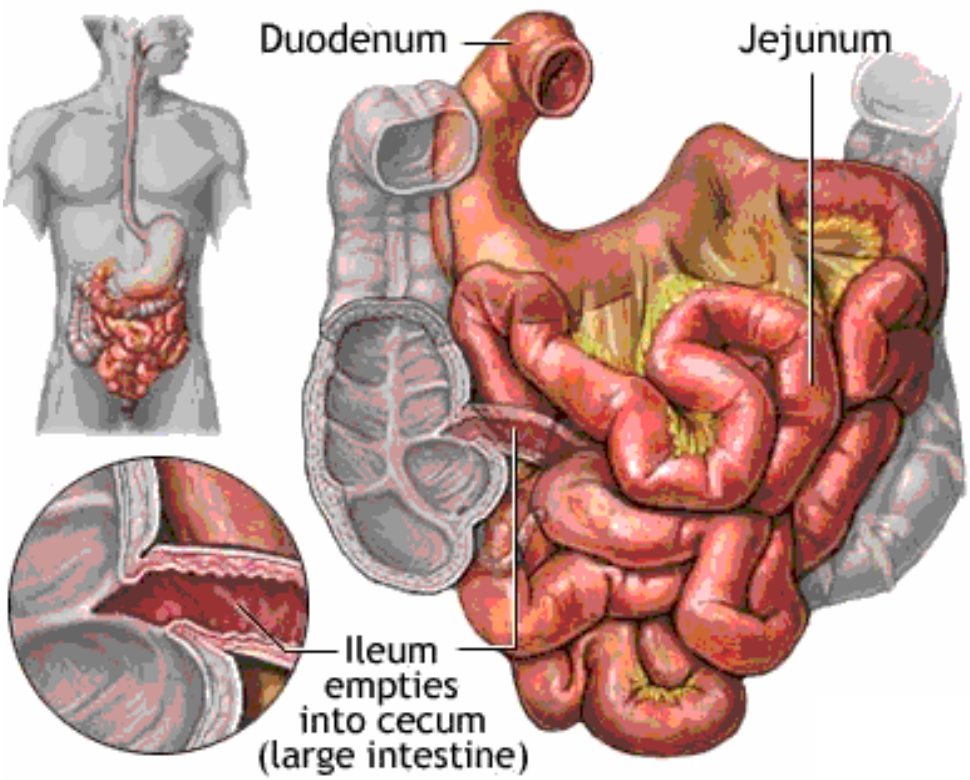

Figure 1-1 Diagram of small intestine

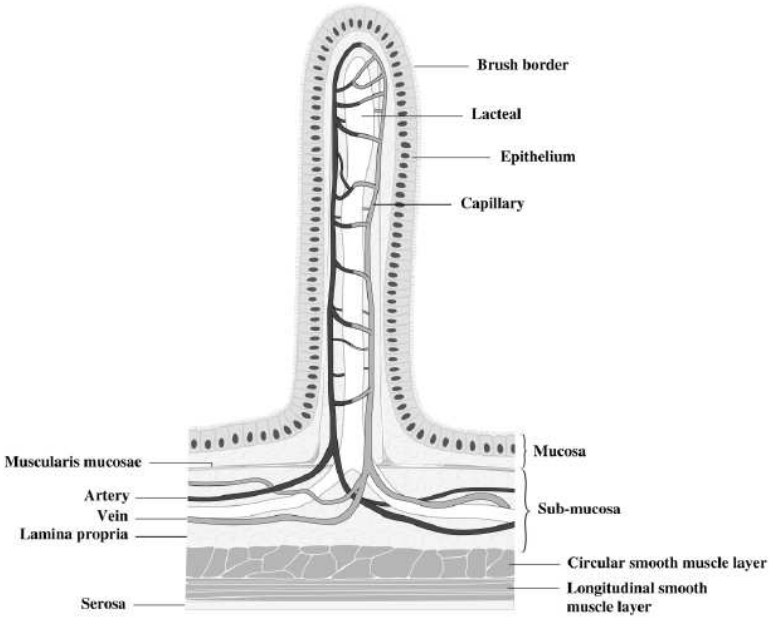

a)

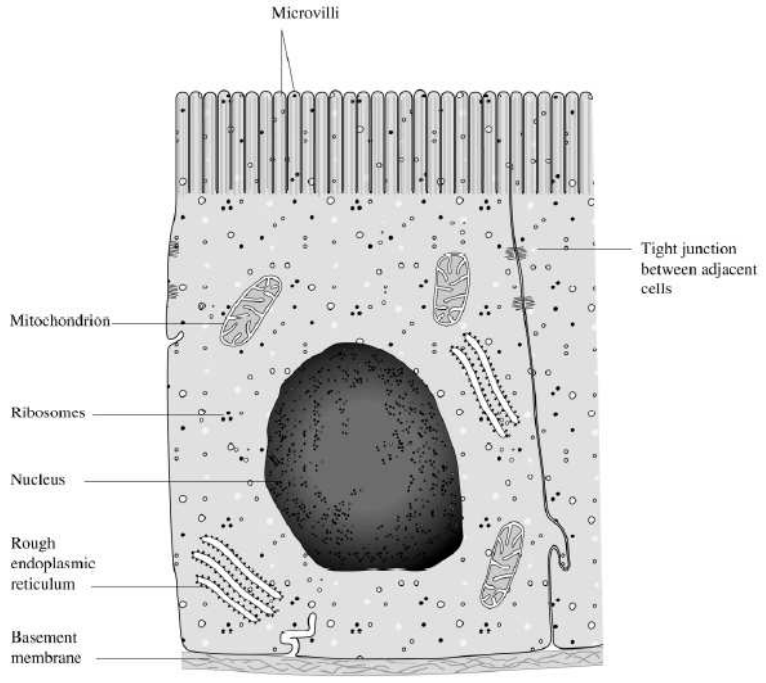

b)

Figure 1-2 Diagram of (a) villus and (b) microvilli (DeSesso and Jacobson 2001)

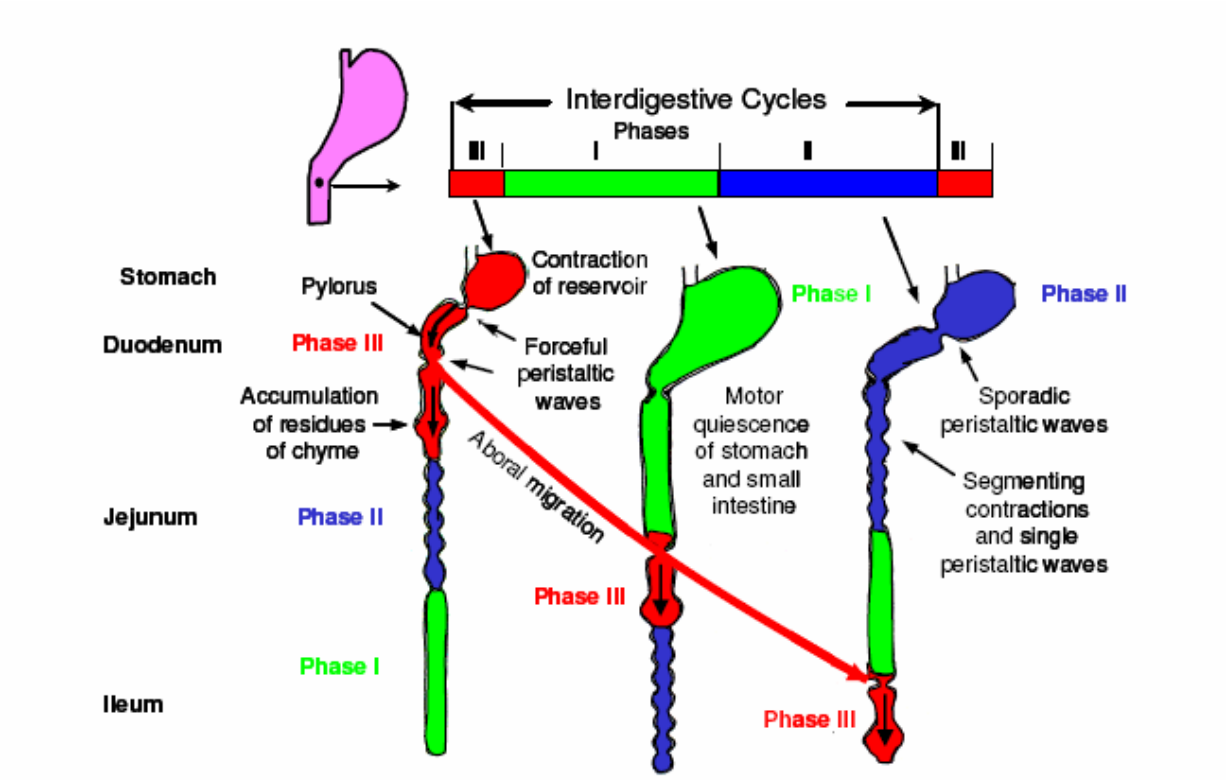

Figure 1-3 Aboral migration of phase III (Ehrlein and Schemann)

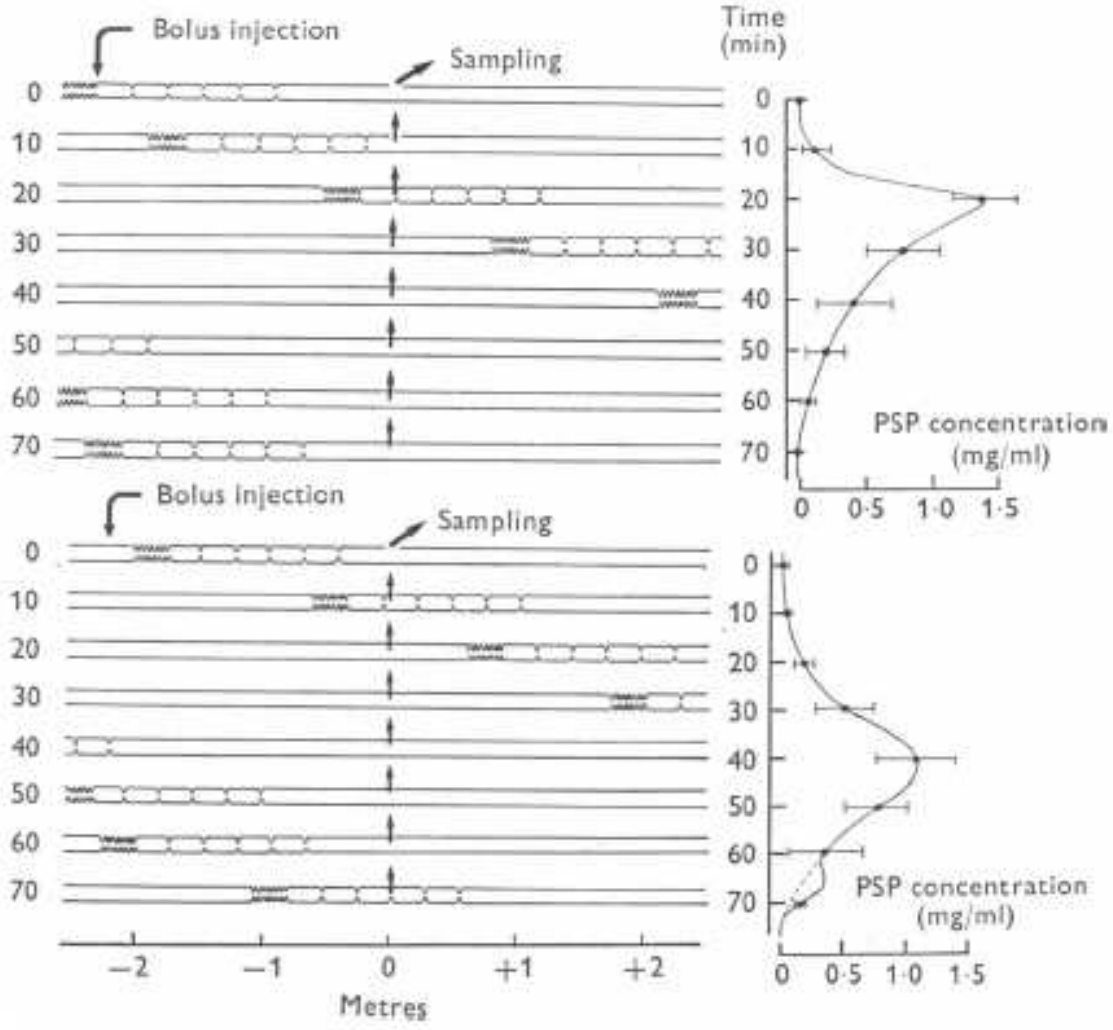

Figure 1-4 Timing of bolus injection and intestinal transit (Bueno, Fioramonti et al. 1975)

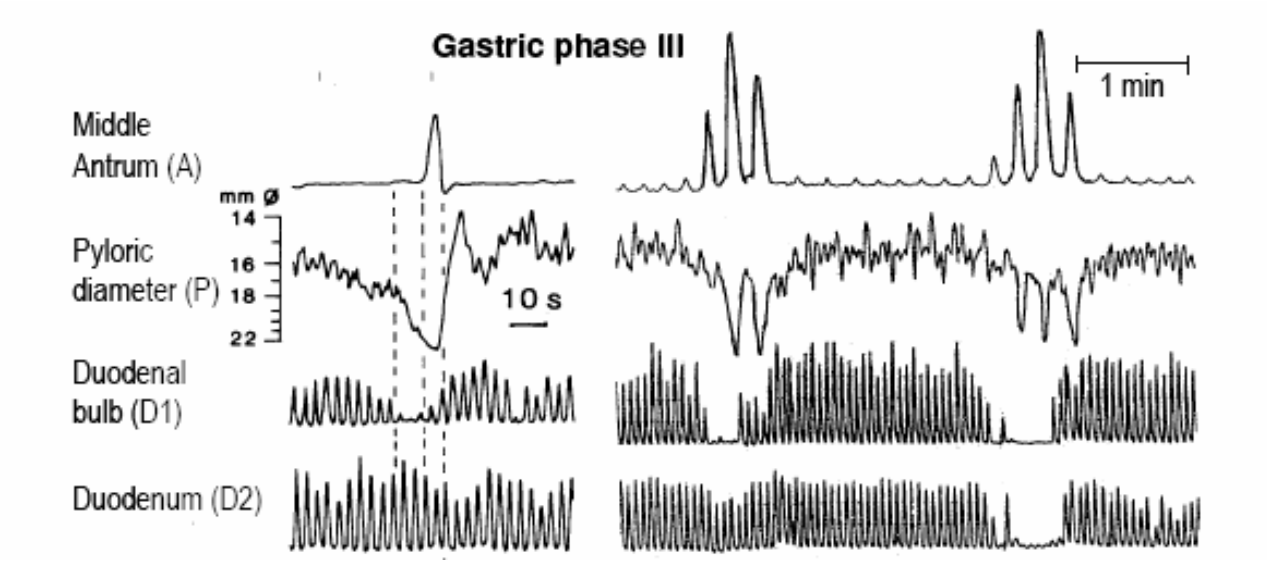

Figure 1-5 Contractile coordination between antrum and duodenum (Ehrlein and Schemann)

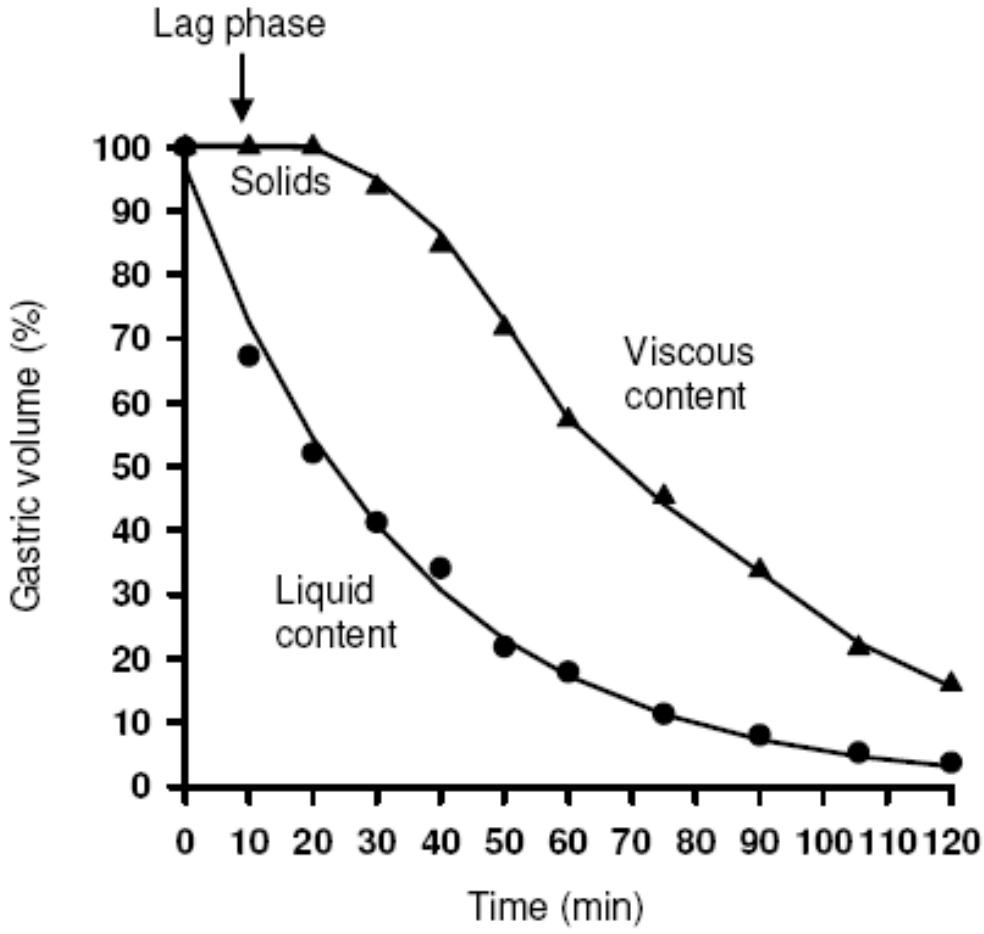

Figure 1-6 Gastric emptying rates for non-nutrient liquids and solids (Ehrlein and Schemann)

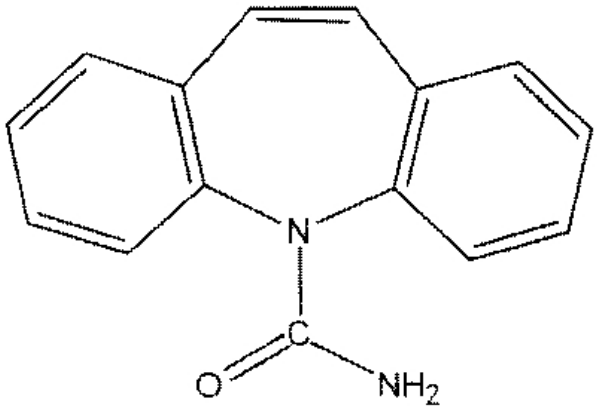

(a)

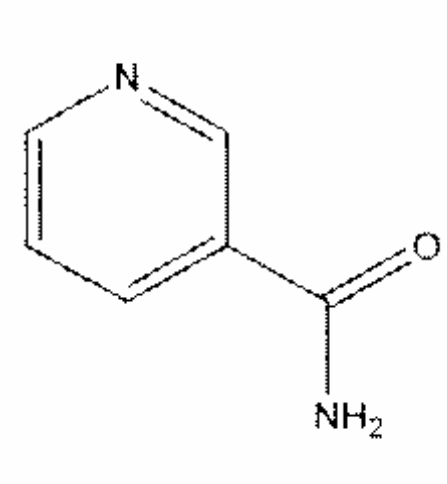

(b)

Figure 1-7 Chemical structures of (a) carbamazepine and (b) nicotinamide

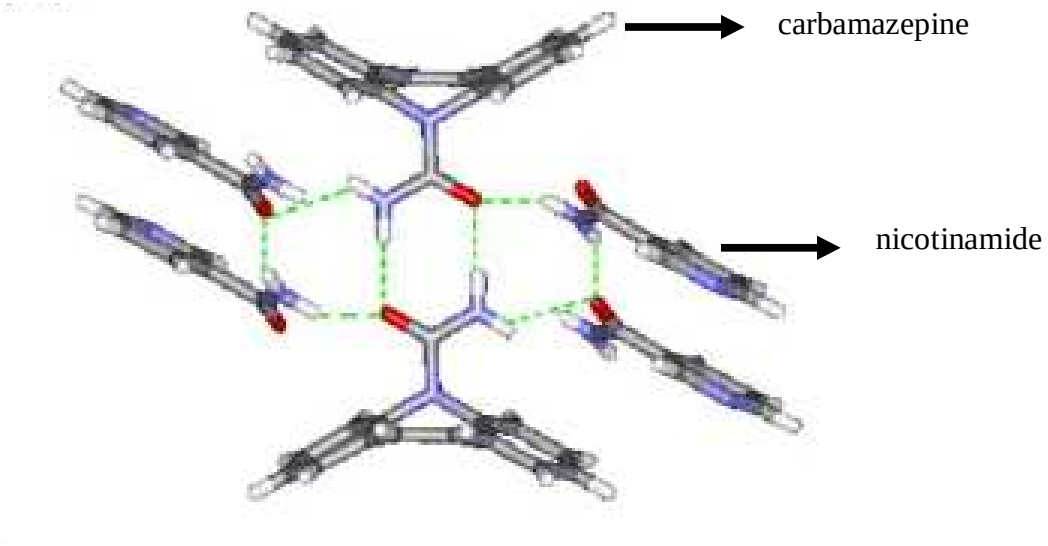

Figure 1-8 Molecular assembly of CBZ:NCT (Fleischman, Kuduva et al. 2003)

References

A.D.A.M. Medical Encyclopedia [Internet] (2007). Small Intestine. Atlanta (GA), A.D.A.M. Inc. **2007**.

Bueno, L., et al. (1975). "Rate of Flow of Digesta and Electrical-Activity of Small-Intestine in Dogs and Sheep." Journal of Physiology-London **249**(1): 69-85.

Childs, S. L., et al. (2004). "Crystal engineering approach to forming cocrystals of amine hydrochlorides with organic acids. Molecular complexes of fluoxetine hydrochloride with benzoic, succinic, and fumaric acids." Journal of the American Chemical Society **126**(41): 13335-13342.

Code, C. F. and J. A. Marlett (1975). "Interdigestive Myo-Electric Complex of Stomach and Small Bowel of Dogs." Journal of Physiology-London **246**(2): 289-309.

DeSesso, J. M. and C. F. Jacobson (2001). "Anatomical and physiological parameters affecting gastrointestinal absorption in humans and rats." Food and Chemical Toxicology **39**(3): 209-228.

Ehrlein, H. J. and M. Schemann Gastrointestinal Motility. **2007:** 1-26.

Fleckenstein, P. (1978). "Migrating Electrical Spike Activity in Fasting Human Small-Intestine." American Journal of Digestive Diseases **23**(9): 769-775.

Fleckenstein, P. and A. Oigaard (1978). "Electrical Spike Activity in Human Small-Intestine - Multiple Electrode Study of Fasting Diurnal-Variations." American Journal of Digestive Diseases **23**(9): 776-780.

Fleischman, S. G., et al. (2003). "Crystal engineering of the composition of pharmaceutical phases: Multiple-component crystalline solids involving carbamazepine." Crystal Growth & Design **3**(6): 909-919.

Kaneniwa, N., et al. (1987). "Dissolution Behavior of Carbamazepine Polymorphs." Yakugaku Zasshi-Journal of the Pharmaceutical Society of Japan **107**(10): 808-813.

Kerlin, P. and S. Phillips (1982). "Variability of Motility of the Ileum and Jejunum in Healthy Humans." Gastroenterology **82**(4): 694-700.

Kobayashi, Y., et al. (2000). "Physicochemical properties and bioavailability of carbamazepine polymorphs and dihydrate." International Journal of Pharmaceutics **193**(2): 137-146.

McNamara, D. P., et al. (2006). "Use of a glutaric acid cocrystal to improve oral bioavailability of a low solubility API." Pharmaceutical Research **23**(8): 1888-1897.

Murphy, D., et al. (2002). "Solution-mediated phase transformation of anhydrous to dihydrate carbamazepine and the effect of lattice disorder." International Journal of Pharmaceutics **246**(1-2): 121-134.

Oberle, R. L., et al. (1990). "The Influence of the Interdigestive Migrating Myoelectric Complex on the Gastric-Emptying of Liquids." Gastroenterology **99**(5): 1275-1282.

Remenar, J. F., et al. (2003). "Crystal engineering of novel cocrystals of a triazole drug with 1,4-dicarboxylic acids." Journal of the American Chemical Society **125**(28): 8456-8457.

Sanghvi, R., et al. (2007). "Stacking complexation by nicotinamide: A useful way of enhancing drug solubility." International Journal of Pharmaceutics **336**(1): 35-41.

Szurszewski, J. H. (1969). "A Migrating Electric Complex of Canine Small Intestine." American Journal of Physiology **217**(6): 1757-1763.

Takamatsu, N., et al. (2002). "Variability in cimetidine absorption and plasma double peaks following oral administration in the fasted state in humans: correlation with antral gastric motility (vol 53, pg 37, 2002)." European Journal of Pharmaceutics and Biopharmaceutics **54**(2): 255-255.

Ungell, A. L., et al. (1998). "Membrane transport of drugs in different regions of the intestinal tract of the rat." Journal of Pharmaceutical Sciences **87**(3): 360-366.

Vantrappen, G., et al. (1977). "Interdigestive Motor Complex of Normal Subjects and Patients with Bacterial Overgrowth of Small-Intestine." Journal of Clinical Investigation **59**(6): 1158-1166.

Yu, L. X., et al. (1996). "Transport approaches to the biopharmaceutical design of oral drug delivery systems: Prediction of intestinal absorption." Advanced Drug Delivery Reviews **19**(3): 359-376.

Chapter II

Development of the Pulsatile Emptying Transit (PET) Oral Absorption Model

Introduction

Absorption is one of the processes that influence the pharmacokinetics of a drug. Other processes include distribution, metabolism, and excretion. Pharmacokinetic models have traditionally used first order absorption assumptions to describe the oral absorption rate of drugs from the gastrointestinal tract. However, oral drug absorption is a complex process affected by physicochemical properties of the drug, drug formulation, and gastrointestinal physiology factors. The absorption rates of many drugs are not well described by a first order absorption rate (Zhou 2003). Consequentially, erroneous predictions for dosage regimens may occur when first order oral absorption assumptions are made in pharmacokinetic modeling. Developing absorption models that can more accurately represent the *in vivo* rate and extent of absorption from the gastrointestinal tract can improve dosage regimen predictions for orally delivered drugs.

The development of oral absorption modeling has evolved over the past half century and the models can generally be classified into three categories: quasi-equilibrium, steady state, and dynamic models (Yu, Lipka et al. 1996). The pH-partition hypothesis and absorption potential are examples of quasi-equilibrium models and are useful in forming drug absorption trends. According to the pH-partition hypothesis, only unionized forms of compounds can be passively absorbed across lipid membrane so the

disassociation constant is an important characteristic that determines absorption across a membrane (Schanker, Tocco et al. 1958). Although exceptions to the pH-partition hypothesis have been found, it is still a useful concept to consider when evaluating the absorption capability of a compound.

The absorption potential model built upon concepts of the pH-partition hypothesis to take into account the effects of solubility and dose on drug absorption (Dressman, Amidon et al. 1985) According to the absorption potential model the following equation was proposed:

$$AP = \log\left(\frac{PF_{un}}{Do}\right) \quad (2.1)$$

where AP is the absorption potential, P is the partition coefficient, F_{un} is the fraction unionized at pH 6.5 and Do is a dimensionless number known as the dose number and is defined as the ratio of dose concentration to drug solubility:

$$Do = \frac{D/V_o}{C_s} \quad (2.2)$$

where D is the dose, V_o is the volume of water taken with the dose (250 mL) and C_s is the solubility of drug in the gastrointestinal tract fluid. When several drugs that varied widely in their physicochemical properties were evaluated to test the ability of the absorption potential concept to predict fraction of absorbed, it was found that the absorption potential strongly correlated with fraction absorbed (Dressman, Amidon et al. 1985).

While quasi-equilibrium models have been useful in qualitatively understanding drug absorption, quantitative absorption models that took into account gastrointestinal physiology needed to be developed to estimate the fraction of dose absorbed. Two

approaches to estimate the fraction of drug absorbed include the steady state macroscopic mass balance approach and microscopic mass balance approach. In the macroscopic mass balance approach, the small intestine is assumed to be a cylindrical tube where R is the radius and L is the length of the tube and a solution of drug flows through the intestine. Applying mass balance principles, the difference in amount of drug that enters the intestine and leaves the intestine is equal to the amount of drug absorbed, which is described by the following equation (Sinko, Leesman et al. 1991):

$$-\frac{dM}{dt} = Q\cdot(C_o - C_{out}) = 2\pi RP_{eff}\int_0^L Cdz \qquad (2.3)$$

where M is the amount of drug, Q is the volumetric flow rate, C_o and C_{out} are the inlet and outlet concentrations, respectively. Under the steady state assumption the fraction of dose absorbed is given by the following equation:

$$F_a = 1 - \frac{C_{out}}{C_o} = 2An\int_0^1 C^* dz^* \qquad (2.4)$$

where C^* and z^* are dimensionless concentration and position, respectively.

$$C^* = \frac{C}{C_o}, \qquad z^* = \frac{z}{L} \qquad (2.5)$$

An is the dimensionless absorption number and represents the ratio between the intestinal residence time and effective absorption rate constant (Amidon, Lennernas et al. 1995):

$$An = \frac{\pi RLPeff}{Q} \qquad (2.6)$$

The macroscopic balance approach is useful for drugs that are already in solution form or have a high solubility. However to include drug dissolution effects on absorption, the microscopic balance approach was developed. The microscopic balance approach was

used to estimate the fraction of drug absorbed for suspensions of poorly soluble drugs (Oh, Curl et al. 1993). Similar to the macroscopic balance approach, the microscopic balance approach assumes a steady state condition and the small intestine is assumed to be a cylindrical tube with radius = R and length = L. A mass balance on the solid drug leads to the following equation which describes the change in particle radius with respect to intestinal position:

$$\frac{dr_p}{dz} = -\frac{D\pi\pi^2}{Q\rho} \cdot \frac{(C_s - C_L)}{r_p} \qquad (2.7)$$

From a mass balance on the solution phase, the following equation is derived to describe the change in intestinal lumen concentration (C_L) with respect to intestinal position:

$$\frac{dC_L}{dz} = \frac{D \cdot \left(N_o / V_o\right) \cdot 4\pi^2 R^2}{Q} \cdot r_p (C_s - C_L) - \frac{Peff \cdot 2\pi R}{Q} \cdot C_L \qquad (2.8)$$

where r_p is the particle radius, ρ is the drug density, N_o/V_o is the particle number density, and D is the drug diffusion coefficient. Dimensionless forms of the equations were derived by letting:

$$z^* = \frac{z}{L}, \qquad r^* = \frac{r_p}{r_o}, \qquad C^* = \frac{C_L}{C_s} \qquad (2.9)$$

The dimensionless forms of the equations are:

$$\frac{dr^*}{dz^*} = -\frac{Dn}{3} \cdot \frac{1 - C^*}{r^*} \qquad (2.10)$$

$$\frac{dC^*}{dz^*} = Dn \cdot Do \cdot r^* (1 - C^*) - 2\,An \cdot C^* \qquad (2.11)$$

where, the dose number, Do, and absorption number, An, were previously defined in equations 2.2 and 2.6, respectively. Dn is another dimensionless parameter known as the dissolution number and it is the ratio of the intestinal residence time to the dissolution

time of a particle with an initial radius of r_o. From mass balance of drug in the small intestine, the fraction of dose absorbed is given by the following equation:

$$F_a = 1 - [r^*(1)]^3 - \frac{C^*(1)}{Do} \qquad (2.12)$$

where $r^*(1)$ and $C^*(1)$ are the dimensionless particle radius and dimensionless intestinal concentration at the end of the intestine. A typical three-dimensional plot of the fraction of dose absorbed as a function of dose number and dissolution number that can be attained with the microscopic balance approach is shown in Figure 2-4. The plot shows for a well absorbed compound (An = 1) at dose number and dissolution number close to 1 the fraction of dose absorbed changes rapidly. Since the macroscopic and microscopic balance approaches were derived with respect to intestinal position rather than time, the outputs of these models were not incorporated into time dependent pharmacokinetic models. As a result, only an estimate of extent of absorption was outputted by these models.

Dispersion and compartmental models fall under the category of dynamic models because they output both the rate and extent of absorption. A major advantage of dynamic models over previously discussed models is that absorption rates are simulated and can be inputted into traditional pharmacokinetic models to simulate plasma concentration-time profiles. One of the first approaches used to simulate time dependent absorption processes was a dispersion model developed by Ni, Ho et al. According to the model, the absorption rate can be determined by solving the following equation:

$$\frac{\partial C}{\partial t} = \alpha \frac{\partial^2 C}{\partial z^2} - \nu \frac{\partial C}{\partial z} - K_a C \qquad (2.13)$$

where C is the drug concentration, z is the axial distance from the stomach, K_a is the absorption rate constant, and α is the diffusion coefficient for longitudinal spreading (Ni, Ho et al. 1980). Analytical solutions for simple cases of the dispersion model have been found, however the solutions are complex.

The development of compartmental models offers an alternative way to model dynamic oral absorption. The compartmental modeling approach involves using one or more series of mixing tanks to represent the gastrointestinal tract. A number of absorption models have been developed using the compartmental approach to simulate a wide range of pharmaceutical scenarios(Goodacre and Murray 1981; Dressman, Fleisher et al. 1984) (Dressman and Fleisher 1986; Oberle and Amidon 1987; Hintz and Johnson 1989; Luner and Amidon 1993). It was not until the compartmental and transit model (CAT) was developed that transit of drug through the intestine and the optimal number of compartments to describe that transit was considered in the development of compartmental oral absorption models. To determine the number of mixing tanks that would best describe drug transit through the small intestine, data that measured 400 small intestine transit times was analyzed. It was determined that seven mixing tanks best described the transit of contents through the small intestine (Yu and Amidon 1998). The absorption rates estimated by the CAT model were incorporated into a pharmacokinetic model that predicted the plasma concentration-time profile of cefatrizine well (Figure 2-5). Numerous extensions to the CAT model have been made and the new model is currently called the advanced CAT (ACAT) model. The ability of the ACAT program to simulate plasma concentration-time profiles of several drugs has been demonstrated (Agoram, Woltosz et al. 2001). The commercial success of the ACAT model has

demonstrated the value of oral absorption modeling to the pharmaceutical industry. However, oral absorption models continue to evolve and additional uses of these models other than just the estimation of rate and extent of absorption can significantly benefit the drug development process and improve the therapeutic outcomes of patients.

In addition to estimating the rate and extent of oral absorption, the variability associated with these estimates is important to determine when decisions about developing a dosage regimen need to be made, especially for drugs with narrow therapeutic indexes. Dynamic oral absorption models that can incorporate sources of variability and quantify their effects therefore may be of great value in delineating variability in plasma concentration-time profiles attributable to oral drug absorption processes. They may also help elucidate how drug physicochemical factors or drug formulation factors can be altered to maintain safe and effective plasma drug concentrations within a reasonable amount of confidence.

A source of variability that can affect the rate and extent of oral absorption during the fasted state is the migrating motor complex (MMC). The MMC is a rhythmically recurring cycle of contractile activity that occurs in the stomach and small intestine (Code and Marlett 1975). It consists of three phases of contractile activity. Phase I is a quiescent phase. Phase II has irregular and infrequent contractions. Phase III has a burst of regular frequent contractions and is commonly referred to as the "housekeeper wave" because of its ability to propel remaining stomach and intestinal contents aborally. The housekeeper function of the MMC affects the gastric emptying rate and small intestinal transit time of drugs (Bueno, Fioramonti et al. 1975; Oberle, Chen et al. 1990). Variability in oral absorption due to the MMC can occur due to drug being taken at

different phases of the MMC and different MMC cycle lengths between individuals. A new type of dynamic absorption model was developed based on mass balance and stochastic modeling concepts that incorporate the effects of the migrating motor complex to estimate the rate, extent, and variability of oral drug absorption during the fasted state. The purpose of this report is to describe the development of the program.

Theoretical

In the Pulsatile Emptying Transit (PET) model, the GI tract is described by the stomach, duodenum, jejunum, and ileum. Absorption rates obtained from the PET model are inputted into a two compartment pharmacokinetic model to obtain a plasma concentration time profile. The first compartment represents the central compartment while the second compartment represents a peripheral compartment. Figure 2-6 shows a schematic of the model.

Initially the dose of drug and 250 mL of water is delivered to the stomach. Drug empties from the stomach in a pulsatile manner. The intestinal transit of the pulses is directly related to the contractile activity. Drug pulses are propelled forward only during Late Phase II/Phase III of the MMC. Thus the transit time of the pulses is related to the dosing time relative to the time until the end of the next Phase III (TTPIII) and to the time it takes for Phase III to migrate to the distal ileum.

The following assumptions are made:

1. No absorption takes place in the stomach
2. No absorption takes place in the colon
3. The volume of each pulse is constant

4. Phase III activity is always present somewhere in the stomach or small intestine

5. The drug in each pulse is well mixed

TTPIII is a parameter that can have a value between zero and the MMC cycle time. The MMC cycle length used was 150 minutes.

Physiological:

In the model, the migrating motor complex consists of three phases (Phase I, Phase II, and Phase III). The lengths of Phase I, Phase II, and Phase III in the stomach used in the model were 117 minutes, 18 minutes, and 15 minutes, respectively.

To describe the motility of the MMC in the small intestine, available literature on the propagation velocity of Phase III was found.

Pulsatile Gastric Emptying:

Gastric emptying is predominantly a pulsatile process (Malbert, Mathis et al. 1994; Anvari, Dent et al. 1995). In the model, pulses of liquid, containing solid and dissolved drug, empty from the stomach into the duodenum every 30 seconds. A total of 75 pulses empty into the small intestine. The first pulse empties from the stomach into the intestine after an initial time lag and the last pulse empties into the intestine 37 minutes later. Each pulse is assumed to be well-mixed and the pulses do not mix with other pulses inside the intestine.

The gastric emptying of liquids is assumed to be a first order process. The amount of drug and volume of liquid in each pulse is determined from:

$$\textit{Drug amount in pulse} = M_o e^{-k_e t}\left(1 - e^{-k_e i}\right) \quad (2.14)$$

$$\textit{Liquid volume in pulse} = V_o e^{-k_e t}\left(1 - e^{-k_e i}\right) \quad (2.15)$$

where M_o = dose and V_o = volume of water taken with the dose, k_e = gastric emptying rate, t = time, i = time interval between pulses

The value of the first order gastric emptying rate constant for 200 mL of water was reported in the literature and depends on the phase of the migrating motor complex in the stomach (Oberle, Chen et al. 1990). During phase I, the lag time = 7 minutes and in early phase II, the lag time = 4 minutes. The gastric emptying rate, $k_e = 0.11\ min^{-1}$ for both phase I and II. The gastric half emptying time ($GE_{1/2}$) for phase I and phase 2 is 13.3 min and 10.3 min, respectively. During late phase II and phase III, the lag time = 2 minutes and $k_e = 0.236\ min^{-1}$ ($GE_{1/2}$ = 5 min).

Intestinal Residence Time:

In the model, the intestinal residence time of each pulse is dependant on the phase of the migrating motor complex in the duodenum at the time of gastric emptying. For example, a pulse that empties into the duodenum during phase I, spends time in the duodenum until the next Phase III pushes it into the jejunum and thus it has a longer intestinal residence time than a pulse that empties into the small intestine during phase III, which is immediately propelled to the jejunum once it enters the duodenum.

Dissolution profile:

The Weibull equation is often used to describe *in vitro* dissolution profiles. A modified version of the Weibull equation was used in the model. According to the Weibull equation, the amount of drug dissolved approaches the original amount of solid drug at an infinite time. However, the model assumes that drug can not continue to

dissolve once the solution is saturated. To take this into account, the Weibull equation was modified so that the dissolution rate decreases when the concentration approaches the solubility of the drug. The modified Weibull equation is given by:

$$M = M_{pulse}\left(1 - e^{-\frac{(t-tlag)^b}{A}}\right)\frac{(C_s - C_l)}{C_s} \quad (2.16)$$

where b = shape factor, A = time scale factor, tlag = lag time, C_s = the drug solubility, and C_l = the drug concentration in the intestinal lumen.

An advantage of using the Weibull equation is that different dissolution profile shapes can be simulated by adjusting the shape factor, time scale factor, and lag time. The effect of adjusting these parameters on the dissolution profile shape is shown in Figure 2-1, Figure 2-2, and Figure 2-3.

Dissolution rate:

Taking the derivative of the modified Weibull equation with respect to time gives the dissolution rate.

$$dissolution\ rate = M_{pulse} \cdot \frac{b(t - tlag)^{(b-1)}}{A} e^{-\frac{(t-tlag)^b}{A}} \frac{(C_s - C_L)}{C_s} \quad (2.17)$$

Absorption rate:

The absorption rate is determined by the product of the flux of the drug (j_w) and the absorption surface area (A).

$$absorption\ rate = j_w A = Peff \cdot C_L \cdot A = 2 \cdot Peff \cdot C_L \cdot \pi R L_p \quad (2.18)$$

Mass balance for each pulse:

A mass balance of drug in each pulse is given by:

$$\begin{pmatrix} Amount\ of\ drug \\ in\ pulse\ at\ time\ 0 \end{pmatrix} = \begin{pmatrix} Amount\ of\ solid \\ drug\ at\ time\ t \end{pmatrix} + \begin{pmatrix} Amount\ of\ drug \\ in\ solution\ at\ time\ t \end{pmatrix} + \begin{pmatrix} Amount\ of\ drug \\ absorbed\ at\ time\ t \end{pmatrix} \quad (2.19)$$

A mass balance of the solution phase in each pulse is given by:

$$\begin{pmatrix} rate\ of\ mass\ accumulation \\ at\ time\ t \end{pmatrix} = \begin{pmatrix} rate\ of\ mass\ dissolved \\ at\ time\ t \end{pmatrix} - \begin{pmatrix} rate\ of\ mass\ absorbed \\ at\ time\ t \end{pmatrix} \quad (2.20)$$

$$M\big|_{t} - M\big|_{t+dt} + M_{pulse} \cdot \frac{b(t-tlag)^{(b-1)}}{A} e^{-\frac{(t-tlag)^{b}}{A}} \frac{(C_s - C_L)}{C_s} dt - 2 \cdot Peff \cdot C_L \cdot \pi RL_p dt = 0 \quad (2.21)$$

$$\frac{dM}{dt} = M_{pulse} \cdot \frac{b(t-tlag)^{(b-1)}}{A} e^{-\frac{(t-tlag)^{b}}{A}} \frac{(C_s - C_L)}{C_s} - 2 \cdot Peff \cdot C_L \cdot \pi RL_p \quad (2.22)$$

$$\frac{1}{V_{pulse}} \frac{dM}{dt} = \frac{M_{pulse}}{V_{pulse}} \cdot \frac{b(t-tlag)^{(b-1)}}{A} e^{-\frac{(t-tlag)^{b}}{A}} \frac{(C_s - C_L)}{C_s} - \frac{2 \cdot Peff \cdot C_L \cdot \pi RL_p}{V_{pulse}} \quad (2.23)$$

$$\frac{dC_L}{dt} = \frac{M_{pulse}}{V_{pulse}} \cdot \frac{b(t-tlag)^{(b-1)}}{A} e^{-\frac{(t-tlag)^{b}}{A}} \frac{(C_s - C_L)}{C_s} - \frac{2 \cdot Peff \cdot C_L}{R} \quad (2.24)$$

Fraction Dose Absorbed:

The fraction dose absorbed is obtained by summing the amount of drug absorbed from each pulse and dividing by the dose.

$$Fabs = \frac{\sum_{n=1}^{75} (\text{amount of drug absorbed pulse}_n)}{Dose} \quad (2.25)$$

Methods

Method of Solution

The differential equations describing the model were solved numerically using a Runge-Kutta-Fehlberg routine that was programmed into Visual Basic in Excel.

Model Parameter Values

The values of the parameters inputted into the PET model and 2-compartment PK are listed in Appendix A.

Results and Discussion

A simulated amount of drug in solution-time profile at different regions of the gastrointestinal tract is presented in Figure 2-7a. The dose was given 80 minutes prior to the end of phase III (TTPIII) in the stomach. Pulses of drug empty into the duodenum from the stomach and the drug remaining in the stomach dissolves. The model assumes that no absorption takes place in the stomach. The amount of drug in solution in the stomach is a result of drug dissolving in the stomach and drug gastric emptying. Initially the amount of drug in solution increases in the stomach due to drug dissolution occurring in the stomach and little gastric emptying. The amount of drug in solution decreases in the stomach as more of the drug in solution is emptied into the duodenum. In the duodenum, both solid drug and drug in solution empty in pulses from the stomach, solid drug dissolves, and drug in solution is absorbed. The increase in amount of drug in solution in the duodenum is a result of dissolution in the duodenum and gastric emptying. When the amount of drug absorbed from the duodenum exceeds the sum of the amount of

drug dissolving and drug in solution emptying from the stomach, the amount of drug in solution in the duodenum decreases. When phase III of the MMC reaches the duodenum, all of the drug in the duodenum is propelled to the jejunum. In the jejunum, when the amount of drug absorbed exceeds the amount of drug dissolving, the amount of drug in solution decreases. When phase III of the MMC reaches the jejunum, all drug in the jejunum is propelled to the ileum. In the ileum, when the amount of drug absorbed exceeds the amount of drug dissolving, the amount of drug in solution decreases.

Figure 2-7b shows that dosing 18 minutes prior to the end of phase III leads to a different amount of drug in solution-time profile than Figure 2-7a. During phase III, the gastric emptying rate of 200 mL of water is approximately twice the emptying rate during phase I and phase II. Therefore, not as much drug can dissolve in the stomach when dosed near or during phase III. In addition, when drug is emptied from the stomach during phase III, the drug spends very little time in the duodenum because after a pulse of drug empties from the stomach, phase III contractions in the duodenum immediately propel the pulse to the jejunum.

Figure 2-8 shows a plot of dissolution rate (t85) vs. TTPIII vs. C_{max} for a drug with a high solubility (33 mg/mL) and high permeability (0.1 cm/min). The drug is classified as Class I under the Biopharmaceutics Classification System (BCS). The plot shows that for drugs with high dissolution rates (85% of the dose dissolves within 15 minutes) a significantly higher C_{max} (> 10%) is obtained if drug is dosed near or during phase III.

Figure 2-9 shows a plot of effective permeability (P_{eff}) vs. TTPIII vs. C_{max} for a drug in solution. The plot shows that dosing this drug near or during phase III results in a

significantly higher C_{max} when the effective permeability of the drug is higher than 0.04 cm/minute, approximately the effective permeability of naproxen in the human jejunum.

Together, Figures 2-8 and 2-9 suggest that the rates of absorption of BCS Class I compounds are not all rate limited by gastric emptying. Metoprolol is often used as a reference compound in the determination of whether a drug has high permeability or not. The effective permeability of metoprolol is 0.008 cm/min. In terms of dissolution, a drug that dissolves 85% within 15 minutes is considered to be a drug with a high dissolution rate. The majority of Class I drugs have effective permeabilities higher than metoprolol, but lower than naproxen and have a high dissolution rate. Simulations with the PET model suggest that absorption of these Class I drugs would not be rate limited by gastric emptying and C_{max} would not be greatly affected by dosing these drugs near orduring phase III.

Summary

The emptying of contents from the stomach in the fasted state is predominantly a pulsatile process that is influenced by the phase of the MMC. The MMC also affects the residence time of contents in the small intestine. An oral absorption model, the PET model, was developed to take into account these MMC effects. The PET model was coupled to a compartmental pharmacokinetic model to estimate plasma concentration-time profiles. Simulations with the PET model suggest that the maximum plasma concentration (C_{max}) of drugs with effective permeabilities less than 0.04 cm/min would not be significantly affected (< 10%) by the phase of the MMC in which the drug was dosed. Also, for drugs with dissolution rates where less than 85% of the dose dissolves

within 15 minutes, C_{max} is not significantly affected by the phase of the MMC in which the drug was dosed.

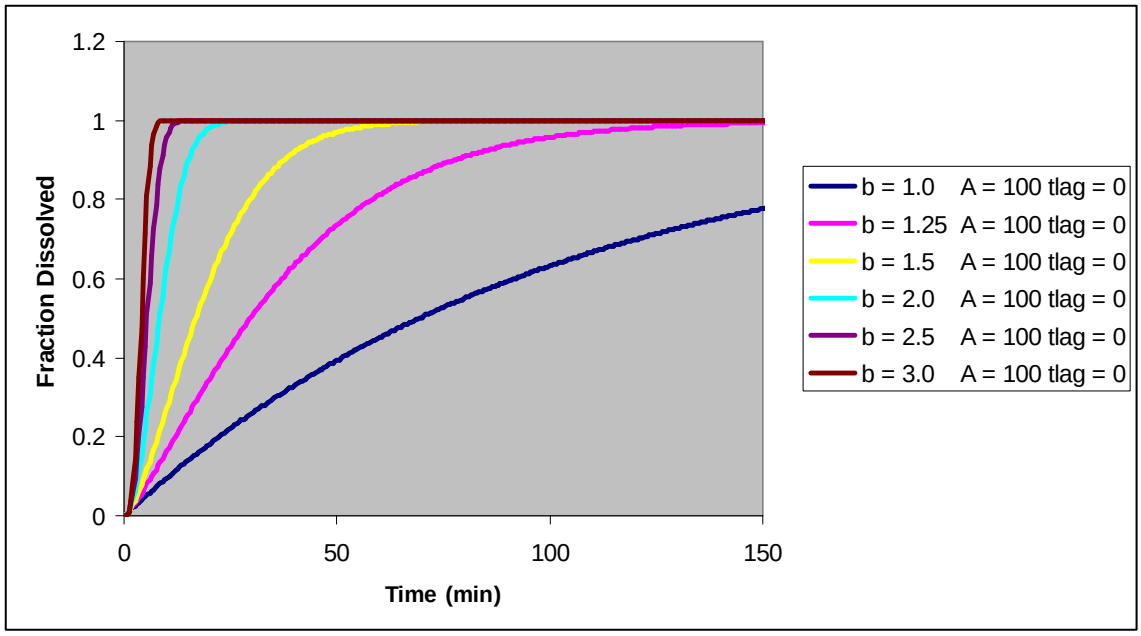

Figure 2-1 Weibull disolution varying shape factor (b).

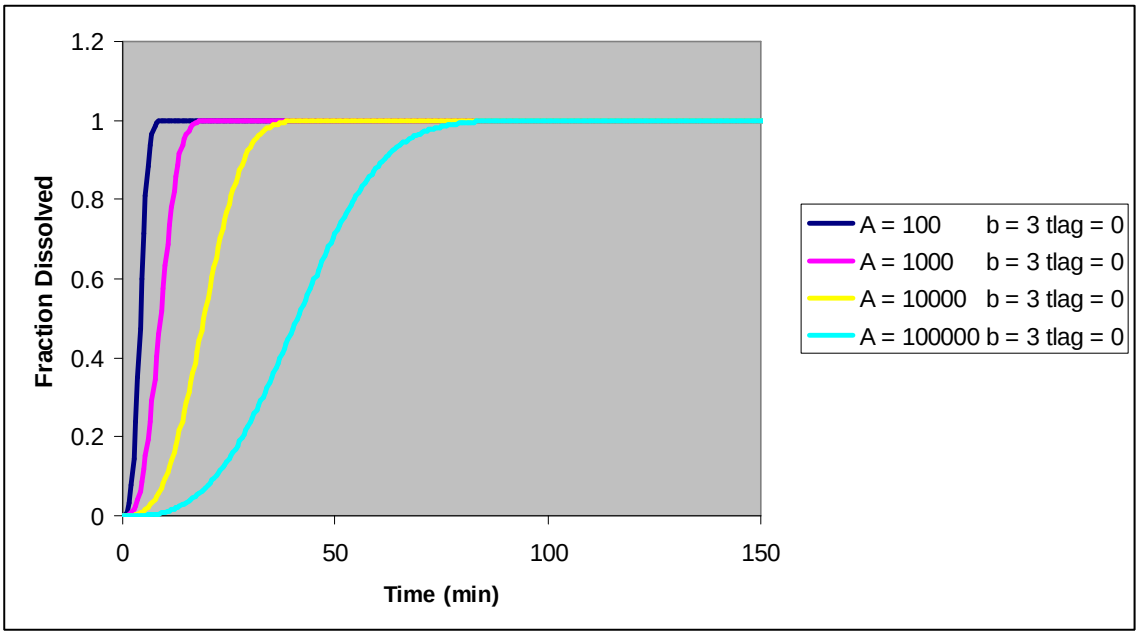

Figure 2-2 Weibull dissolution varying time scale factor (A).

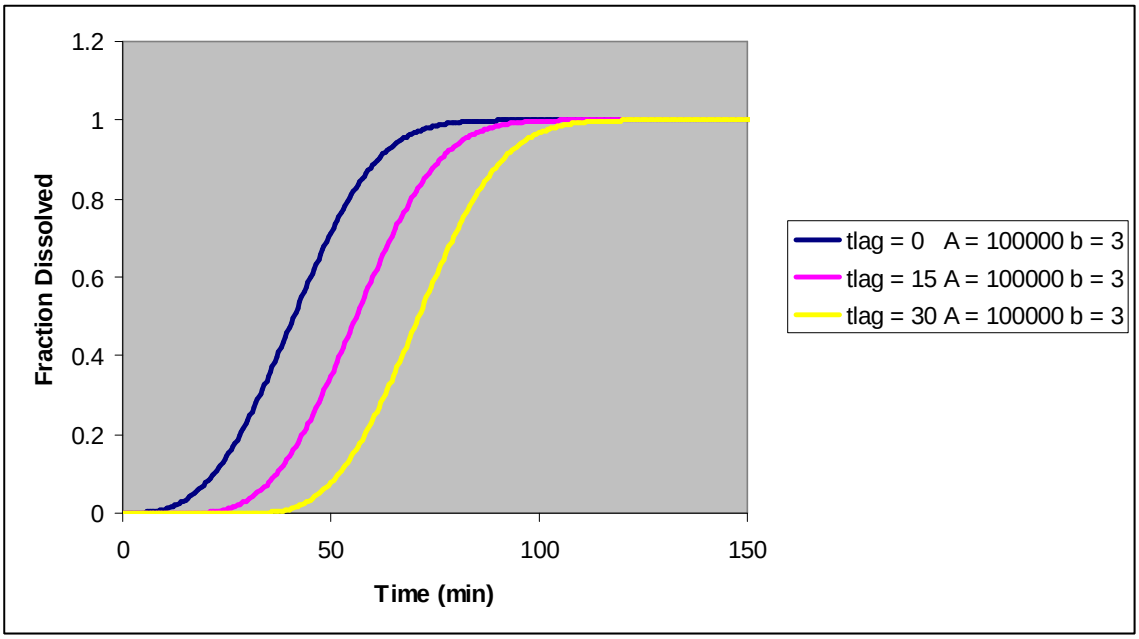

Figure 2-3 Weibull dissolution varying time lag (t_{lag}).

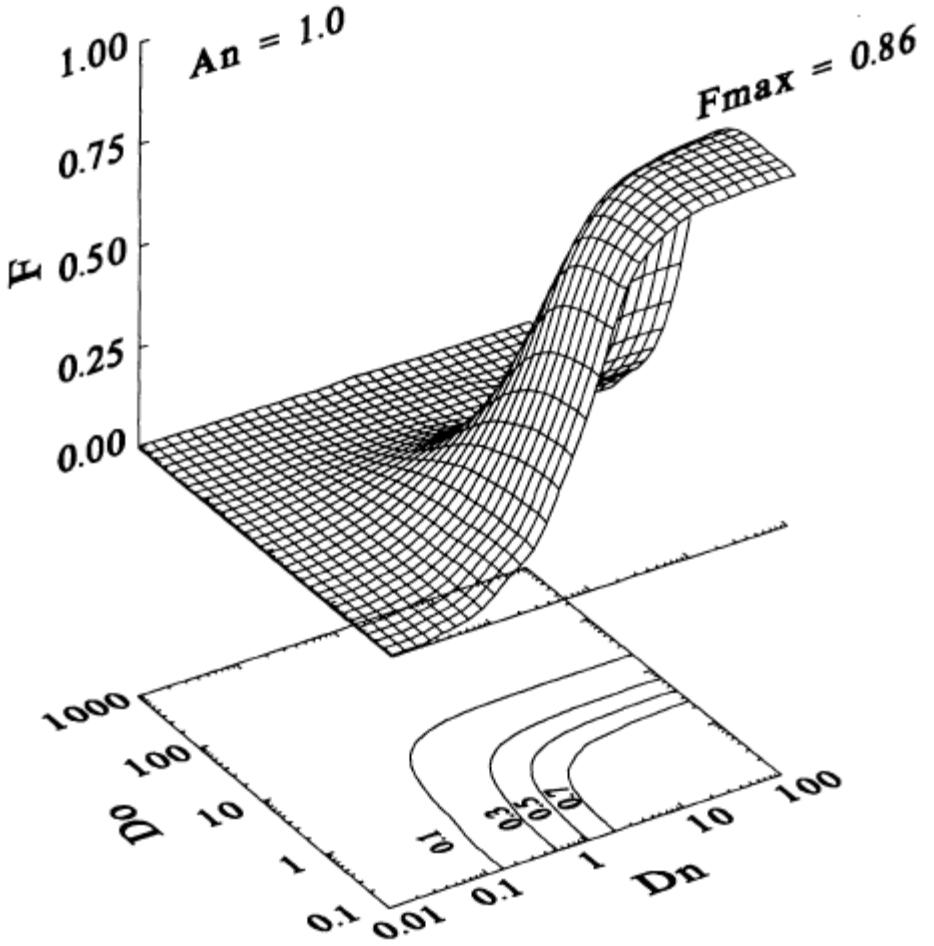

Figure 2-4 3-D plot of fraction of dose absorbed vs. dose number (Do) vs. dissolution number (Dn). (Oh, Curl et al. 1993)

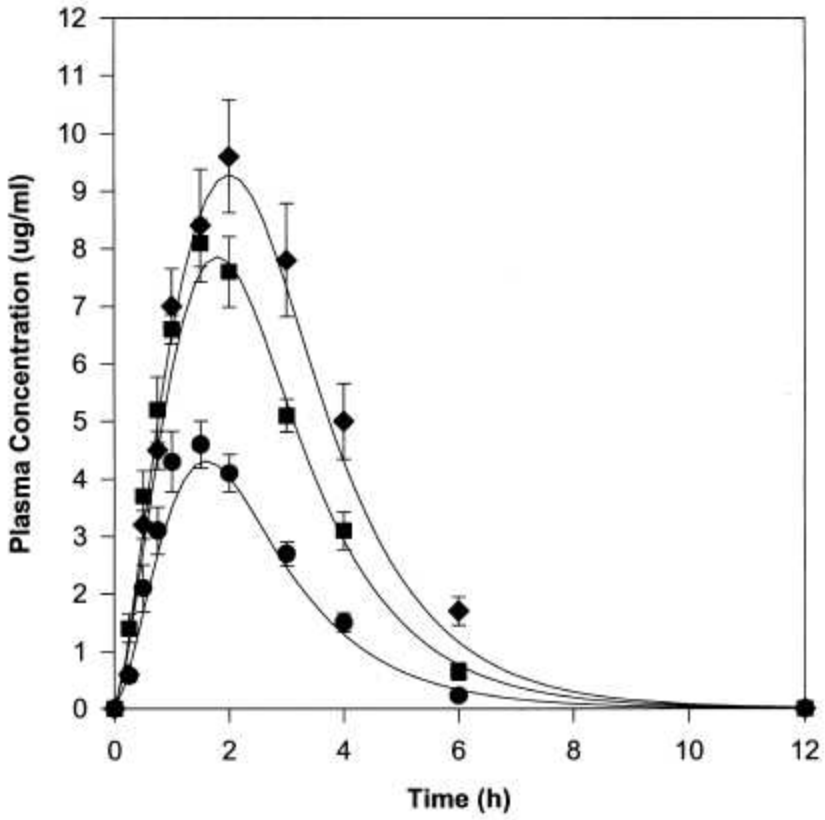

Figure 2-5 Simulated plasma concentration-time profiles for ceftirizine. (Yu and Amidon 1998)

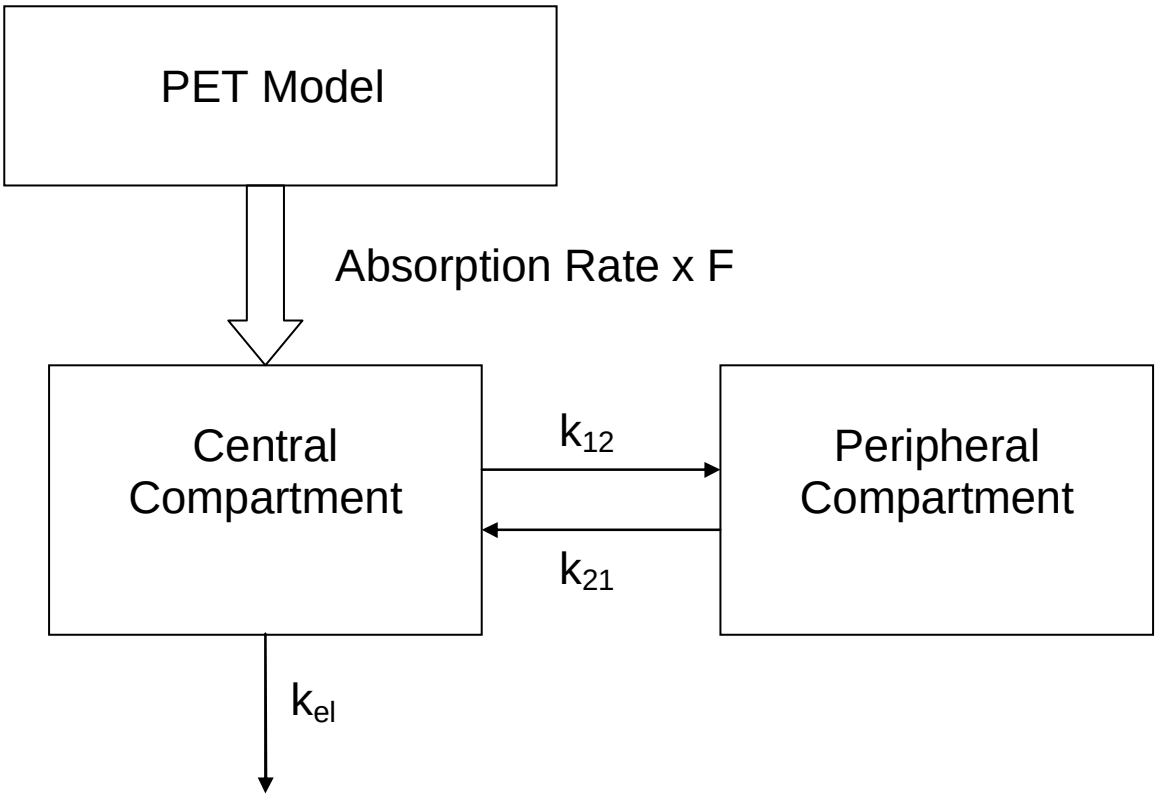

Figure 2-6 Schematic of PET model with 2-compartment pharmacokinetic model

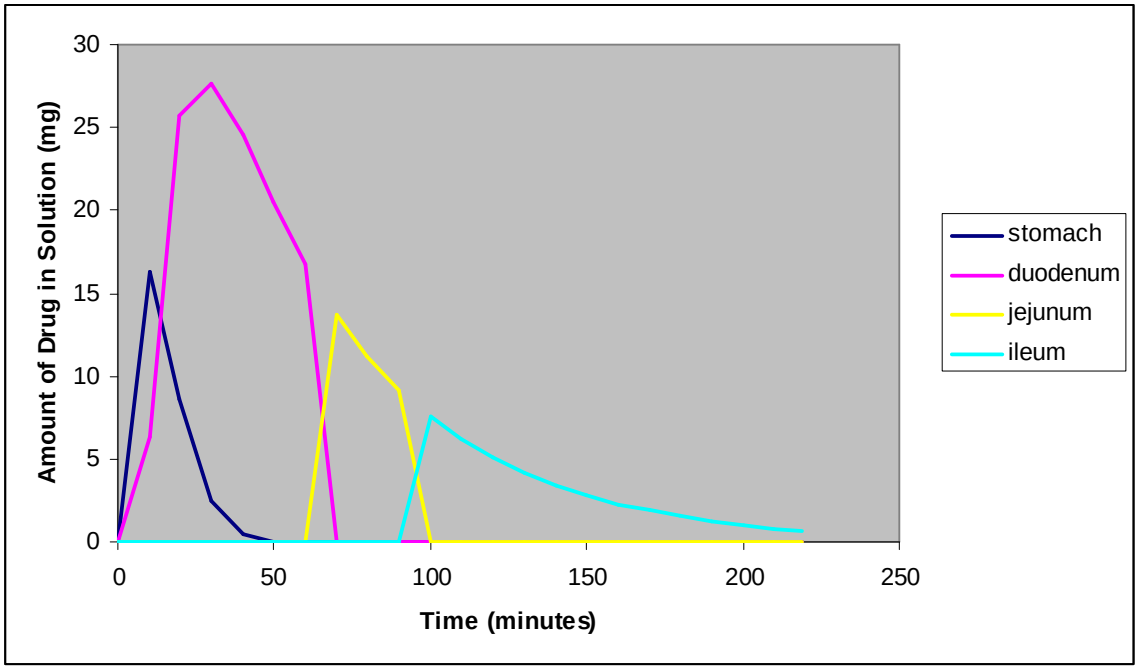

a)

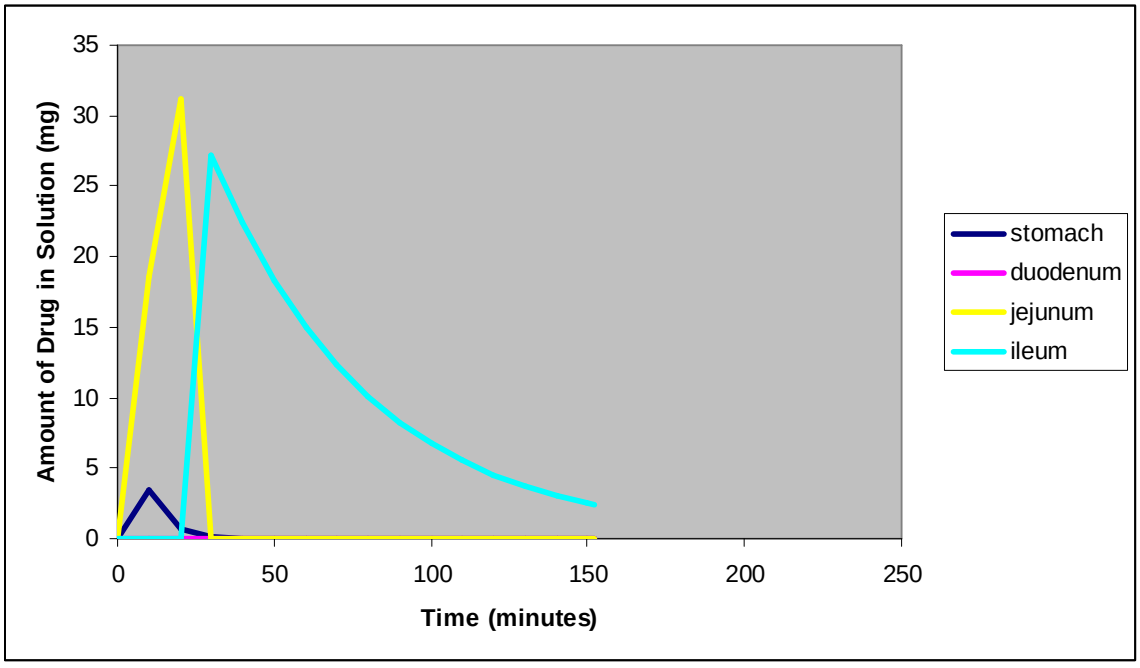

b)

Figure 2-7 Amount of drug in solution at different regions of the gastrointestinal tract vs. time (a) TTP = 80 min (b) TTP = 18 min

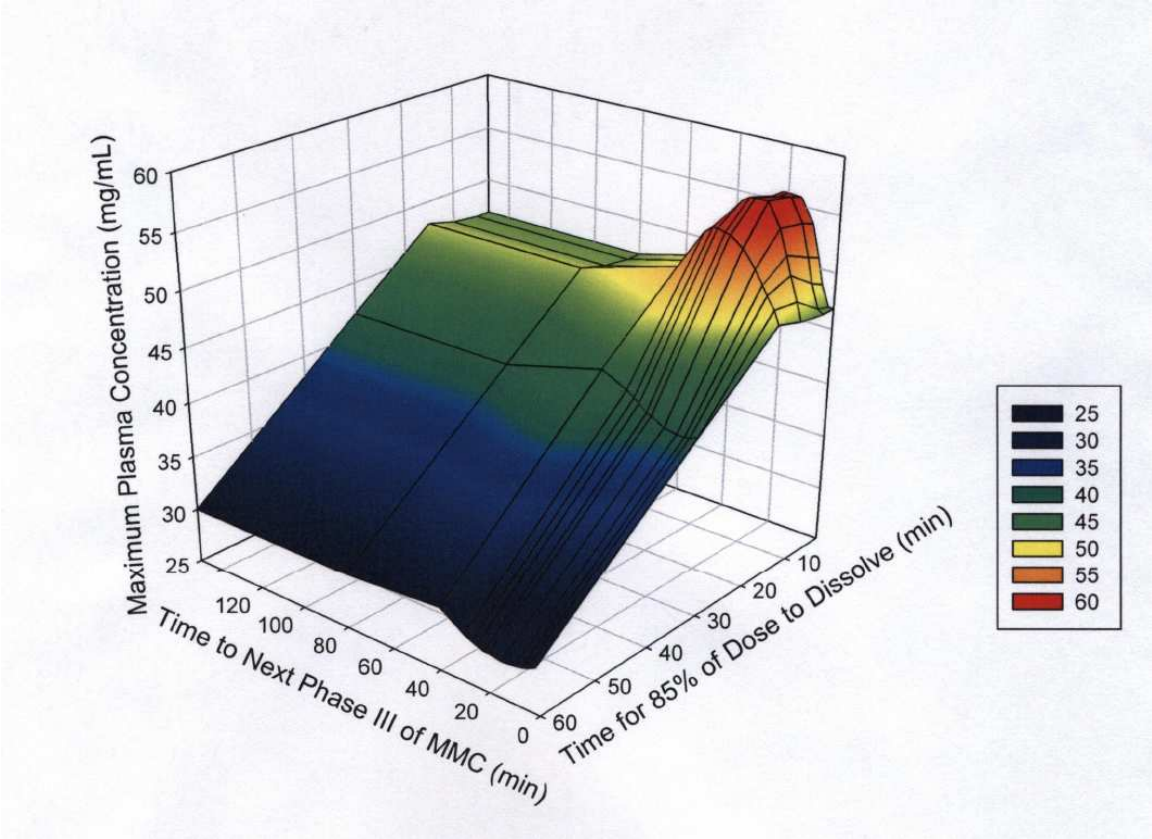

Figure 2-8 3-D plot of C_{max} vs TTPIII vs. t85

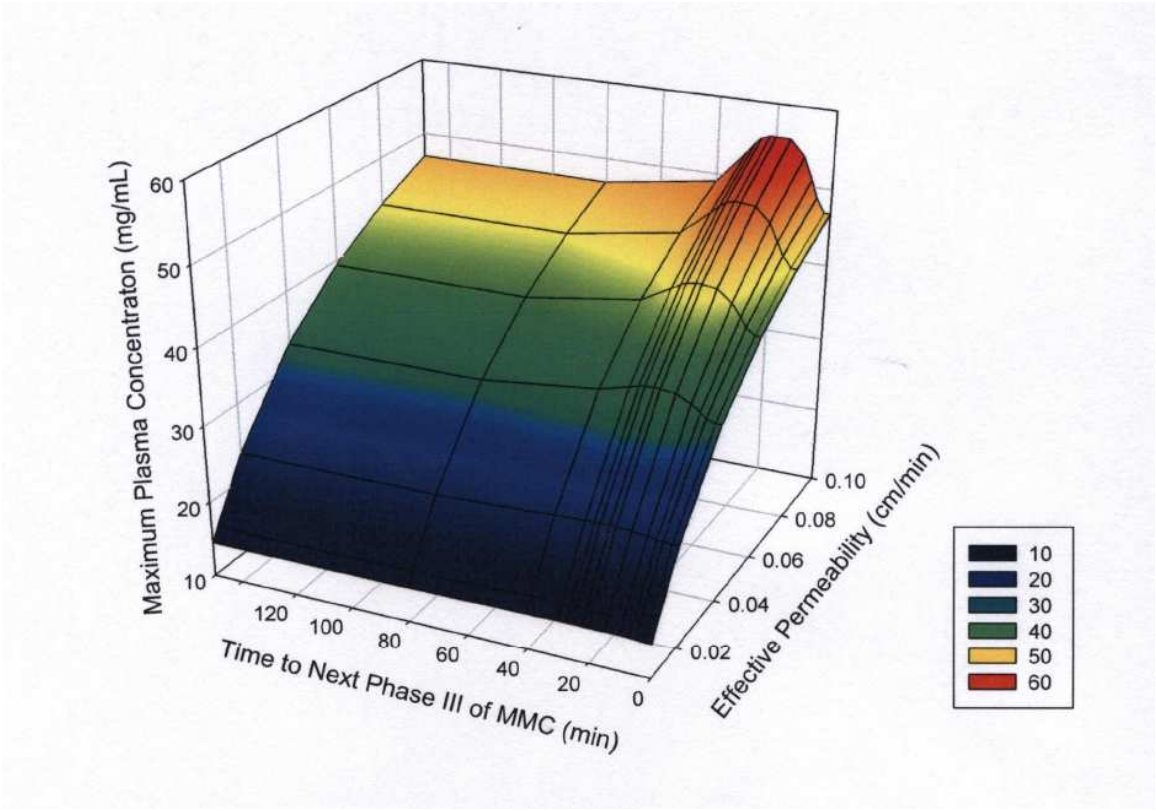

Figure 2-9 3-D plot of C_{max} vs. TTPIII vs. P_{eff}

References

Agoram, B., et al. (2001). "Predicting the impact of physiological and biochemical processes on oral drug bioavailability." Advanced Drug Delivery Reviews **50**: S41-S67.

Amidon, G. L., et al. (1995). "A Theoretical Basis for a Biopharmaceutic Drug Classification - the Correlation of in-Vitro Drug Product Dissolution and in-Vivo Bioavailability." Pharmaceutical Research **12**(3): 413-420.

Anvari, M., et al. (1995). "Mechanics of Pulsatile Transpyloric Flow in the Pig." Journal of Physiology-London **488**(1): 193-202.

Bueno, L., et al. (1975). "Rate of Flow of Digesta and Electrical-Activity of Small-Intestine in Dogs and Sheep." Journal of Physiology-London **249**(1): 69-85.

Code, C. F. and J. A. Marlett (1975). "Interdigestive Myo-Electric Complex of Stomach and Small Bowel of Dogs." Journal of Physiology-London **246**(2): 289-309.

Dressman, J. B., et al. (1985). "Absorption Potential - Estimating the Fraction Absorbed for Orally-Administered Compounds." Journal of Pharmaceutical Sciences **74**(5): 588-589.

Dressman, J. B. and D. Fleisher (1986). "Mixing-Tank Model for Predicting Dissolution Rate Control of Oral Absorption." Journal of Pharmaceutical Sciences **75**(2): 109-116.

Dressman, J. B., et al. (1984). "Physicochemical Model for Dose-Dependent Drug Absorption." Journal of Pharmaceutical Sciences **73**(9): 1274-1279.

Goodacre, B. C. and P. J. Murray (1981). "A Mathematical-Model of Drug Absorption." Journal of Clinical and Hospital Pharmacy **6**(2): 117-133.

Hintz, R. J. and K. C. Johnson (1989). "The Effect of Particle-Size Distribution on Dissolution Rate and Oral Absorption." International Journal of Pharmaceutics **51**(1): 9-17.

Luner, P. E. and G. L. Amidon (1993). "Description and Simulation of a Multiple Mixing Tank Model to Predict the Effect of Bile Sequestrants on Bile-Salt Excretion." Journal of Pharmaceutical Sciences **82**(3): 311-318.

Malbert, C. H., et al. (1994). "Vagal Control of Transpyloric Flow and Pyloric Resistance." Digestive Diseases and Sciences **39**(12): S24-S27.

Ni, P. F., et al. (1980). "Theoretical-Model Studies of Intestinal Drug Absorption .5. Non-Steady-State Fluid-Flow and Absorption." International Journal of Pharmaceutics **5**(1): 33-47.

Oberle, R. L. and G. L. Amidon (1987). "The Influence of Variable Gastric-Emptying and Intestinal Transit Rates on the Plasma-Level Curve of Cimetidine - an Explanation for the Double Peak Phenomenon." Journal of Pharmacokinetics and Biopharmaceutics **15**(5): 529-544.

Oberle, R. L., et al. (1990). "The Influence of the Interdigestive Migrating Myoelectric Complex on the Gastric-Emptying of Liquids." Gastroenterology **99**(5): 1275-1282.

Oh, D. M., et al. (1993). "Estimating the Fraction Dose Absorbed from Suspensions of Poorly Soluble Compounds in Humans - a Mathematical-Model." Pharmaceutical Research **10**(2): 264-270.

Schanker, L. S., et al. (1958). "Absorption of Drugs from the Rat Small Intestine." Journal of Pharmacology and Experimental Therapeutics **123**(1): 81-88.

Sinko, P. J., et al. (1991). "Predicting Fraction Dose Absorbed in Humans Using a Macroscopic Mass Balance Approach." Pharmaceutical Research **8**(8): 979-988.

Yu, L. X. and G. L. Amidon (1998). "Characterization of small intestinal transit time distribution in humans." International Journal of Pharmaceutics **171**(2): 157-163.

Yu, L. X. and G. L. Amidon (1998). "Saturable small intestinal drug absorption in humans: modeling and interpretation of cefatrizine data." European Journal of Pharmaceutics and Biopharmaceutics **45**(2): 199-203.

Yu, L. X., et al. (1996). "Transport approaches to the biopharmaceutical design of oral drug delivery systems: Prediction of intestinal absorption." Advanced Drug Delivery Reviews **19**(3): 359-376.

Zhou, H. H. (2003). "Pharmacokinetic strategies in deciphering atypical drug absorption profiles." Journal of Clinical Pharmacology **43**(3): 211-227.

Chapter III

A Pharmacokinetic Model Incorporating Gastrointestinal Motility Variation Coupled with Discontinuous Gastrointestinal Absorption to Examine the Appearance and Absence of Double Peaks in Oral Ranitidine Plasma Concentration-Time Profiles

Introduction

The appearance of double peaks in ranitidine plasma concentration-time profiles has been widely reported (Garg, Weidler et al. 1983; Shim and Hong 1989; Williams, Dukes et al. 1992; Yin, Tomlinson et al. 2003). Other drugs that have also shown double peaks in plasma concentration-time profiles include furosemide (Hammarlund, Paalzow et al. 1984), cimetidine (Takamatsu, Welage et al. 2002), celiprolol (Lipka, Lee et al. 1995), and penicillamine (Bergstrom, Kay et al. 1981). Several hypotheses have been proposed for the occurrence of double peaks in plasma concentration-time profiles including: enterohepatic recirculation (Miller 1984), discontinuous absorption (Plusquellec, Campistron et al. 1987), and variable gastric emptying and intestinal transit rates (Oberle and Amidon 1987).

Enterohepatic recirculation is an unlikely explanation for the appearance of double peaks in ranitidine plasma concentration-time profiles. After intravenous administration of 50 mg ranitidine in patients, it was found that only 0.7 to 2.6% of the dose was recovered in bile after 24 hours. Similarly, after 300 mg/day of ranitidine was administered orally to patients, only 0.1 to 1% of the daily dose was excreted in the bile

(Klotz and Walker 1990). The low amounts of ranitidine recovered in the bile after both intravenous and oral dosing suggest that significant ranitidine enterohepatic recirculation does not occur and other explanations for the double peak phenomena need to be considered.

Another explanation for the appearance of double peaks in ranitidine plasma concentration-time profiles is discontinuous absorption sites, where a non-absorbing gastrointestinal segment lies between two sites of absorption (Plusquellec, Campistron et al. 1987). Evidence for discontinuous absorption sites for ranitidine in the small intestine of humans has been reported. Ranitidine is well absorbed at the proximal (duodeno-jejunal junction) and distal (ileum) parts of the small intestine. However it is poorly absorbed in the middle part of the small intestine (mid jejunum) (Gramatte, Eldesoky et al. 1994). Simulations with a pharmacokinetic model that incorporated discontinuous absorption sites support the discontinuous absorption site hypothesis. The model was able to simulate double peaks similar to those actually observed in ranitidine concentration-time profiles (Suttle, Pollack et al. 1992). Although a discontinuous absorption site seems to be a plausible explanation for the appearance of double peaks in ranitidine plasma concentration-time profiles, the explanation does not account for the absence of double peaks that has been observed in ranitidine plasma concentration-time profiles (Williams, Dukes et al. 1992; Yin, Tomlinson et al. 2003).

An alternative explanation for double peaks in plasma concentration-time profiles is variable gastric emptying rates and intestinal transit due to the migrating motor complex. The migrating motor complex (MMC) is a rhythmically recurring cycle of contractile activity that occurs in the stomach and small intestine (Code and Marlett

1975). It consists of three phases of contractile activity. Phase I is a quiescent phase. Phase II has irregular and infrequent contractions. Phase III has a burst of regular frequent contractions and is commonly referred to as the "housekeeper wave" because of its ability to propel remaining stomach and intestinal contents aborally. The housekeeper function of the MMC affects the gastric emptying rate and small intestinal transit time of drugs (Bueno, Fioramonti et al. 1975; Oberle, Chen et al. 1990). Using a pharmacokinetic model that incorporated variability in gastrointestinal transit, it was concluded that the dosing time relative to stomach phasic activity and variable gastric emptying are important factors in the occurrence of double peaks in cimetidine plasma concentration-time profiles (Oberle and Amidon 1987).

Since both discontinuous absorption sites for ranitidine and variability in gastrointestinal motility due to the migrating motor complex have been shown to occur in humans, it is conceivable that these two explanations for the appearance and absence of double peaks observed in ranitidine plasma concentration-time profiles do not have to be independent of the other. The present study was undertaken to develop a pharmacokinetic model that takes into account both discontinuous absorption sites and variability in gastrointestinal motility due to the motor migrating complex. Simulations with this model may provide new insights into double peak phenomena observed in ranitidine plasma concentration-time profiles.

Theoretical

In the Pulsatile Emptying Transit (PET) model, the GI tract is described by the stomach and small intestine, which is divided into duodenum, jejunum, and ileum. The

stomach is considered to be a reservoir for ingested drug and liquid. In the stomach, drug dissolution occurs, but minimal drug absorption takes place. The contents in the stomach are assumed to be well-mixed.

Physiological:

The migrating motor complex (MMC) is a rhythmically contractile cycle that takes place in the stomach and small intestine. A major purpose of the MMC is to clear any undigested contents from the GI tract. There are three phases of the MMC. Phase I is a quiescent phase, with no contractile activity. Phase II has infrequent contractile activity and Phase III has repeated contractile activity and is known as the housekeeper wave. The MMC plays a role in gastric emptying and flow of intestinal contents.

A MMC cyclelength of 150 minutes was used. The lengths of Phase I, Phase II, and Phase III in the stomach used in the model were 117 minutes, 18 minutes, and 15 minutes, respectively.

Pulsatile Gastric Emptying:

Pulses of liquid, containing solid and dissolved drug, empty from the stomach into the small intestine every 30 seconds. A total of 75 pulses empty into the small intestine. The first pulse empties from the stomach into the intestine after a lag time dependant on the MMC at the time of dosing and the last pulse empties into the intestine 37 minutes later. Each pulse is well-mixed and the pulses do not mix with other pulses within the intestine.

The gastric emptying of liquids observes a first order process. The amount of drug and volume of liquid in each pulse is determined from:

$$\textit{Drug amount in pulse} = M_o e^{-k_e t}\left(1 - e^{-k_e i}\right) \qquad (3.1)$$

$$\textit{Liquid volume in pulse} = V_o e^{-k_e t}\left(1 - e^{-k_e i}\right) \qquad (3.2)$$

where M_o = dose, k_e = first order gastric emptying rate, t = time, and V_o = volume taken with dose

The value of the first order gastric emptying rate constant depends on the phase of the migrating motor complex in the stomach. During phase I, lag time = 7 minutes and in early phase II, lag time = 4 minutes. The gastric emptying rate was $k_e = 0.11\ min^{-1}$ for both of these phases ($GE_{1/2}$ = 13.3 min and $GE_{1/2}$ = 10.3 min, respectively). During late phase II and phase III, lag time = 2 minutes and $k_e = 0.236\ min^{-1}$ ($GE_{1/2}$ = 5 min).

Intestinal Residence Time:

Once a pulse empties into the small intestine, the drug in the pulse has a finite amount of time to be absorbed, the pulse intestinal residence time. In the model, the intestinal residence time of each pulse is dependant on the phase III of the migrating motor complex in the intestine at the time of gastric emptying. For example, a pulse that empties into the small intestine during phase I spends more time in the duodenum and thus has a longer intestinal residence time than a pulse that empties into the small intestine during phase III, which is quickly propelled to the jejunum and spends little time in the duodenum.

Dissolution profile:

The Weibull equation is often used to describe *in vitro* dissolution data. A modified version of the Weibull equation was used to model the dissolution profile of drug. According to the Weibull equation, the amount of drug dissolved approaches the original amount of solid drug at an infinite time. However, drug can not continue to dissolve once the solution is saturated. To take this into account, the Weibull equation was modified so that the dissolution rate decreases when the concentration approaches the solubility of the drug. The modified Weibull equation is given by:

$$M = M_{pulse}\left(1 - e^{-\frac{(t-tlag)^b}{A}}\right)\frac{(C_s - C_l)}{C_s} \qquad (3.3)$$

where M_{pulse} = Amount of drug in pulse, tlag = lag time, A = time scale factor, and b = shape factor, C_s = drug solubility, and C_l = drug concentration in the intestinal lumen An advantage of using the Weibull equation is that different dissolution rates can be explored by changing these parameters.

Dissolution Rate:

Taking the derivative of the modified Weibull equation with respect to time gives the dissolution rate.

$$dissolution\ rate = M_{pulse} \cdot \frac{b(t - tlag)^{(b-1)}}{A} e^{-\frac{(t-tlag)^b}{A}} \frac{(C_s - C_L)}{C_s} \qquad (3.4)$$

Absorption Rate:

The absorption rate is determined by the product of the flux of the drug (j_w) and the absorption surface area (A).

$$j_w = k_w(C_L - 0) = Peff \cdot C_L = Peff \cdot \frac{M}{V} \qquad (3.5)$$

$$absorption\ rate = j_w A = \frac{P_{eff} M}{V_p} \cdot A = \frac{P_{eff} M}{V_p} \cdot 2\pi RL_p \qquad (3.6)$$

Pulse mass balance:

A mass balance of drug in each pulse is given by:

$$\begin{pmatrix} Amount\ of\ drug \\ in\ pulse\ at\ time\ 0 \end{pmatrix} = \begin{pmatrix} Amount\ of\ solid \\ drug\ at\ time\ t \end{pmatrix} + \begin{pmatrix} Amount\ of\ drug \\ in\ solution\ at\ time\ t \end{pmatrix} + \begin{pmatrix} Amount\ of\ drug \\ absorbed\ at\ time\ t \end{pmatrix} \qquad (3.7)$$

A mass balance of the solution phase in each pulse is given by:

$$\begin{pmatrix} rate\ of\ mass \\ accumulation\ at\ time\ t \end{pmatrix} = \begin{pmatrix} rate\ of\ mass \\ dissolved\ at\ time\ t \end{pmatrix} - \begin{pmatrix} rate\ of\ mass \\ absorbed\ at\ time\ t \end{pmatrix} \qquad (3.8)$$

$$M\big|_t - M\big|_{t+dt} + M_{pulse} \cdot \frac{b(t - tlag)^{(b-1)}}{A} e^{-\frac{(t-tlag)^b}{A}} \frac{(C_s - C_L)}{C_s} dt - \frac{Peff \cdot M}{V_p} \cdot 2\pi RL_p dt = 0 \qquad (3.9)$$

$$\frac{dM}{dt} = M_{pulse} \cdot \frac{b(t - tlag)^{(b-1)}}{A} e^{-\frac{(t-tlag)^b}{A}} \frac{(C_s - C_L)}{C_s} - \frac{2 \cdot Peff \cdot M}{V_p} \cdot \pi RL_p \qquad (3.10)$$

$$\frac{1}{V_{pulse}} \frac{dM}{dt} = \frac{M_{pulse}}{V_{pulse}} \cdot \frac{b(t - tlag)^{(b-1)}}{A} e^{-\frac{(t-tlag)^b}{A}} \frac{(C_s - C_L)}{C_s} - \frac{2 \cdot Peff \cdot C_L \cdot \pi RL_p}{V_{pulse}} \qquad (3.11)$$

$$\frac{dC_L}{dt} = \frac{M_{pulse}}{V_{pulse}} \cdot \frac{b(t - tlag)^{(b-1)}}{A} e^{-\frac{(t-tlag)^b}{A}} \frac{(C_s - C_L)}{C_s} - \frac{2 \cdot Peff \cdot C_L}{R} \qquad (3.12)$$

The rate of mass absorbed from each pulse is given by:

$$\frac{dM_{abs}}{dt} = \frac{2 \cdot Peff \cdot C_L}{R} \cdot V_{pulse} \qquad (3.13)$$

Differential Equations were solved numerically using the Runge-Kutta-Fehlberg method which was programmed into Visual Basic in Excel.

Methods

The absorption rate obtained from the PET model was inputted into a 2 compartment pharmacokinetic model. All parameters inputted into the model were obtained from the literature except for the human duodenal and ileal effective permeabilities of ranitidine which have not been reported. All simulations were based on a single dose of drug with time = 0 representing the time of dosing. Pharmacokinetic parameters were varied in each simulation to assess their influence on the concentration-time profile. The effects of phase of dosing and gastric emptying rate were investigated by varying the parameter time to the end of the next phase III (TTPIII). Different permeability values can be inputted in the PET model for the duodenum, jejunum, and ileum. The inputs to the model simulations are listed in Appendix B.

Results

The simulated plasma concentration-time profiles produced when dosing at different times with respect to phase III are presented in Figure 3-2. In simulations where only the time to the end of the next phase III (TTPIII) decreased, the plasma concentration of the first peak (C_{max1}) and time of the first peak (T_{p1}) decreased, the plasma concentration of the second peak (C_{max2}) increased and time of the second peak (T_{p2}) was unchanged. When TTPIII was between 0 and 20 minutes, C_{max1} disappeared and only one peak was observed.

The effects of changes in dissolution rate on the simulated plasma concentration-time profiles are shown in Figure 3-3. Increasing dissolution rate, resulted in increased C_{max1} and C_{max2} decreased T_{p2} and unchanged T_{p1}.

The effects of changes in the effective permeability of the duodenum and ileum on the simulated plasma concentration-time profiles are displayed in Figure 3-4 and Figure 3-5, respectively. Increased effective permeability in the duodenum increased C_{max1} and C_{max2} and decreased T_{p1} and T_{p2}. At increasingly high effective permeabilities in the duodenum, the second peak becomes less pronounced. Increased effective permeability in the ileum has no effect on C_{max1} and T_{p1}, but increases C_{max2} and decreases T_{p2}.

The effects of the intravenous pharmacokinetic parameters on simulated plasma concentration-time profiles are displayed in Figures 3-6, 3-7, 3-8, and 3-9. Increasing k_{12} decreases C_{max1} and C_{max2}, has no effect on T_{p1}, and increases T_{p2}. Increasing k_{21}, increases C_{max1} and C_{max2}, has no effect on T_{p1}, and increases T_{p2}. Increasing k_{out}, decreases C_{max1} and C_{max2}, has no effect on T_{p1}, and decreases T_{p2}. Increasing V_c, decreases C_{max1} and C_{max2} and has no effect on T_{p1} and T_{p2}.

Discussion

Factors that affect oral absorption (drug dissolution, variable gastric emptying, variable effective permeabilities along the intestine, and intestinal transit times) were taken into account in the present model. The model is described by the stomach, duodenum, jejunum and ileum. The transit of gastrointestinal contents was modeled to be dependent on the migrating motor complex.

Twelve plots showing a diversity of shapes for orally administered ranitidine plasma concentration-time profiles are shown in Figure 3-1. Each plot has two plasma concentration-time profiles taken from a single individual one week apart. The dotted plots were taken one week after the solid plots. The majority of the plasma concentration-time profiles show double peaks. Among the plasma concentration-time profiles that have double peaks, differences in the heights and timing of appearance for the first and second peaks are very apparent. Even within the same individual, the heights and time of appearance for the first and second peaks differ slightly when ranitidine is given one week later.

Simulations with the PET model show that the heights of the two peaks in ranitidine plasma concentration-time profiles can be affected by several parameters including TTPIII, drug dissolution rate, effective permeability values, and intravenous PK parameters. All of these parameters may differ between individuals. The wide variability in the shapes of the concentration-time profiles between individuals is striking and suggests that the shape of each of the profiles is a result of the combination of these parameters in the individual and each individual has different combinations of these parameters.

However within individuals, effective permeability patterns along the intestine and intravenous PK parameters are not expected to vary significantly. Thus, the absorption pattern of ranitidine along the small intestine is a characteristic of an individual. Given similar flow patterns in the small intestine, one would expect to see similarly shaped concentration-time profiles within the same individual. The data showing pairs of concentration-time profiles obtained one week apart from 12 individuals

show this to be the true except for one pair of concentration-time profiles. Simulations with the PET model show that dosing at different phases of the MMC, produce slight changes in the peak heights and time shifts in plasma concentration time profiles, but the overall shape of the profiles are extremely similar the majority of the time. In simulations, exceptions occurred when drug was given during phase III of the motor migrating complex which produced plasma concentration-time profiles with single peaks. When drug is dosed during phase III, little drug is absorbed in the duodenum because drug is rapidly propelled to the jejunum by phase III contractions in the duodenum. Assuming that the MMC phase that the dose of ranitidine is given is random, the occurrence of single peaks rather than double peaks in ranitidine plasma concentration curves is expected to occur infrequently, approximately 15% of the time.

Summary

Simulations with the PET model with a discontinuous PK model support discontinuous absorption sites as an explanation for the appearance of double peaks in ranitidine plasma concentration-time profiles. Simulations also suggest that single peaks may occur when drug is dosed during phase III of the migrating motor complex. When drug is dosed during phase III, absorption in the duodenum, a high absorption site, may be bypassed resulting in a single peak. Since phase III makes up roughly 15% of the MMC cycle, single peak plasma concentration-time profiles are expected to appear infrequently. Simulations with the PET model show that similarly shaped concentration-time profiles can be expected for the same individual the majority of the time. For an individual, simulations show that the height and timing of peaks in plasma concentration-

time profiles can differ depending on the phase of dosing; however, the general shape of the double peaks is similar. Exceptions occurred when simulations produced single peak plasma concentration curves when ranitidine was dosed during phase III of the MMC. Simulations show that slight differences in peak heights and timing of peaks may also be caused by differences in drug dissolution rate.

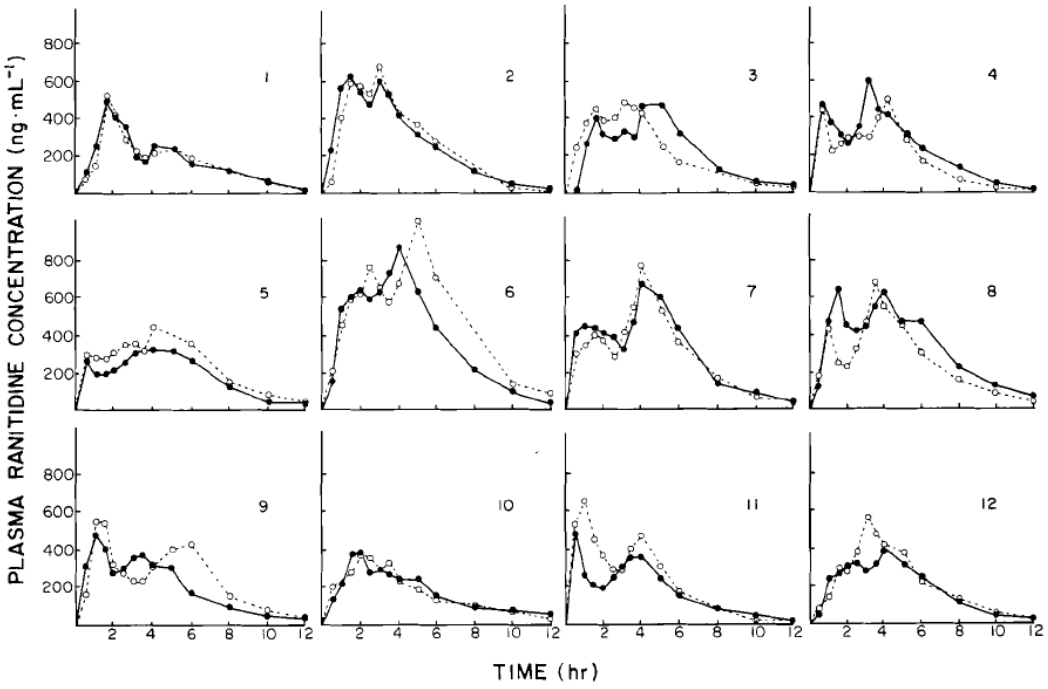

Figure 3-1 Oral ranitidine plasma concentration-time profiles for 12 patients (Shim and Hong 1989)

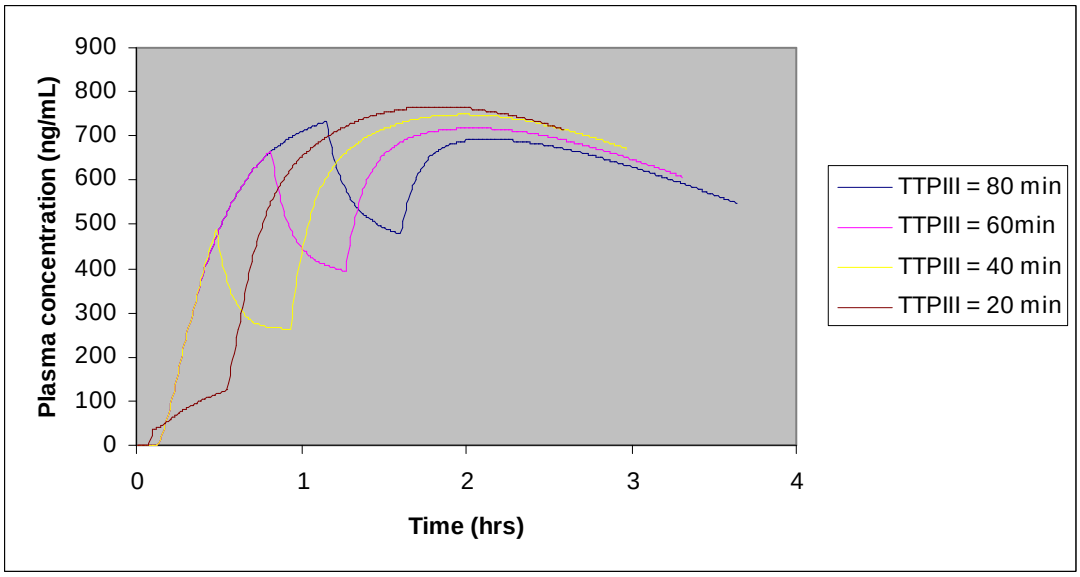

Figure 3-2 Plasma concentration-time profile varying time to next phase III (TTPIII)

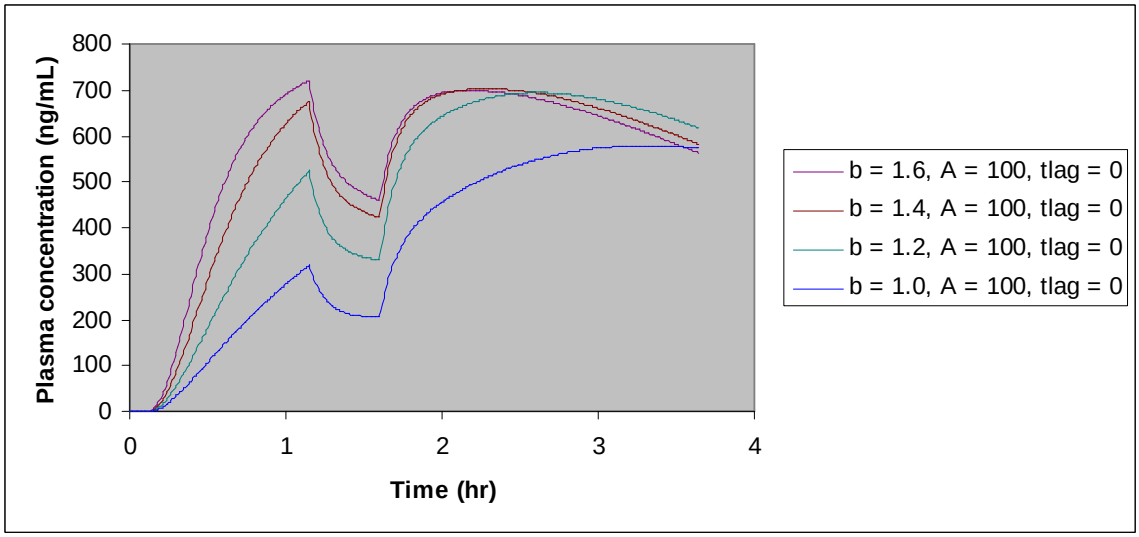

Figure 3-3 Plasma concentration-time profile varying dissolution rate (t85)

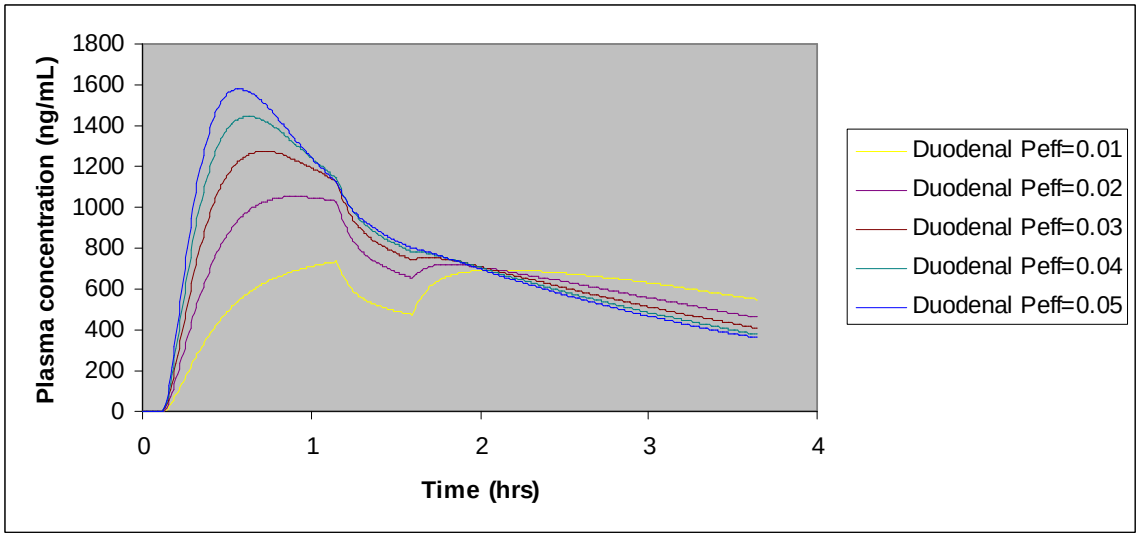

Figure 3-4 Plasma concentration-time profile varying P_{eff} in the duodenum

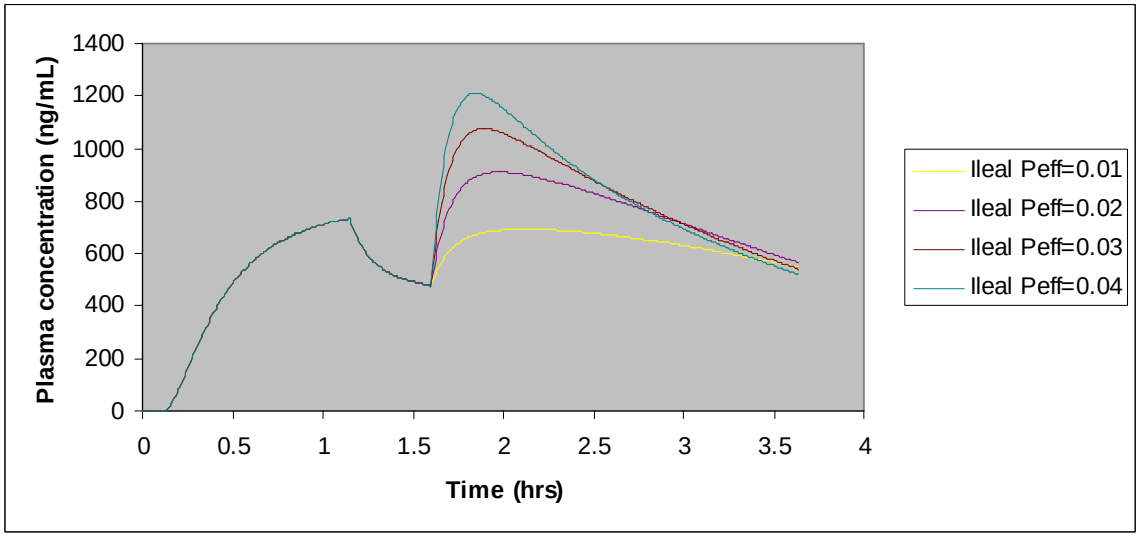

Figure 3-5 Plasma concentration-time profile varying P_{eff} in the ileum

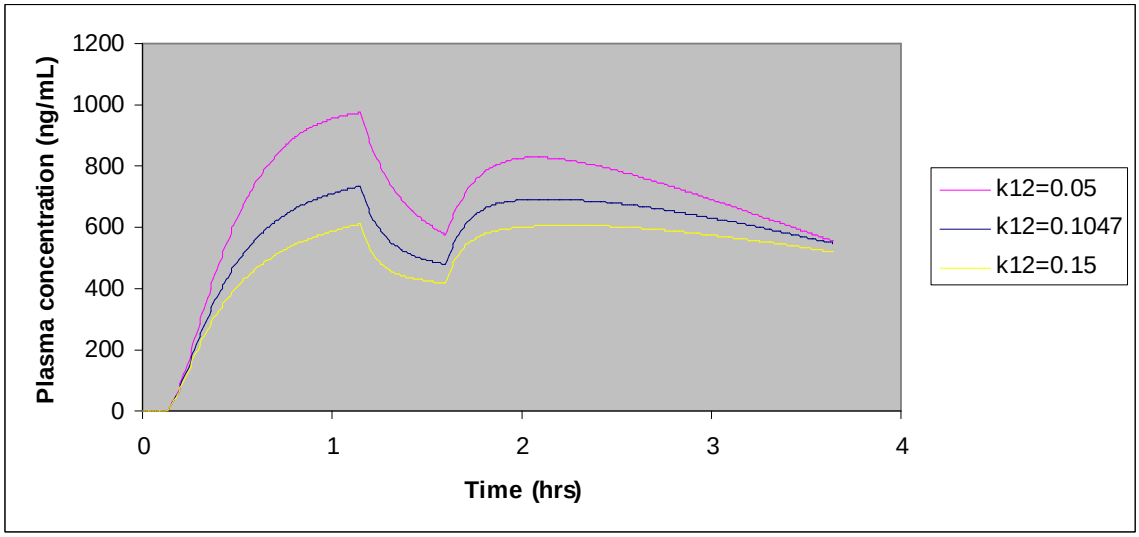

Figure 3-6 Plasma concentration-time profile varying k_{12}

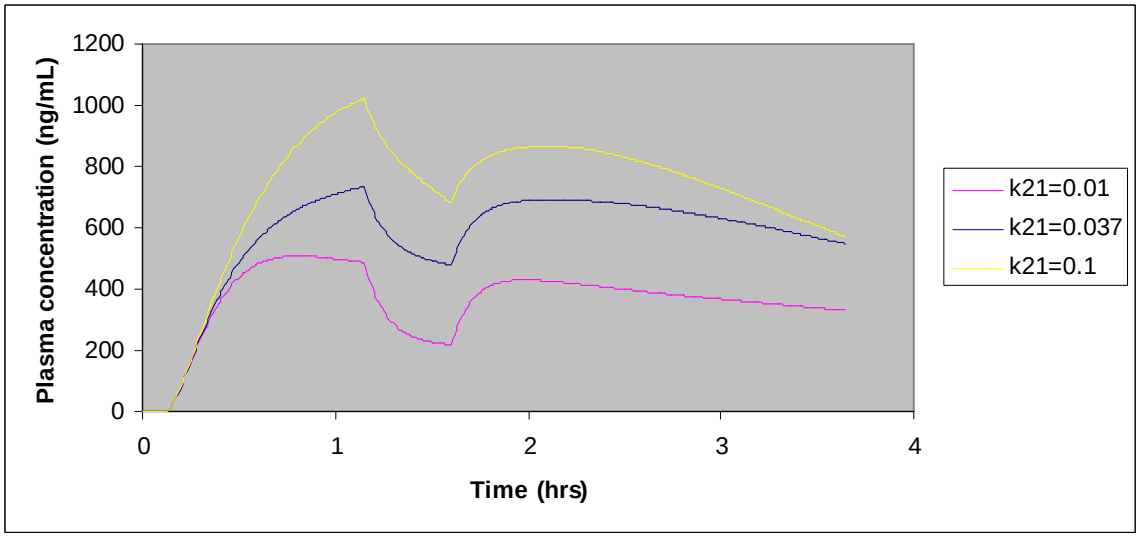

Figure 3-7 Plasma concentration-time profile varying k_{21}

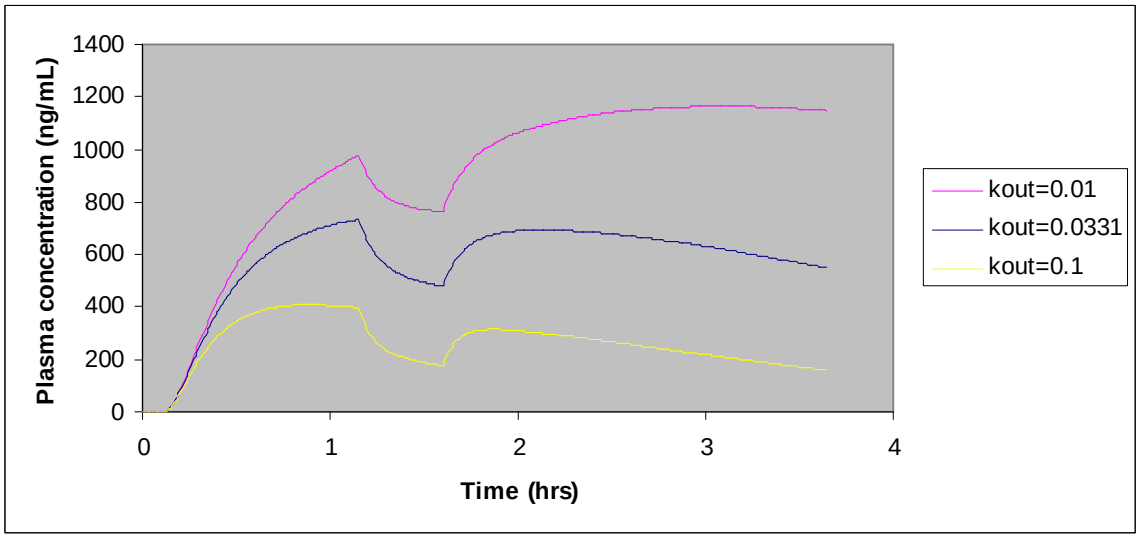

Figure 3-8 Plasma concentration-time profile varying k_{out}

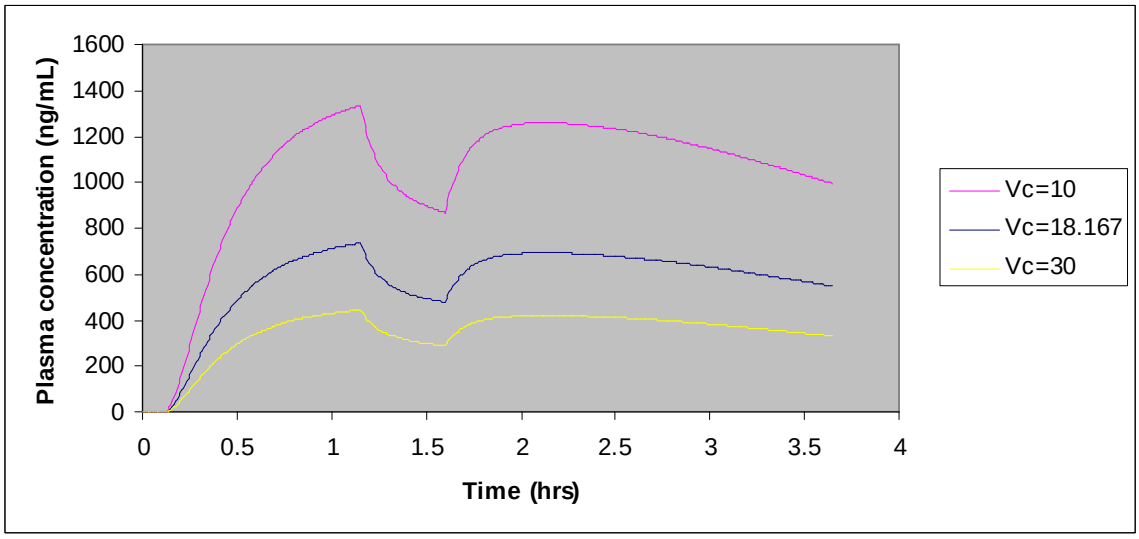

Figure 3-9 Plasma concentration-time profile varying V_c

References

Bergstrom, R. F., et al. (1981). "Penicillamine Kinetics in Normal Subjects." Clinical Pharmacology & Therapeutics **30**(3): 404-413.

Bueno, L., et al. (1975). "Rate of Flow of Digesta and Electrical-Activity of Small-Intestine in Dogs and Sheep." Journal of Physiology-London **249**(1): 69-85.

Code, C. F. and J. A. Marlett (1975). "Interdigestive Myo-Electric Complex of Stomach and Small Bowel of Dogs." Journal of Physiology-London **246**(2): 289-309.

Garg, D. C., et al. (1983). "Ranitidine Bioavailability and Kinetics in Normal-Male Subjects." Clinical Pharmacology & Therapeutics **33**(4): 445-452.

Gramatte, T., et al. (1994). "Site-Dependent Small-Intestinal Absorption of Ranitidine." European Journal of Clinical Pharmacology **46**(3): 253-259.

Hammarlund, M. M., et al. (1984). "Pharmacokinetics of Furosemide in Man after Intravenous and Oral-Administration - Application of Moment Analysis." European Journal of Clinical Pharmacology **26**(2): 197-207.

Klotz, U. and S. Walker (1990). "Biliary-Excretion of H2-Receptor Antagonists." European Journal of Clinical Pharmacology **39**(1): 91-92.

Lipka, E., et al. (1995). "Celiprolol double-peak occurrence and gastric motility: Nonlinear mixed effects modeling of bioavailability data obtained in dogs." Journal of Pharmacokinetics and Biopharmaceutics **23**(3): 267-286.

Miller, R. (1984). "Pharmacokinetics and Bioavailability of Ranitidine in Humans." Journal of Pharmaceutical Sciences **73**(10): 1376-1379.

Oberle, R. L. and G. L. Amidon (1987). "The Influence of Variable Gastric-Emptying and Intestinal Transit Rates on the Plasma-Level Curve of Cimetidine - an Explanation for the Double Peak Phenomenon." Journal of Pharmacokinetics and Biopharmaceutics **15**(5): 529-544.

Oberle, R. L., et al. (1990). "The Influence of the Interdigestive Migrating Myoelectric Complex on the Gastric-Emptying of Liquids." Gastroenterology **99**(5): 1275-1282.

Plusquellec, Y., et al. (1987). "A Double-Peak Phenomenon in the Pharmacokinetics of Veralipride after Oral-Administration - a Double-Site Model for Drug Absorption." Journal of Pharmacokinetics and Biopharmaceutics **15**(3): 225-239.

Shim, C. K. and J. S. Hong (1989). "Intersubject and Intrasubject Variations of Ranitidine Pharmacokinetics after Oral-Administration to Normal-Male Subjects." Journal of Pharmaceutical Sciences **78**(12): 990-994.

Suttle, A. B., et al. (1992). "Use of a Pharmacokinetic Model Incorporating Discontinuous Gastrointestinal Absorption to Examine the Occurrence of Double Peaks in Oral Concentration-Time Profiles." Pharmaceutical Research **9**(3): 350-356.

Takamatsu, N., et al. (2002). "Variability in cimetidine absorption and plasma double peaks following oral administration in the fasted state in humans: correlation with antral gastric motility (vol 53, pg 37, 2002)." European Journal of Pharmaceutics and Biopharmaceutics **54**(2): 255-255.

Williams, M. F., et al. (1992). "Influence of Gastrointestinal Site of Drug Delivery on the Absorption Characteristics of Ranitidine." Pharmaceutical Research **9**(9): 1190-1194.

Yin, O. Q. P., et al. (2003). "A modified two-portion absorption model to describe double-peak absorption profiles of ranitidine." Clinical Pharmacokinetics **42**(2): 179-192.

Chapter IV

Applying Solubility Product and Solution Complexation Relationships to Preliminary Cocrystal Dissolution Studies

Introduction

Dissolution is a process that affects the rate and extent of absorption of orally administered pharmaceutical solids from the gastrointestinal tract and therefore is a key process for drug absorption and drug effectiveness. Before a drug can be absorbed from the gastrointestinal tract, it needs to be dissolved in the gastrointestinal fluid. The drug dissolution rate can be the rate limiting step in absorption and can prevent sufficient amounts of drug from being absorbed by the gastrointestinal tract to elicit the desired therapeutic effect. Altering solid state properties of compounds through the formation of salts, solvates, polymorphs or amorphous solids is a strategy commonly used to try to obtain more favorable compound dissolution rates (Huang and Tong 2004; Rodriguez-Spong, Price et al. 2004). The formation of solid state complexes or cocrystals offers an additional option to alter solid state properties of compounds without changing covalent bonds. The formation of cocrystals may be particularly helpful for compounds that are non-ionizable and when the other commonly used methods for altering solid state properties do not produce the desired results (Stahly 2007). Although the utility of forming cocrystals to alter dissolution rates has been demonstrated for several

compounds it is not well understood how dissolution rate may be affected by cocrystal component selection.

A mechanistic understanding of cocrystal dissolution may aid in the rational selection of components for the formation of cocrystals to achieve a desired dissolution rate for a compound. The dissolution rate of pharmaceutical solids is commonly described by the following equation (Brunner 1904; Nernst 1904):

$$\frac{dm}{dt} = \frac{DS}{h}(C_s - C) \qquad (4.1)$$

where, dm/dt is the dissolution rate, m is the mass of solute dissolved at time t, D is the diffusion coefficient, S is the surface area of the dissolving solid, C is the concentration of the dissolved solute in the bulk solution at time t, and C_s is the solubility of the solute in a thin unstirred layer of solvent with a thickness h. The driving force for dissolution is the concentration gradient across the unstirred layer of solvent. According to the Brunner-Nernst equation, increasing the solubility of the pharmaceutical solid increases the concentration gradient across the unstirred layer of solvent and thus can increase the dissolution rate of the compound.

Understanding the solubility behavior of cocrystals in solutions of cocrystal components may increase our knowledge of how selecting different cocrystal components would affect the dissolution rate of cocrystals. Theoretical analysis and experimental results presented elsewhere (Nehm, Rodriguez-Spong et al. 2006) show that the solubility of cocrystal is dependent on the concentration of cocrystal components in solution and the cocrystal solubility product and the binding constants of complexes formed in solution can explain this dependence. The purpose of the studies presented in

this manuscript is to use solubility product and solution complexation concepts to investigate how cocrystal components may affect cocrystal dissolution.

Theoretical

In search of caffeine cocrystals that would dissolve less rapidly in aqueous solutions than caffeine itself, an equation to estimate the relative dissolution rates of a cocrystal and the active pharmaceutical ingredient (API) was derived using mass transport film theory concepts (Higuchi and Pitman 1973). The relative rate of dissolution (R) of caffeine:gentisic acid cocrystal and caffeine was found to be well estimated by the following equation:

$$R = \frac{A_{To}}{S_A} \qquad (4.2)$$

where A_{To} is the stoichiometric solubility of the cocrystal in the dissolution medium and S_A is the solubility of the uncomplexed drug in the dissolution medium. Equation 2 states that the relative rates of dissolution can be estimated by the ratio of the stoichiometric solubility of the cocrystal and solubility of the API. The validity of the equation depends on whether the stoichiometric solubility of the cocrystal in the dissolution media is representative of the solubility of the cocrystal at the solid/liquid interface of the diffusion layer. Salts can increase their own dissolution rate by acting as their own buffers to change the pH in the diffusion layer, thus increasing the solubility of the parent compound in the unstirred diffusion layer (Berge, Bighley et al. 1977). Cocrystals may similarly increase their own dissolution rates by mechanisms that can increase cocrystal solubility within the unstirred diffusion layer. To investigate this mechanism, solubility

product and solution complexation relationships were used to construct phase solubility diagrams.

Mathematical models that explain the shape of phase solubility diagrams for 1:1 carbamazepine:nicotinamide cocrystal (CBZ:NCT) in ethanol, 2-propanol and ethyl acetate have been derived using solubility product and solution complexation relationships and are presented elsewhere (Nehm, Rodriguez-Spong et al. 2006). When dissolution of 1:1 cocrystal of an API (A) and ligand (B) leads to the formation of soluble complexes, the equilibrium reactions are given by:

$$AB_{solid} \overset{K_{sp}}{\rightleftharpoons} A_{soln} + B_{soln} \qquad (4.3)$$

$$A_{soln} + B_{soln} \overset{K_{1:1}}{\rightleftharpoons} AB_{soln} \qquad (4.4)$$

When the activity coefficients are unity, the equilibrium constants for these reactions can be described by the solubility product

$$K_{sp} = [A][B] \qquad (4.5)$$

and the binding constant for the 1:1 complex formed in solution

$$K_{1:1} = \frac{[AB]}{[A][B]} \qquad (4.6)$$

where [A], [B] and [AB] are the molar concentrations at equilibrium of the A cocrystal component, B cocrystal component, and soluble AB complex, respectively.

Mass balances for A and B in solution give

$$[A]_T = [A] + [AB] \qquad (4.7)$$

$$[B]_T = [B] + [AB] \qquad (4.8)$$

A or B can exist in solution either as free species or as a 1:1 soluble complex.

Substituting equation 7 into equation 8 gives

$$[AB] = K_{1:1}K_{sp} \qquad (4.9)$$

The 1:1 soluble complex concentration is a constant and is determined by taking the product of the solubility product and 1:1 complexation constant.

Substituting equation 11 into equations 9 and 10 gives

$$[A]_T = [A] + K_{1:1}K_{sp} \qquad (4.10)$$

$$[B]_T = [B] + K_{1:1}K_{sp} \qquad (4.11)$$

When CBZ:NCT cocrystal is dissolved in pure solvent, the resulting measured cocrystal solubility is the stoichiometric cocrystal solubility, where:

$$[A] = [B] = \sqrt{K_{sp}} \qquad (4.12)$$

At the stoichiometric solubility for a 1:1 cocrystal AB, the free concentrations of A and B are equal and the total A and B concentrations are given by:

$$[A]_{To} = \sqrt{K_{sp}} + K_{1:1}K_{sp} \qquad (4.13)$$

$$[B]_{To} = \sqrt{K_{sp}} + K_{1:1}K_{sp} \qquad (4.14)$$

At nonstoichiometric conditions for a 1:1 cocrystal AB, the free concentrations of A and B are not equal. The free concentrations of A and B have an inverse relationship given by the solubility product. Increasing the ligand concentration, [B], decreases [A] and thus decreases cocrystal solubility. Decreasing the ligand concentration, [B], increases [A] and thus can increase the cocrystal solubility. Substituting equation 7 into equation 12 gives:

$$[A]_T = \frac{K_{sp}}{[B]} + K_{1:1}K_{sp} \qquad (4.15)$$

Substituting equation 13 into equation 14 gives:

$$[A]_T = \frac{K_{sp}}{[B]_T - K_{1:1}K_{sp}} + K_{1:1}K_{sp} \qquad (4.16)$$

The maximum value for the free concentration of A, [A], is given by the intrinsic solubility of A, $[A]_o$, in the dissolution medium. The maximum value of $[A]_T$ is given by:

$$[A]_{Tmax} = \frac{K_{sp}}{[B]_T - K_{1:1}K_{sp}} + K_{1:1}K_{sp} = [A]_o + K_{1:1}K_{sp} \qquad (4.17)$$

where

$$[B]_T = [B] + K_{1:1}K_{sp} = \frac{K_{sp}}{[A]_o} + K_{1:1}K_{sp} \qquad (4.18)$$

The minimum value for [A] occurs when the free B concentration is equal to the intrinsic solubility of B, $[B]_o$. The minimum value for $[A]_T$ is given by:

$$[A]_{Tmin} = \frac{K_{sp}}{[B]_T - K_{1:1}K_{sp}} + K_{1:1}K_{sp} = \frac{K_{sp}}{[B]_o} + K_{1:1}K_{sp} \qquad (4.19)$$

where

$$[B]_T = [B]_o + K_{1:1}K_{sp} \qquad (4.20)$$

If nonstoichiometric conditions exist in the unstirred layer, the relative dissolution rate between cocrystal and API may deviate from equation 2 and using nonstoichiometric cocrystal solubility values may give better estimates of the relative dissolution rate. Nonstoichiometric conditions may occur in the unstirred layer if the cocrystal components, A and B, diffuse through the unstirred layer at different rates resulting in unequal concentrations of A and B in the unstirred layer.

Methods

Materials:

Anhydrous monoclinic carbamazepine (CBZ(III); lot #093K1544 USP Grade and 99.8% pure) and nicotinamide (NCT(I); lot #093K0018) were purchased from Sigma Chemical Company (St. Louis, MO) and used as received. Ethyl acetate and 2-propanol were of HPLC grade and were purchased from Fisher Scientific (Fair Lawn, NJ). Anhydrous ethanol (200 proof) was of USP grade and was purchased from Pharmco (Brookfield, CT). All solvents were used as received.

Preparation of Carbamazepine:Nicotinamide (CBZ:NCT):

CBZ:NCT cocrystals (1:1 molar ratio) were prepared by dissolving NCT(I) (0.35 g; 2.83 mmol) in ethyl acetate (50 g) and adding CBZ(III) (0.67 g; 2.83 mmol) at 40 ± 5 °C with constant stirring. The solution was quickly cooled to 25 °C in an ice water bath and allowed to crystallize over 2 h. Crystals of CBZ:NCT were harvested by vacuum filtration and dried at room temperature (22-23 °C) under reduced pressure (25 mmHg) on Whatman #50 filter paper (Maidstone, England) for 30 minutes to remove loosely bound solvent. The cocrystal form was confirmed by x-ray powder diffraction. CBZ:NCT was stored at 5 °C over anhydrous calcium sulfate.

X-ray Powder Diffraction (XRPD):

XRPD analyses were carried out on a Rigaku Miniflex X-ray diffractometer (Tokyo, Japan) using Cu Kα radiation (λ = 1.54 Å), tube voltage of 30 kV, and tube

current of 15 mA. The intensities were measured at 2-theta values from 2.5° to 40° at a continuous scan rate of 2.5°/min.

Compact Formation:

Either 80 mg of CBZ(III) or CBZ:NCT powder was placed in a rotating disk die and compressed with a hydraulic press (Fred Carver, Inc., Summit, NJ) to form a 1.2 cm diameter compact. All compacts were inspected for cracks on the surface. If any imperfections were seen, the compact was not used in the experiments. Sometimes an entire compact would detach from the rotating disk die upon almost immediately after being submerged in the solvent. If this occurred, compact compression conditions were changed to prevent this from occurring. Studies looking at compact compression conditions and dissolution rate have found that different compact compression conditions for CBZ:NCT did not significantly affect the dissolution rate (Spong 2005). Table 4-1 shows the compression conditions used for CBZ and CBZ:NCT in each solvent.

Dissolution Experiments:

Intrinsic dissolution rates of CBZ(III) and CBZ:NCT in ethanol, 2-propanol and ethyl acetate were determined with rotating disk experiments. Experiments were conducted in a jacketed beaker containing 250 mL of solvent. The solvent was maintained at 25 °C with a circulating temperature bath running through the jacketed beaker. The rotating disk was attached to an overhead synchronous motor (Cole-Parmer Scientific, Niles, IL) and rotated at 100 rpm. A Servodyne Mixer Controller (Cole-Parmer Scientific, Niles, IL) was used to control and monitor the rotation speed of the

disk. A lid for the jacketed beaker and parafilm were used to prevent evaporation of solvent. Samples of 0.5 mL were taken from the dissolution medium at three minute intervals for 30 minutes. The amount of dissolution medium taken out for sampling was replaced with the same amount of pure solvent. Samples taken from the dissolution media were filtered with a 0.22 μm nylon filter and directly analyzed with high performance liquid chromotagraphy (HPLC). All experiments were done in triplicate, except for the CBZ:NCT dissolution experiments in ethanol, which were repeated four times.

High Performance Liquid Chromatography (HPLC):

The HPLC instrument (Waters, Milford, Massachusetts) was equipped with a UV diode array detector (Waters, Milford, Massachusetts) and contained a Xterra™ C_{18} (5 μm particle size, 6 x 250 mm) column (Waters, Milford, Massachusetts). The maximum wavelength for absorbance for CBZ was set to 285.1 nm. The maximum wavelength for absorbance for NCT was set to 260.7 nm. A 12 minute isocratic method was used. The mobile phase consisted of 70/30 water/acetonitrile with 0.1% trifluoroacetic acid and ran at a flow rate of 1 mL/min. The injection volume was 25 μL. Each sample was injected twice and the values obtained from the two injections were averaged. .

Statistical Analysis

A student's t-test was used to test statistically whether a difference between the predicted and measured relative rates of dissolution was observed.

Solubility, K_{sp} and $K_{1:1}$ Values

Solubilities for CBZ, NCT, and CBZ:NCT in ethanol, 2-propranol, and ethyl acetate are reported elsewhere (Nehm, Rodriguez-Spong et al. 2006) and listed in Table 4-2. Ksp and K1:1 values for CBZ:NCT for the three organic solvents are also reported (Nehm, Rodriguez-Spong et al. 2006) and listed in Table 4-3.

Mathematical Modeling of Phase Solubility Diagrams

Mathematical models that consider equilibria and solid state complex have been reported elsewhere (Nehm, Rodriguez-Spong et al. 2006). For the present analysis, mass balances were done starting with cocrystal components rather than cocrystal. The equations that describe phase solubility diagrams for 1:1 and 1:2 cocrystals where complexes form in solution are given in the appendix.

Results and Discussion

Theoretical phase solubility diagrams for CBZ:NCT cocrystal as a function of the ligand (NCT) are plotted with reported CBZ:NCT cocrystal solubility values in ethanol, 2-propanolol, and ethyl acetate solutions in Figures 4-1, 4-2, and 4-3, respectively. Solubility studies conducted by Nehm et al. show that addition of the ligand, NCT, in excess of the stoichiometric composition reduces the solubility of CBZ:NCT cocrystal in three organic solvents. Since the solubility studies were conducted with CBZ:NCT cocrystal in pure solvent or in NCT solutions, NCT was always either equal to or in excess of the stoichiometric composition. Solubility experiments where NCT was below the stoichiometric composition have not been conducted. In solutions where soluble complexes form, theoretical phase solubility diagrams suggest that decreasing NCT

below the stoichiometric composition would increase the solubility of CBZ:NCT cocrystal. Therefore decreasing the ligand concentration below the stoichiometric composition in the unstirred diffusion layer during dissolution is a possible mechanism to achieve higher dissolution rates for 1:1 cocrystals than predicted by equation 2. During the dissolution of 1:1 cocrystals, nonstoichiometric conditions may occur in the unstirred layer due to the difference in diffusion rates between the free cocrystal components through the unstirred layer. The diffusion coefficient for each species in the unstirred layer can be estimated using the Stokes-Einstein equation:

$$D = \frac{k_B T}{6\pi\eta r} \qquad (4.21)$$

where k_B = Boltzman constant, T = temperature, η = viscosity of the suspending fluid, and r = radius of sphere.

Rewriting the Stokes-Einstein equation in terms of mass gives:

$$D = \frac{k_B T}{6\pi\eta \cdot \left(\frac{3}{4\pi} \cdot \frac{m}{\rho}\right)^{1/3}} \qquad (4.22)$$

where m = mass and ρ = density

Assuming $\rho_1 = \rho_2$, the ratio of the cocrystal component diffusion coefficients can be determined from:

$$\frac{D_1}{D_2} = \frac{\dfrac{k_B T}{6\pi\eta\left(\frac{3}{4\pi} \cdot \frac{m_1}{\rho_1}\right)^{1/3}}}{\dfrac{k_B T}{6\pi\eta\left(\frac{3}{4\pi} \cdot \frac{m_2}{\rho_2}\right)^{1/3}}} = \left(\frac{m_2}{m_1}\right)^{1/3} \qquad (4.23)$$

The ratio of carbemazepine to nicotinamide diffusion coefficients using equation 25 is 0.80.

Theoretical and experimental relative dissolution rates between cocrystal CBZ:NCT (1:1) and single component crystal CBZ in three organic solvents are presented in Table 4-4. The theoretical relative dissolution rates were calculated using the ratio of stoichiometric CBZ:NCT cocrystal solubility to single CBZ crystal solubility. Although differences between the experimental and theoretical relative dissolution rates were observed in all three solvents, the differences were found not to be statistically significant. To detect a statistically significant difference in the relative dissolution rates a much greater change in dissolution rates than what was observed in the described experiments are necessary.

Summary

Theoretical phase solubility diagrams for CBZ:NCT cocrystals in organic solvents show that cocrystal solubility can either increase or decrease when the ligand, NCT, concentration differs from the stoichiometric composition. If non-stoichiometric cocrystal solubilities exist in the unstirred boundary layer during dissolution, relative dissolution rates determined experimentally would be expected to deviate from equation 2. However, results of preliminary experiments described above do not show a statistically significant difference between relative dissolution rates determined experimentally and equation 2. The lack of a statistically significant result may be due to the small differences in diffusion coefficients between carbamazepine and nicotinamide.

Dissolution studies with other cocrystals in different solvent systems may demonstrate greater increases in the rates of dissolution for cocrystal compared to the API.

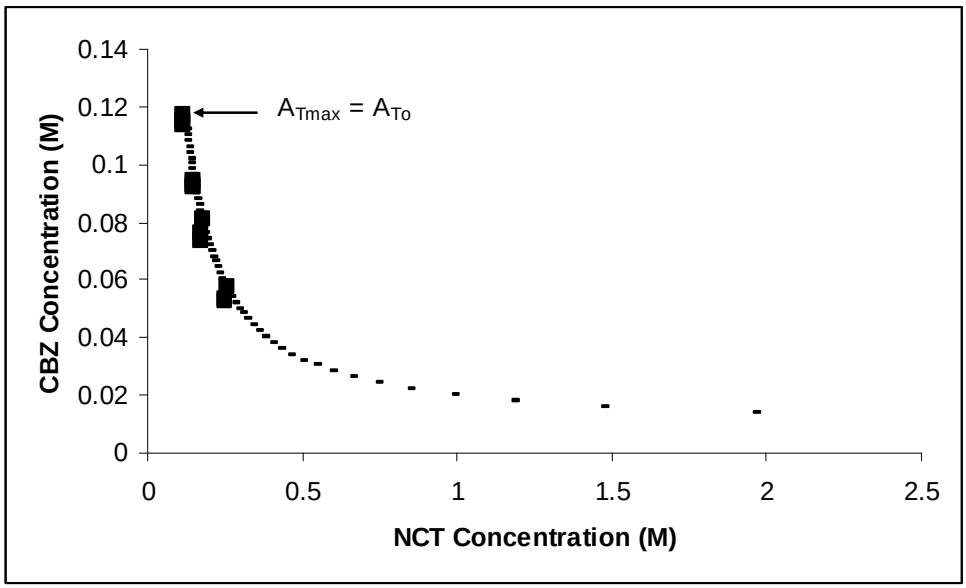

Figure 4-1 Theoretical phase solubility diagram of CBZ:NCT in ethanol at 25 ºC (---) overlayed on experimental measurements (■) from (Nehm, Rodriguez-Spong et al. 2006).

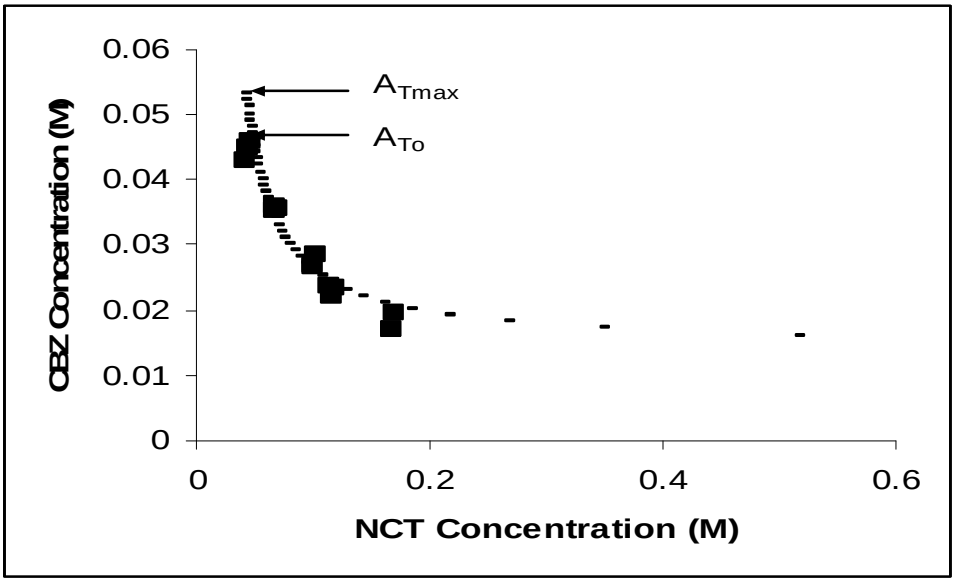

Figure 4-2 Theoretical phase solubility diagram of CBZ:NCT in 2-propanol at 25 ºC (---) overlayed on experimental measurements (■) from (Nehm, Rodriguez-Spong et al. 2006).

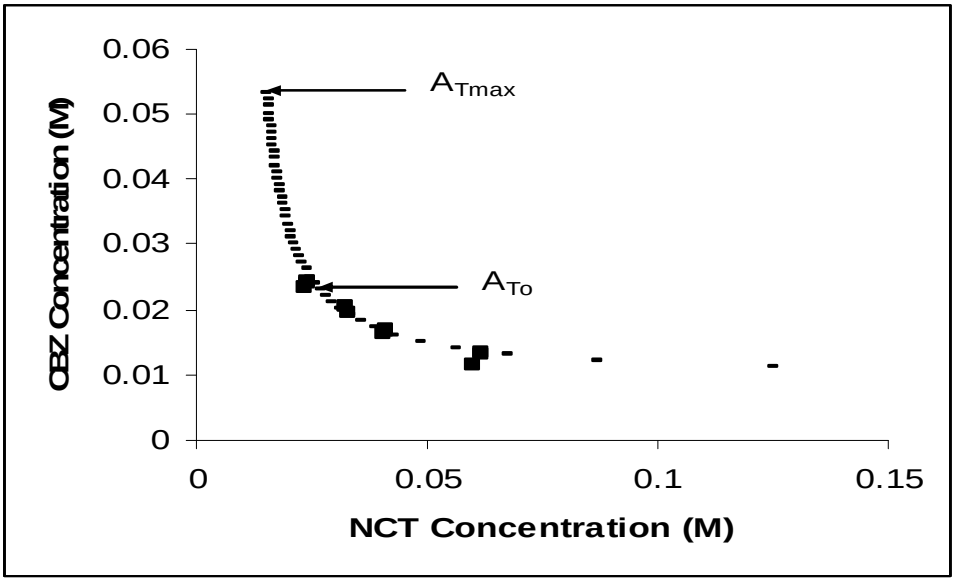

Figure 4-3 Theoretical phase solubility diagram of CBZ:NCT in ethyl acetate at 25 ºC (---) overlayed on experimental measurements (■) from (Nehm, Rodriguez-Spong et al. 2006).

Table 4-1: Compression conditions for compact formation.

Compact	Ethanol	Ethyl Acetate	2-propanol
CBZ (80 mg)	5000 psi for 30 min	5000 psi for 30 min	4500 psi for 30 min
CBZ:NCT (80 mg)	2000 psi for 15 min	3000 psi for 30 min	5000 psi for 30 min

Table 4-2 Solubilities of CBZ:NCT, CBZ(III) and NCT in three organic solvents at 25 °C. Data from (Nehm, Rodriguez-Spong et al. 2006).

compound	ethanol (M)	2-propanol (M)	ethyl acetate (M)
CBZ/NCT (1:1)	$0.116^{b} \pm 0.003$	$0.044^{c} \pm 0.003$	$0.024^{d} \pm 0.001$
CBZ(III)	$0.1080^{b} \pm 0.0001$	$0.039^{c,e} \pm 0.003$	$0.0440^{d,e} \pm 0.0001$
NCT(I)	0.841 ± 0.008	0.496 ± 0.004	0.098 ± 0.002

[a] Solubility values are the mean ± standard deviation of $n = 3$. [b] Statistically significant difference in solubilties, $P < 0.05$. [c] Statistically insignificant difference in solubilities, $P > 0.10$. [d] Statistically significant difference in solubilities, $P < 0.001$. [e] Statistically insignificant difference in solubilities, $P > 0.05$.

Table 4-3 K_{sp} and $K_{1:1}$ for CBZ:NCT in three organic solvents at 25 ºC. Data from (Nehm, Rodriguez-Spong et al. 2006).

solvent	K_{sp} (M^2)	K_{11} (M^{-1})
ethanol	0.0129 ± 0.0006^a	0.3 ± 0.3^a
2-propanol	0.0016 ± 0.0001	6.3 ± 0.7
ethyl acetate	0.00045 ± 0.00003	12.7 ± 1.8

[a] Standard error in each solvent system.

Table 4-4: Comparison of estimated $\left(\frac{A_{To}^{*}}{S_A^{*}}\right)$ and experimental $\left(\frac{DR_{AB}}{DR_A}\right)$ relative dissolution rates in three organic solvents at 25 ºC.

Solvent	$\frac{A_{To}^{*}}{S_A^{*}}$	$\frac{DR_{AB}}{DR_A}$	% Difference from $\frac{A_{To}}{S_A}$
Ethanol	1.074 ± 0.028[a]	0.848 ± 0.170[a]	-20%
Ethyl Acetate	0.545 ± 0.023[b]	0.473 ± 0.206[b]	-15%
2-propanol	1.128 ± 0.116[c]	1.286 ± 0.176[c]	+14%

[a] Statistically insignificant difference in ratios, p-value > 0.05. [b] Statistically insignificant difference in ratios, p-value > 0.05. [c] Statistically insignificant difference in ratios, p-value > 0.05. [*] A_{To} and S_A data from (Nehm, Rodriguez-Spong et al. 2006).

References

Berge, S. M., et al. (1977). "Pharmaceutical Salts." Journal of Pharmaceutical Sciences **66**(1): 1-19.

Brader, M. L., et al. (2002). "Hybrid insulin cocrystals for controlled release delivery." Nature Biotechnology **20**(8): 800-804.

Brunner, E. (1904). "Reaction rate in heterogenous systems." Zeitschrift Fur Physikalische Chemie--Stochiometrie Und Verwandtschaftslehre **47**(1): 56-102.

Childs, S. L., et al. (2004). "Crystal engineering approach to forming cocrystals of amine hydrochlorides with organic acids. Molecular complexes of fluoxetine hydrochloride with benzoic, succinic, and fumaric acids." Journal of the American Chemical Society **126**(41): 13335-13342.

Higuchi, T. and I. H. Pitman (1973). "Caffeine Complexes with Low Water Solubility - Synthesis and Dissolution Rates of 1-1 and 1-2 Caffeine-Gentisic Acid Complexes." Journal of Pharmaceutical Sciences **62**(1): 55-58.

Huang, L. F. and W. Q. Tong (2004). "Impact of solid state properties on developability assessment of drug candidates." Advanced Drug Delivery Reviews **56**(3): 321-334.

McNamara, D. P., et al. (2006). "Use of a glutaric acid cocrystal to improve oral bioavailability of a low solubility API." Pharmaceutical Research **23**(8): 1888-1897.

Nehm, S. J., et al. (2006). "Phase solubility diagrams of cocrystals are explained by solubility product and solution complexation." Crystal Growth & Design **6**(2): 592-600.

Nernst, N. (1904). "Theory on the reaction rate in heterogenous systems." Zeitschrift Fur Physikalische Chemie--Stochiometrie Und Verwandtschaftslehre **47**(1): 52-55.

Remenar, J. F., et al. (2003). "Crystal engineering of novel cocrystals of a triazole drug with 1,4-dicarboxylic acids." Journal of the American Chemical Society **125**(28): 8456-8457.

Rodriguez-Spong, B., et al. (2004). "General principles of pharmaceutical solid polymorphism: a supramolecular perspective." Advanced Drug Delivery Reviews **56**(3): 241-274.

Spong, B. R. (2005). Enhancing the pharmaceutical behavior of poorly soluble drugs through the formation of cocrystals and mesophases. Ph.D. Thesis, University of Michigan.

Stahly, G. P. (2007). "Diversity in single- and multiple-component crystals. The search for and prevalence of polymorphs and cocrystals." Crystal Growth & Design **7**(6): 1007-1026.

Chapter V

Conclusions

An oral absorption model, the Pulsatile Emptying and Transit (PET) model, was developed to take into account the effects of variable gastrointestinal motility on oral absorption. When coupled to a compartmental pharmacokinetic model, simulations with the PET model suggested that the maximum plasma concentration (C_{max}) of drugs with effective permeabilities less than 0.04 cm/min would not be significantly affected (less than 10%) by the phase of the MMC in which the drug was dosed. Also, for drugs with dissolution rates where less than 85% of the dose dissolves within 15 minutes, C_{max} is not significantly affected by the phase of the MMC in which the drug was dosed. C_{max} is a measure of bioequivalence used to evaluate how quickly the drug is absorbed. In summary, the results of the simulations suggest that the MMC will not significantly affect the rate of drug absorption unless the drug has an extremely high effective permeability and rapid dissolution rate.

The PET model was also used to examine the appearance and absence of double peaks in oral ranitidine plasma concentration-time profiles. Simulations with a region dependent permeability PET model with compartmental PK support discontinuous absorption sites as an explanation for the appearance of double peaks in ranitidine plasma concentration-time profiles. Simulations also suggest that single peaks may occur when drug is dosed during phase III of the migrating motor complex. When drug is dosed during phase III, absorption in the duodenum, a high absorption site, may be bypassed

resulting in a single peak. Since phase III makes up roughly 15% of the MMC cycle, single peak plasma concentration-time profiles are expected to appear infrequently. Simulations with the PET model show that similarly shaped concentration-time profiles can be expected for the same individual the majority of the time. For an individual, simulations show that the height and timing of peaks in plasma concentration-time profiles can differ depending on the phase of dosing; however, the general shape of the double peaks is similar. Exceptions occurred when simulations produced single peak plasma concentration curves when ranitidine was dosed during phase III of the MMC.

In the ranitidine simulations, although the plasma concentration levels are similar to those observed in patients, the times of the dip between the double peaks in the simulations (1.5 hours after dosing) tended to occur earlier than those observed in patients (2-3 hours after dosing). A possible reason for this inconsistency between the simulated and observed plasma concentration-time profiles is that in the model, the jejunum permeability was the same way throughout the whole jejunum. However, the decrease in ranitidine permeability in the jejunum occurs after the proximal jejunum. Therefore dividing the jejunum into a proximal and distal region in the model may give simulations that better coincide with the timing of the dip in the observed plasma concentration-time profile.

In addition to modeling oral absorption, solubility product and solution complexation relationships were used to model preliminary cocrystal dissolution studies Theoretical phase solubility diagrams for CBZ:NCT cocrystals in organic solvents showed that cocrystal solubility can either increase or decrease when the ligand, NCT, concentration differs from the stoichiometric composition. If non-stoichiometric

cocrystal solubilities exist in the unstirred boundary layer during dissolution, relative dissolution rates determined experimentally would be expected to deviate from the ratio of the stoichiometric CBZ:NCT cocrystal solubility and CBZ(III) solubility . However, results of the preliminary dissolution experiments did not show a statistically significant difference between relative dissolution rates determined experimentally and the ratio of the stoichiometric CBZ:NCT cocrystal solubility and CBZ(III) solubility. The lack of a statistically significant result may be due to the small differences in diffusion coefficients between carbamazepine and nicotinamide. Dissolution studies with other cocrystals in different solvent systems may demonstrate greater increases in the rates of dissolution for cocrystal compared to the API.

Appendices

Appendix A

Parameter values used for simulations in Chapter II

Figure	Dose (mg)	Cs (mg/mL)	Peff (cm/min)	tlag (min)	b	A (1/min)	TTPIII (min)	Cyclelength (min)	Fraction Unmet	k12 (1/min)	k21 (1/min)	kout (1/min)	Vc (mL)
2-7a	40	33	0.01746	0	1.94	100	80	150	0.219	0.09767	0.0215	0.0245	51.76
2-7b	40	33	0.01746	0	1.94	100	18	150	0.219	0.09767	0.0215	0.0245	51.76

Figure	Dose (mg)	Cs (mg/mL)	Peff (cm/min)	tlag (min)	b	A (1/min)	TTPIII (min)	Cyclelength (min)	Fraction Unmet	k12 (1/min)	k21 (1/min)	kout (1/min)	Vc (mL)
2-8	40	33	0.1	0	1.28	100	0	150	0.219	0.09767	0.0215	0.0245	51.76
2-8	40	33	0.1	0	1.28	100	2	150	0.219	0.09767	0.0215	0.0245	51.76
2.8	40	33	0.1	0	1.28	100	5	150	0.219	0.09767	0.0215	0.0245	51.76
2-8	40	33	0.1	0	1.28	100	7	150	0.219	0.09767	0.0215	0.0245	51.76
2-8	40	33	0.1	0	1.28	100	10	150	0.219	0.09767	0.0215	0.0245	51.76
2.8	40	33	0.1	0	1.28	100	15	150	0.219	0.09767	0.0215	0.0245	51.76
2-8	40	33	0.1	0	1.28	100	20	150	0.219	0.09767	0.0215	0.0245	51.76
2-8	40	33	0.1	0	1.28	100	22	150	0.219	0.09767	0.0215	0.0245	51.76
2.8	40	33	0.1	0	1.28	100	25	150	0.219	0.09767	0.0215	0.0245	51.76
2-8	40	33	0.1	0	1.28	100	27	150	0.219	0.09767	0.0215	0.0245	51.76
2-8	40	33	0.1	0	1.28	100	30	150	0.219	0.09767	0.0215	0.0245	51.76
2.8	40	33	0.1	0	1.28	100	40	150	0.219	0.09767	0.0215	0.0245	51.76
2-8	40	33	0.1	0	1.28	100	80	150	0.219	0.09767	0.0215	0.0245	51.76
2-8	40	33	0.1	0	1.28	100	150	150	0.219	0.09767	0.0215	0.0245	51.76
2-8	40	33	0.1	0	1.54	100	0	150	0.219	0.09767	0.0215	0.0245	51.76
2-8	40	33	0.1	0	1.54	100	2	150	0.219	0.09767	0.0215	0.0245	51.76
2.8	40	33	0.1	0	1.54	100	5	150	0.219	0.09767	0.0215	0.0245	51.76
2-8	40	33	0.1	0	1.54	100	7	150	0.219	0.09767	0.0215	0.0245	51.76
2-8	40	33	0.1	0	1.54	100	10	150	0.219	0.09767	0.0215	0.0245	51.76
2.8	40	33	0.1	0	1.54	100	15	150	0.219	0.09767	0.0215	0.0245	51.76

Figure	Dose (mg)	Cs (mg/mL)	Peff (cm/min)	tlag (min)	b	A (1/min)	TTPIII (min)	Cyclelength (min)	Fraction Unmet	k12 (1/min)	k21 (1/min)	kout (1/min)	Vc (mL)
2-8	40	33	0.1	0	1.54	100	20	150	0.219	0.09767	0.0215	0.0245	51.76
2-8	40	33	0.1	0	1.54	100	22	150	0.219	0.09767	0.0215	0.0245	51.76
2.8	40	33	0.1	0	1.54	100	25	150	0.219	0.09767	0.0215	0.0245	51.76
2-8	40	33	0.1	0	1.54	100	27	150	0.219	0.09767	0.0215	0.0245	51.76
2-8	40	33	0.1	0	1.54	100	30	150	0.219	0.09767	0.0215	0.0245	51.76
2.8	40	33	0.1	0	1.54	100	40	150	0.219	0.09767	0.0215	0.0245	51.76
2-8	40	33	0.1	0	1.54	100	80	150	0.219	0.09767	0.0215	0.0245	51.76
2-8	40	33	0.1	0	1.54	100	150	150	0.219	0.09767	0.0215	0.0245	51.76
2-8	40	33	0.1	0	1.94	100	0	150	0.219	0.09767	0.0215	0.0245	51.76
2-8	40	33	0.1	0	1.94	100	2	150	0.219	0.09767	0.0215	0.0245	51.76
2.8	40	33	0.1	0	1.94	100	5	150	0.219	0.09767	0.0215	0.0245	51.76
2-8	40	33	0.1	0	1.94	100	7	150	0.219	0.09767	0.0215	0.0245	51.76
2-8	40	33	0.1	0	1.94	100	10	150	0.219	0.09767	0.0215	0.0245	51.76
2.8	40	33	0.1	0	1.94	100	15	150	0.219	0.09767	0.0215	0.0245	51.76
2-8	40	33	0.1	0	1.94	100	20	150	0.219	0.09767	0.0215	0.0245	51.76
2-8	40	33	0.1	0	1.94	100	22	150	0.219	0.09767	0.0215	0.0245	51.76
2.8	40	33	0.1	0	1.94	100	25	150	0.219	0.09767	0.0215	0.0245	51.76
2-8	40	33	0.1	0	1.94	100	27	150	0.219	0.09767	0.0215	0.0245	51.76
2-8	40	33	0.1	0	1.94	100	30	150	0.219	0.09767	0.0215	0.0245	51.76
2.8	40	33	0.1	0	1.94	100	40	150	0.219	0.09767	0.0215	0.0245	51.76
2-8	40	33	0.1	0	1.94	100	80	150	0.219	0.09767	0.0215	0.0245	51.76
2-8	40	33	0.1	0	1.94	100	150	150	0.219	0.09767	0.0215	0.0245	51.76
2-8	40	33	0.1	0	2.28	100	0	150	0.219	0.09767	0.0215	0.0245	51.76
2-8	40	33	0.1	0	2.28	100	2	150	0.219	0.09767	0.0215	0.0245	51.76
2.8	40	33	0.1	0	2.28	100	5	150	0.219	0.09767	0.0215	0.0245	51.76
2-8	40	33	0.1	0	2.28	100	7	150	0.219	0.09767	0.0215	0.0245	51.76
2-8	40	33	0.1	0	2.28	100	10	150	0.219	0.09767	0.0215	0.0245	51.76
2.8	40	33	0.1	0	2.28	100	15	150	0.219	0.09767	0.0215	0.0245	51.76
2-8	40	33	0.1	0	2.28	100	20	150	0.219	0.09767	0.0215	0.0245	51.76
2-8	40	33	0.1	0	2.28	100	22	150	0.219	0.09767	0.0215	0.0245	51.76

Figure	Dose (mg)	Cs (mg/mL)	Peff (cm/min)	tlag (min)	b	A (1/min)	TTPIII (min)	Cyclelength (min)	Fraction Unmet	k12 (1/min)	k21 (1/min)	kout (1/min)	Vc (mL)
2.8	40	33	0.1	0	2.28	100	25	150	0.219	0.09767	0.0215	0.0245	51.76
2-8	40	33	0.1	0	2.28	100	27	150	0.219	0.09767	0.0215	0.0245	51.76
2-8	40	33	0.1	0	2.28	100	30	150	0.219	0.09767	0.0215	0.0245	51.76
2.8	40	33	0.1	0	2.28	100	40	150	0.219	0.09767	0.0215	0.0245	51.76
2-8	40	33	0.1	0	2.28	100	80	150	0.219	0.09767	0.0215	0.0245	51.76
2-8	40	33	0.1	0	2.28	100	150	150	0.219	0.09767	0.0215	0.0245	51.76
2-8	40	33	0.1	0	3.26	100	0	150	0.219	0.09767	0.0215	0.0245	51.76
2-8	40	33	0.1	0	3.26	100	2	150	0.219	0.09767	0.0215	0.0245	51.76
2.8	40	33	0.1	0	3.26	100	5	150	0.219	0.09767	0.0215	0.0245	51.76
2-8	40	33	0.1	0	3.26	100	7	150	0.219	0.09767	0.0215	0.0245	51.76
2-8	40	33	0.1	0	3.26	100	10	150	0.219	0.09767	0.0215	0.0245	51.76
2.8	40	33	0.1	0	3.26	100	15	150	0.219	0.09767	0.0215	0.0245	51.76
2-8	40	33	0.1	0	3.26	100	20	150	0.219	0.09767	0.0215	0.0245	51.76
2-8	40	33	0.1	0	3.26	100	22	150	0.219	0.09767	0.0215	0.0245	51.76
2.8	40	33	0.1	0	3.26	100	25	150	0.219	0.09767	0.0215	0.0245	51.76
2-8	40	33	0.1	0	3.26	100	27	150	0.219	0.09767	0.0215	0.0245	51.76
2-8	40	33	0.1	0	3.26	100	30	150	0.219	0.09767	0.0215	0.0245	51.76
2.8	40	33	0.1	0	3.26	100	40	150	0.219	0.09767	0.0215	0.0245	51.76
2-8	40	33	0.1	0	3.26	100	80	150	0.219	0.09767	0.0215	0.0245	51.76
2-8	40	33	0.1	0	3.26	100	150	150	0.219	0.09767	0.0215	0.0245	51.76
2-8	40	33	0.1	0	5.72	100	0	150	0.219	0.09767	0.0215	0.0245	51.76
2-8	40	33	0.1	0	5.72	100	2	150	0.219	0.09767	0.0215	0.0245	51.76
2.8	40	33	0.1	0	5.72	100	5	150	0.219	0.09767	0.0215	0.0245	51.76
2-8	40	33	0.1	0	5.72	100	7	150	0.219	0.09767	0.0215	0.0245	51.76
2-8	40	33	0.1	0	5.72	100	10	150	0.219	0.09767	0.0215	0.0245	51.76
2.8	40	33	0.1	0	5.72	100	15	150	0.219	0.09767	0.0215	0.0245	51.76
2-8	40	33	0.1	0	5.72	100	20	150	0.219	0.09767	0.0215	0.0245	51.76
2-8	40	33	0.1	0	5.72	100	22	150	0.219	0.09767	0.0215	0.0245	51.76
2.8	40	33	0.1	0	5.72	100	25	150	0.219	0.09767	0.0215	0.0245	51.76
2-8	40	33	0.1	0	5.72	100	27	150	0.219	0.09767	0.0215	0.0245	51.76

Figure	Dose (mg)	Cs (mg/mL)	Peff (cm/min)	tlag (min)	b	A (1/min)	TTPIII (min)	Cyclelength (min)	Fraction Unmet	k12 (1/min)	k21 (1/min)	kout (1/min)	Vc (mL)
2-8	40	33	0.1	0	5.72	100	30	150	0.219	0.09767	0.0215	0.0245	51.76
2.8	40	33	0.1	0	5.72	100	40	150	0.219	0.09767	0.0215	0.0245	51.76
2-8	40	33	0.1	0	5.72	100	80	150	0.219	0.09767	0.0215	0.0245	51.76
2-8	40	33	0.1	0	5.72	100	150	150	0.219	0.09767	0.0215	0.0245	51.76

Figure	Dose (mg)	Cs (mg/mL)	Peff (cm/min)	tlag (min)	b	A (1/min)	TTPIII (min)	Cyclelength (min)	Fraction Unmet	k12 (1/min)	k21 (1/min)	kout (1/min)	Vc (mL)
2-9	40	33	0.008	0	8	100	0	150	0.219	0.09767	0.0215	0.0245	51.76
2-9	40	33	0.008	0	8	100	2	150	0.219	0.09767	0.0215	0.0245	51.76
2-9	40	33	0.008	0	8	100	5	150	0.219	0.09767	0.0215	0.0245	51.76
2-9	40	33	0.008	0	8	100	7	150	0.219	0.09767	0.0215	0.0245	51.76
2-9	40	33	0.008	0	8	100	10	150	0.219	0.09767	0.0215	0.0245	51.76
2.9	40	33	0.008	0	8	100	15	150	0.219	0.09767	0.0215	0.0245	51.76
2-9	40	33	0.008	0	8	100	20	150	0.219	0.09767	0.0215	0.0245	51.76
2-9	40	33	0.008	0	8	100	22	150	0.219	0.09767	0.0215	0.0245	51.76
2-9	40	33	0.008	0	8	100	25	150	0.219	0.09767	0.0215	0.0245	51.76
2-9	40	33	0.008	0	8	100	27	150	0.219	0.09767	0.0215	0.0245	51.76
2-9	40	33	0.008	0	8	100	30	150	0.219	0.09767	0.0215	0.0245	51.76
2-9	40	33	0.008	0	8	100	40	150	0.219	0.09767	0.0215	0.0245	51.76
2.9	40	33	0.008	0	8	100	80	150	0.219	0.09767	0.0215	0.0245	51.76
2-9	40	33	0.008	0	8	100	150	150	0.219	0.09767	0.0215	0.0245	51.76
2-9	40	33	0.01	0	8	100	0	150	0.219	0.09767	0.0215	0.0245	51.76
2-9	40	33	0.01	0	8	100	2	150	0.219	0.09767	0.0215	0.0245	51.76
2-9	40	33	0.01	0	8	100	5	150	0.219	0.09767	0.0215	0.0245	51.76
2-9	40	33	0.01	0	8	100	7	150	0.219	0.09767	0.0215	0.0245	51.76
2-9	40	33	0.01	0	8	100	10	150	0.219	0.09767	0.0215	0.0245	51.76
2.9	40	33	0.01	0	8	100	15	150	0.219	0.09767	0.0215	0.0245	51.76
2-9	40	33	0.01	0	8	100	20	150	0.219	0.09767	0.0215	0.0245	51.76

Figure	Dose (mg)	Cs (mg/mL)	Peff (cm/min)	tlag (min)	b	A (1/min)	TTPIII (min)	Cyclelength (min)	Fraction Unmet	k12 (1/min)	k21 (1/min)	kout (1/min)	Vc (mL)
2-9	40	33	0.01	0	8	100	22	150	0.219	0.09767	0.0215	0.0245	51.76
2-9	40	33	0.01	0	8	100	25	150	0.219	0.09767	0.0215	0.0245	51.76
2-9	40	33	0.01	0	8	100	27	150	0.219	0.09767	0.0215	0.0245	51.76
2-9	40	33	0.01	0	8	100	30	150	0.219	0.09767	0.0215	0.0245	51.76
2-9	40	33	0.01	0	8	100	40	150	0.219	0.09767	0.0215	0.0245	51.76
2.9	40	33	0.01	0	8	100	80	150	0.219	0.09767	0.0215	0.0245	51.76
2-9	40	33	0.01	0	8	100	150	150	0.219	0.09767	0.0215	0.0245	51.76
2-9	40	33	0.02	0	8	100	0	150	0.219	0.09767	0.0215	0.0245	51.76
2-9	40	33	0.02	0	8	100	2	150	0.219	0.09767	0.0215	0.0245	51.76
2-9	40	33	0.02	0	8	100	5	150	0.219	0.09767	0.0215	0.0245	51.76
2-9	40	33	0.02	0	8	100	7	150	0.219	0.09767	0.0215	0.0245	51.76
2-9	40	33	0.02	0	8	100	10	150	0.219	0.09767	0.0215	0.0245	51.76
2.9	40	33	0.02	0	8	100	15	150	0.219	0.09767	0.0215	0.0245	51.76
2-9	40	33	0.02	0	8	100	20	150	0.219	0.09767	0.0215	0.0245	51.76
2-9	40	33	0.02	0	8	100	22	150	0.219	0.09767	0.0215	0.0245	51.76
2-9	40	33	0.02	0	8	100	25	150	0.219	0.09767	0.0215	0.0245	51.76
2-9	40	33	0.02	0	8	100	27	150	0.219	0.09767	0.0215	0.0245	51.76
2-9	40	33	0.02	0	8	100	30	150	0.219	0.09767	0.0215	0.0245	51.76
2-9	40	33	0.02	0	8	100	40	150	0.219	0.09767	0.0215	0.0245	51.76
2.9	40	33	0.02	0	8	100	80	150	0.219	0.09767	0.0215	0.0245	51.76
2-9	40	33	0.02	0	8	100	150	150	0.219	0.09767	0.0215	0.0245	51.76
2-9	40	33	0.04	0	8	100	0	150	0.219	0.09767	0.0215	0.0245	51.76
2-9	40	33	0.04	0	8	100	2	150	0.219	0.09767	0.0215	0.0245	51.76
2-9	40	33	0.04	0	8	100	5	150	0.219	0.09767	0.0215	0.0245	51.76
2-9	40	33	0.04	0	8	100	7	150	0.219	0.09767	0.0215	0.0245	51.76
2-9	40	33	0.04	0	8	100	10	150	0.219	0.09767	0.0215	0.0245	51.76
2.9	40	33	0.04	0	8	100	15	150	0.219	0.09767	0.0215	0.0245	51.76
2-9	40	33	0.04	0	8	100	20	150	0.219	0.09767	0.0215	0.0245	51.76
2-9	40	33	0.04	0	8	100	22	150	0.219	0.09767	0.0215	0.0245	51.76
2-9	40	33	0.04	0	8	100	25	150	0.219	0.09767	0.0215	0.0245	51.76

Figure	Dose (mg)	Cs (mg/mL)	Peff (cm/min)	tlag (min)	b	A (1/min)	TTPIII (min)	Cyclelength (min)	Fraction Unmet	k12 (1/min)	k21 (1/min)	kout (1/min)	Vc (mL)
2-9	40	33	0.04	0	8	100	27	150	0.219	0.09767	0.0215	0.0245	51.76
2-9	40	33	0.04	0	8	100	30	150	0.219	0.09767	0.0215	0.0245	51.76
2-9	40	33	0.04	0	8	100	40	150	0.219	0.09767	0.0215	0.0245	51.76
2.9	40	33	0.04	0	8	100	80	150	0.219	0.09767	0.0215	0.0245	51.76
2-9	40	33	0.04	0	8	100	150	150	0.219	0.09767	0.0215	0.0245	51.76
2.9	40	33	0.06	0	3.26	100	0	150	0.219	0.09767	0.0215	0.0245	51.76
2-9	40	33	0.06	0	3.26	100	2	150	0.219	0.09767	0.0215	0.0245	51.76
2-9	40	33	0.06	0	3.26	100	5	150	0.219	0.09767	0.0215	0.0245	51.76
2-9	40	33	0.06	0	3.26	100	7	150	0.219	0.09767	0.0215	0.0245	51.76
2-9	40	33	0.06	0	3.26	100	10	150	0.219	0.09767	0.0215	0.0245	51.76
2-9	40	33	0.06	0	3.26	100	15	150	0.219	0.09767	0.0215	0.0245	51.76
2-9	40	33	0.06	0	3.26	100	20	150	0.219	0.09767	0.0215	0.0245	51.76
2.9	40	33	0.06	0	3.26	100	22	150	0.219	0.09767	0.0215	0.0245	51.76
2-9	40	33	0.06	0	3.26	100	25	150	0.219	0.09767	0.0215	0.0245	51.76
2-9	40	33	0.06	0	3.26	100	27	150	0.219	0.09767	0.0215	0.0245	51.76
2-9	40	33	0.06	0	3.26	100	30	150	0.219	0.09767	0.0215	0.0245	51.76
2-9	40	33	0.06	0	3.26	100	40	150	0.219	0.09767	0.0215	0.0245	51.76
2-9	40	33	0.06	0	3.26	100	80	150	0.219	0.09767	0.0215	0.0245	51.76
2-9	40	33	0.06	0	3.26	100	150	150	0.219	0.09767	0.0215	0.0245	51.76
2.9	40	33	0.08	0	5.72	100	0	150	0.219	0.09767	0.0215	0.0245	51.76
2-9	40	33	0.08	0	5.72	100	2	150	0.219	0.09767	0.0215	0.0245	51.76
2-9	40	33	0.08	0	5.72	100	5	150	0.219	0.09767	0.0215	0.0245	51.76
2-9	40	33	0.08	0	5.72	100	7	150	0.219	0.09767	0.0215	0.0245	51.76
2-9	40	33	0.08	0	5.72	100	10	150	0.219	0.09767	0.0215	0.0245	51.76
2-9	40	33	0.08	0	5.72	100	15	150	0.219	0.09767	0.0215	0.0245	51.76
2-9	40	33	0.08	0	5.72	100	20	150	0.219	0.09767	0.0215	0.0245	51.76
2.9	40	33	0.08	0	5.72	100	22	150	0.219	0.09767	0.0215	0.0245	51.76
2-9	40	33	0.08	0	5.72	100	25	150	0.219	0.09767	0.0215	0.0245	51.76
2-9	40	33	0.08	0	5.72	100	27	150	0.219	0.09767	0.0215	0.0245	51.76
2-9	40	33	0.08	0	5.72	100	30	150	0.219	0.09767	0.0215	0.0245	51.76

Figure	Dose (mg)	Cs (mg/mL)	Peff (cm/min)	tlag (min)	b	A (1/min)	TTPIII (min)	Cyclelength (min)	Fraction Unmet	k12 (1/min)	k21 (1/min)	kout (1/min)	Vc (mL)
2.9	40	33	0.08	0	5.72	100	40	150	0.219	0.09767	0.0215	0.0245	51.76
2-9	40	33	0.08	0	5.72	100	80	150	0.219	0.09767	0.0215	0.0245	51.76
2-9	40	33	0.08	0	5.72	100	150	150	0.219	0.09767	0.0215	0.0245	51.76
2.9	40	33	0.1	0	5.72	100	0	150	0.219	0.09767	0.0215	0.0245	51.76
2-9	40	33	0.1	0	5.72	100	2	150	0.219	0.09767	0.0215	0.0245	51.76
2-9	40	33	0.1	0	5.72	100	5	150	0.219	0.09767	0.0215	0.0245	51.76
2-9	40	33	0.1	0	5.72	100	7	150	0.219	0.09767	0.0215	0.0245	51.76
2-9	40	33	0.1	0	5.72	100	10	150	0.219	0.09767	0.0215	0.0245	51.76
2-9	40	33	0.1	0	5.72	100	15	150	0.219	0.09767	0.0215	0.0245	51.76
2-9	40	33	0.1	0	5.72	100	20	150	0.219	0.09767	0.0215	0.0245	51.76
2.9	40	33	0.1	0	5.72	100	22	150	0.219	0.09767	0.0215	0.0245	51.76
2-9	40	33	0.1	0	5.72	100	25	150	0.219	0.09767	0.0215	0.0245	51.76
2-9	40	33	0.1	0	5.72	100	27	150	0.219	0.09767	0.0215	0.0245	51.76
2-9	40	33	0.1	0	5.72	100	30	150	0.219	0.09767	0.0215	0.0245	51.76
2.9	40	33	0.1	0	5.72	100	40	150	0.219	0.09767	0.0215	0.0245	51.76
2-9	40	33	0.1	0	5.72	100	80	150	0.219	0.09767	0.0215	0.0245	51.76
2-9	40	33	0.1	0	5.72	100	150	150	0.219	0.09767	0.0215	0.0245	51.76

Appendix B

Parameter values used for simulations in Chapter III

Figure	Dose (mg)	Cs (mg/mL)	Peff duodenum/ jejunum/ ileum (cm/min)	tlag (min)	b	A (1/min)	TTPIII (min)	Cyclelength (min)	Fraction Unmet	k12 (1/min)	k21 (1/min)	kout (1/min)	Vc (mL)
3-2	150	100	0.01/ 0.00162/ 0.01	0	8	100	80	150	0.9	0.1047	0.037	0.0331	18.167
3-2	150	100	0.01/ 0.00162/ 0.01	0	8	100	60	150	0.9	0.1047	0.037	0.0331	18.167
3-2	150	100	0.01/ 0.00162/ 0.01	0	8	100	40	150	0.9	0.1047	0.037	0.0331	18.167
3-2	150	100	0.01/ 0.00162/ 0.01	0	8	100	20	150	0.9	0.1047	0.037	0.0331	18.167

Figure	Dose (mg)	Cs (mg/mL)	Peff duodenum/ jejunum/ ileum (cm/min)	tlag (min)	b	A (1/min)	TTPIII (min)	Cyclelength (min)	Fraction Unmet	k12 (1/min)	k21 (1/min)	kout (1/min)	Vc (mL)
3-3	150	100	0.01/ 0.00162/ 0.01	0	1.6	100	80	150	0.9	0.1047	0.037	0.0331	18.167
3-3	150	100	0.01/ 0.00162/ 0.01	0	1.4	100	80	150	0.9	0.1047	0.037	0.0331	18.167
3-3	150	100	0.01/ 0.00162/ 0.01	0	1.2	100	80	150	0.9	0.1047	0.037	0.0331	18.167
3-3	150	100	0.01/ 0.00162/ 0.01	0	1	100	80	150	0.9	0.1047	0.037	0.0331	18.167

Figure	Dose (mg)	Cs (mg/mL)	Peff duodenum/ jejunum/ ileum (cm/min)	tlag (min)	b	A (1/min)	TTPIII (min)	Cyclelength (min)	Fraction Unmet	k12 (1/min)	k21 (1/min)	kout (1/min)	Vc (mL)
3-4	150	100	0.01/ 0.00162/ 0.01	0	8	100	80	150	0.9	0.1047	0.037	0.0331	18.167
3-4	150	100	0.02/ 0.00162/ 0.01	0	8	100	80	150	0.9	0.1047	0.037	0.0331	18.167
3-4	150	100	0.03/ 0.00162/ 0.01	0	8	100	80	150	0.9	0.1047	0.037	0.0331	18.167
3-4	150	100	0.04/ 0.00162/ 0.01	0	8	100	80	150	0.9	0.1047	0.037	0.0331	18.167
3-4	150	100	0.05/ 0.00162/ 0.01	0	8	100	80	150	0.9	0.1047	0.037	0.0331	18.167

Figure	Dose (mg)	Cs (mg/mL)	Peff duodenum/ jejunum/ ileum (cm/min)	tlag (min)	b	A (1/min)	TTPIII (min)	Cyclelength (min)	Fraction Unmet	k12 (1/min)	k21 (1/min)	kout (1/min)	Vc (mL)
3-4	150	100	0.01/ 0.00162/ 0.01	0	8	100	80	150	0.9	0.1047	0.037	0.0331	18.167
3-4	150	100	0.02/ 0.00162/ 0.01	0	8	100	80	150	0.9	0.1047	0.037	0.0331	18.167
3-4	150	100	0.03/ 0.00162/ 0.01	0	8	100	80	150	0.9	0.1047	0.037	0.0331	18.167
3-4	150	100	0.04/ 0.00162/ 0.01	0	8	100	80	150	0.9	0.1047	0.037	0.0331	18.167
3-4	150	100	0.05/ 0.00162/ 0.01	0	8	100	80	150	0.9	0.1047	0.037	0.0331	18.167

Figure	Dose (mg)	Cs (mg/mL)	Peff duodenum/ jejunum/ ileum (cm/min)	tlag (min)	b	A (1/min)	TTPIII (min)	Cyclelength (min)	Fraction Unmet	k12 (1/min)	k21 (1/min)	kout (1/min)	Vc (mL)
3-5	150	100	0.01/ 0.00162/ 0.01	0	8	100	80	150	0.9	0.1047	0.037	0.0331	18.167
3-5	150	100	0.01/ 0.00162/ 0.02	0	8	100	80	150	0.9	0.1047	0.037	0.0331	18.167
3-5	150	100	0.01/ 0.00162/ 0.03	0	8	100	80	150	0.9	0.1047	0.037	0.0331	18.167
3-5	150	100	0.01/ 0.00162/ 0.04	0	8	100	80	150	0.9	0.1047	0.037	0.0331	18.167

Figure	Dose (mg)	Cs (mg/mL)	Peff duodenum/ jejunum/ ileum (cm/min)	tlag (min)	b	A (1/min)	TTPIII (min)	Cyclelength (min)	Fraction Unmet	k12 (1/min)	k21 (1/min)	kout (1/min)	Vc (mL)
3-6	150	100	0.01/ 0.00162/ 0.01	0	8	100	80	150	0.9	0.05	0.037	0.0331	18.167
3-6	150	100	0.01/ 0.00162/ 0.01	0	8	100	80	150	0.9	0.1047	0.037	0.0331	18.167
3-6	150	100	0.01/ 0.00162/ 0.01	0	8	100	80	150	0.9	0.15	0.037	0.0331	18.167

Figure	Dose (mg)	Cs (mg/mL)	Peff duodenum/ jejunum/ ileum (cm/min)	tlag (min)	b	A (1/min)	TTPIII (min)	Cyclelength (min)	Fraction Unmet	k12 (1/min)	k21 (1/min)	kout (1/min)	Vc (mL)
3-7	150	100	0.01/ 0.00162/ 0.01	0	8	100	80	150	0.9	0.1047	0.01	0.0331	18.167
3-7	150	100	0.01/ 0.00162/ 0.01	0	8	100	80	150	0.9	0.1047	0.037	0.0331	18.167
3-7	150	100	0.01/ 0.00162/ 0.01	0	8	100	80	150	0.9	0.1047	0.1	0.0331	18.167

Figure	Dose (mg)	Cs (mg/mL)	Peff duodenum/ jejunum/ ileum (cm/min)	tlag (min)	b	A (1/min)	TTPIII (min)	Cyclelength (min)	Fraction Unmet	k12 (1/min)	k21 (1/min)	kout (1/min)	Vc (mL)
3-8	150	100	0.01/ 0.00162/ 0.01	0	8	100	80	150	0.9	0.1047	0.037	0.01	18.167
3-8	150	100	0.01/ 0.00162/ 0.01	0	8	100	80	150	0.9	0.1047	0.037	0.0331	18.167
3-8	150	100	0.01/ 0.00162/ 0.01	0	8	100	80	150	0.9	0.1047	0.037	0.1	18.167

Figure	Dose (mg)	Cs (mg/mL)	Peff duodenum/ jejunum/ ileum (cm/min)	tlag (min)	b	A (1/min)	TTPIII (min)	Cyclelength (min)	Fraction Unmet	k12 (1/min)	k21 (1/min)	kout (1/min)	Vc (mL)
3-8	150	100	0.01/ 0.00162/ 0.01	0	8	100	80	150	0.9	0.1047	0.037	0.0331	10
3-8	150	100	0.01/ 0.00162/ 0.01	0	8	100	80	150	0.9	0.1047	0.037	0.0331	18.167
3-8	150	100	0.01/ 0.00162/ 0.01	0	8	100	80	150	0.9	0.1047	0.037	0.0331	30

Appendix C

Mathematical phase solubility diagrams

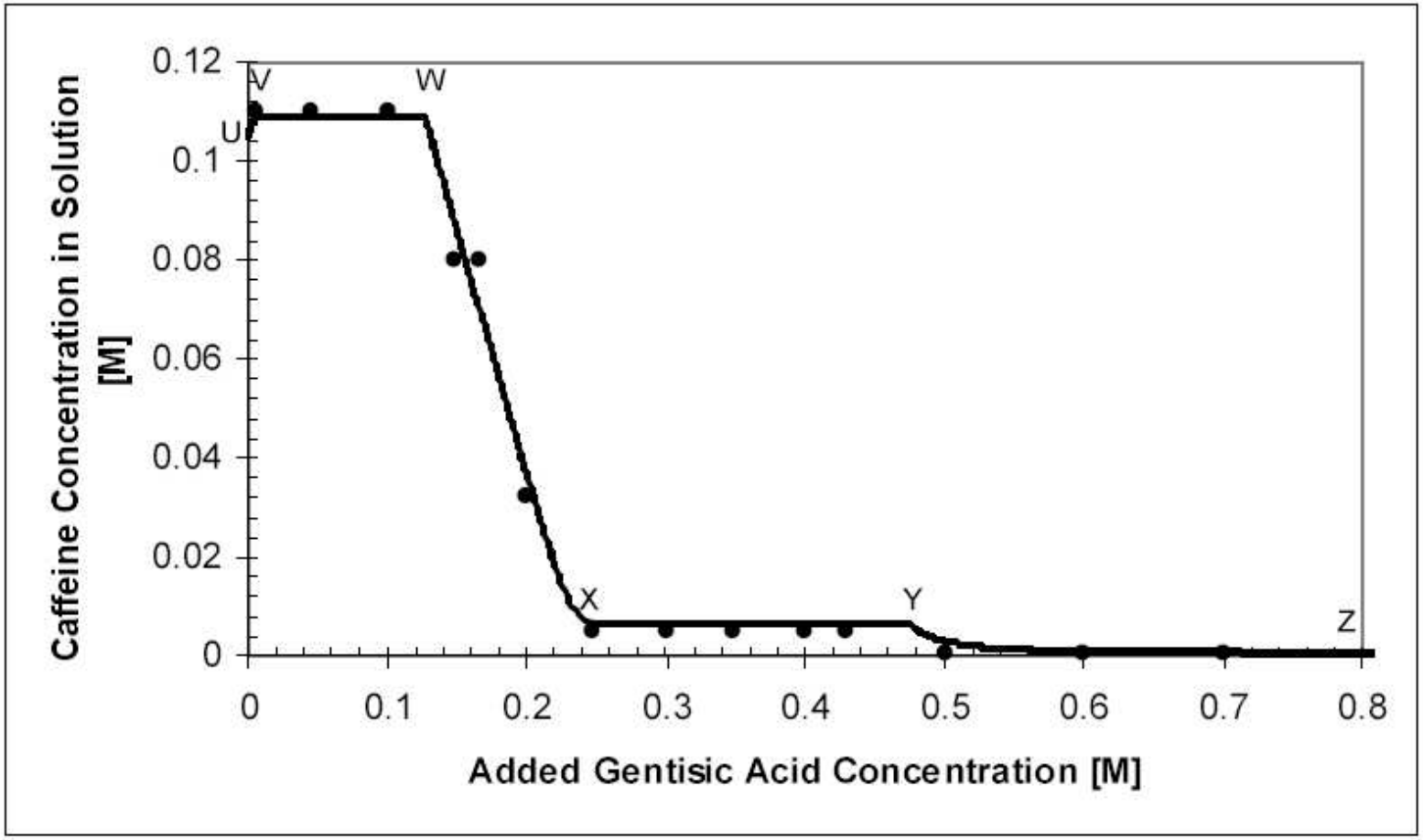

Figure C-1 Mathematical phase solubility diagram overlaid on data from (Higuchi and Pitman 1973)

Table C-1 Solid phases, solution phases, equilibria and equilibria equations in different regions of phase solubility diagram

	U-V	*V-W*	*W-X*	*X-Y*	*Y-Z*
Solid Phases	A	A, AB	AB	AB, AB_2	AB_2
Solution Phases	A, AB, AB_2	A, AB, AB_2	A, AB, AB_2	A, AB, AB_2	A, AB, AB_2
Equilibria	$A + B \overset{K_{sp,1}}{\rightleftharpoons} AB$ $AB + B \overset{K_{1,2}}{\rightleftharpoons} AB_2$	$AB \overset{K_{sp}}{\rightleftharpoons} A + B$ $A + B \overset{K_{1,1}}{\rightleftharpoons} AB$ $AB + B \overset{K_{1,2}}{\rightleftharpoons} AB_2$	$AB \overset{K_{sp}}{\rightleftharpoons} A + B$ $A + B \overset{K_{1,1}}{\rightleftharpoons} AB$ $AB + B \overset{K_{1,2}}{\rightleftharpoons} AB_2$	$AB \overset{K_{sp}}{\rightleftharpoons} A + B$ $AB_2 \overset{K_{sp}}{\rightleftharpoons} A + 2B$ $A + B \overset{K_{1,1}}{\rightleftharpoons} AB$ $AB + B \overset{K_{1,2}}{\rightleftharpoons} AB_2$	$AB_2 \overset{K_{sp}}{\rightleftharpoons} A + 2B$ $A + B \overset{K_{1,1}}{\rightleftharpoons} AB$ $AB + B \overset{K_{1,2}}{\rightleftharpoons} AB_2$
Equilibria Equations	$K_{1,1} = \frac{[AB]}{[A][B]}$ $K_{1,2} = \frac{[AB_2]}{[AB][B]}$	$K_{sp} = [A][B]$ $K_{1,1} = \frac{[AB]}{[A][B]}$ $K_{1,2} = \frac{[AB_2]}{[AB][B]}$	$K_{sp} = [A][B]$ $K_{1,1} = \frac{[AB]}{[A][B]}$ $K_{1,2} = \frac{[AB_2]}{[AB][B]}$	$K_{sp} = [A][B]$ $K_{sp,1,2} = [A][B]^2$ $K_{1,1} = \frac{[AB]}{[A][B]}$ $K_{1,2} = \frac{[AB_2]}{[AB][B]}$	$K_{sp,1,2} = [A][B]^2$ $K_{1,1} = \frac{[AB]}{[A][B]}$ $K_{1,2} = \frac{[AB_2]}{[AB][B]}$

Table C-2 Mass balance in different regions of phase solubility diagram

	U-V	V-W	W-X	X-Y	Y-Z
A_{Total} [moles]	$[A_{Tsoln}]\cdot Volume + A_{Insld}$	$[A_{Tsoln}]\cdot Volume + A_{Insld}$	$[A_{Tsoln}]\cdot Volume + A_{Insld}$	$[A_{Tsoln}]\cdot Volume + A_{Insld}$	$[A_{Tsoln}]\cdot Volume + A_{Insld}$
B_{Total} [moles]	$[B_{Tsoln}]\cdot Volume + B_{Insld}$	$[B_{Tsoln}]\cdot Volume + B_{Insld}$	$[B_{Tsoln}]\cdot Volume + B_{Insld}$	$[B_{Tsoln}]\cdot Volume + B_{Insld}$	$[B_{Tsoln}]\cdot Volume + B_{Insld}$
A_{Tsolid} [moles]	A	$A + AB$	AB	$AB + AB_2$	AB_2
B_{Tsolid} [moles]	0	AB	AB	$AB + 2AB_2$	$2AB_2$
$[A_{Tsoln}]$ [M]	$[A]+[AB]+[AB_2]$	$[A]+[AB]+[AB_2]$	$[A]+[AB]+[AB_2]$	$[A]+[AB]+[AB_2]$	$[A]+[AB]+[AB_2]$
$[B_{Tsoln}]$ [M]	$[B]+[AB]+2[AB_2]$	$[B]+[AB]+2[AB_2]$	$[B]+[AB]+2[AB_2]$	$[B]+[AB]+2[AB_2]$	$[B]+[AB]+2[AB_2]$
[A] [M]	$[A_o]$	$[A_o]$	$\frac{K_{sp}}{[B]}$	$\frac{K_{sp}^{\ 2}}{K_{sp,12}}$	$\frac{K_{sp,12}}{[B]^2}$
[AB] [M]	$K_{11}[A_o][B]$	$K_{11}K_{sp}$	$K_{11}K_{sp}$	$K_{11}K_{sp}$	$\frac{K_{11}K_{sp,12}}{[B]}$
$[AB_2]$ [M]	$K_{11}K_{12}[A_o][B]^2$	$\frac{K_{11}K_{12}K_{sp}^{\ 2}}{[A_o]}$	$K_{11}K_{12}K_{sp}[B]$	$K_{11}K_{12}K_{sp,12}$	$K_{11}K_{12}K_{sp,12}$
[B] [M]	$[B]$	$\frac{K_{sp}}{[A_o]}$	$[B]$	$\frac{K_{sp,12}}{K_{sp}}$	$[B]$

Table C-3 Parameters used for 1:2 Caffeine:Gentisic Acid phase solubility diagram

	Literature Values	*Revised Values*	*Calculated Values*	*Values Used For Phase Solubility Diagram*
A_{total} [moles]	2.317×10^{-3}	—	---	2.317×10^{-3}
Volume [mL]	10	—	---	10
A_0 [M]	0.105	—	---	0.105
$[AB_0]$ [M]	5×10^{-3}	4×10^{-3}	---	4×10^{-3}
$[AB_{2,0}]$ [M]	5×10^{-4}	—	---	5×10^{-4}
K_{sp} [M^2]	N/A	—	4×10^{-5}	4×10^{-5}
$K_{1:1}$ [1/M]	100	—	---	100
$K_{sp,1:2}$ [M^3]	N/A	—	3.2×10^{-6}	3.2×10^{-6}
$K_{1:2}$ [1/M]	NA	—	1.56	1.56

1:1 cocrystal stoichiometric solubility determination

species present in solution: A, B, AB

$$AB_{solid} \overset{K_{sp}}{\Leftrightarrow} A + B \overset{K_{1:1}}{\Leftrightarrow} AB_{so\ln}$$

Mass balance of A

$$A + AB = 1$$

Mass balance of B

$$B + AB = 1$$

The moles of B is equal to the moles of A in solution
Setting mass balance of A = B

$$A + AB = B + AB$$
$$A = B$$

At the 1:1 cocrystal stoichiometric solubility, the moles of B is equal to A

1:2 cocrystal stoichiometric solubility determination

species present in solution: A, B, AB, AB_2

$$AB_{2,solid} \overset{K_{sp,1:2}}{\Leftrightarrow} A + 2B \overset{K_{1:1}}{\Leftrightarrow} AB + B \overset{K_{1:2}}{\Leftrightarrow} AB_{2,so\ln}$$

Mole balance of A

$$A + AB + AB_2 = 1$$

Mole balance of B

$$B + AB + 2AB_2 = 2$$

The moles of B is twice the moles of A in solution
Subtracting mole balance of A from B

$$B - A + AB_2 = 1$$
$$B - A + AB_2 = A + AB + AB_2$$
$$B = 2A + AB$$

At the 1:2 cocrystal solubility, the moles of B is equal to 2A + AB.